Max-Planck-Institut für Polymerforschung

Max Planck Institute for Polymer Research

JOHANNES GUTENBERG UNIVERSITÄT MAINZ

LIGHT-CONTROLLED ADHESION AND DYNAMIC PROCESSES IN LIPID VESICLES

Dissertation zur Erlangung des Grades

“Doktor rerum naturalium (Dr. rer. nat.)“

des Fachbereichs

Chemie, Pharmazie und Geowissenschaften (FB 09),

der Johannes Gutenberg-Universität, Mainz

vorgelegt von

Solveig Mareike Bartelt

Mainz, 2018

The thesis was carried out from January 2016 until December 2018 at the Max Planck Institute for Polymer Research, Mainz.

Dekan:

Prodekan:

Gutachter 1:

Gutachter 2:

Date of oral examination:

I hereby declare that I wrote the dissertation submitted without any unauthorized external assistance and used only sources acknowledged in this work. All textual passages which are appropriate verbatim or paraphrased from published and unpublished texts, as well as all information obtained from oral sources, are duly indicated and listed in accordance with bibliographical rules. In carrying out this research, I complied with the rules of standard scientific practice as formulated in the statutes of Johannes Gutenberg-University Mainz to ensure standard scientific practice.

_____ _____

Solveig Mareike Bartelt

“ What are the three most important rules of the chemist?

Label clearly. Measure twice. Eat elsewhere.”

- Patrick Rothfuss, *The Name of the Wind, 2007*

Table of contents

Seite

List of abbreviations

APS	Ammonium persulfate
ATP	Adenosintripohosphate
BSA	Bovine serum albumine
Cdc42	Cell division control protein 42
CETCH	Crotonyl-CoA/ethylmalonyl-CoA/hydroxybutyryl-CoA
cRGD	Cyclic Arginine-glycine-aspartic acid motif
Cry2	Cryptochrome 2
Cys	Cysteine
Cy5	Cyanine 5 dye
DGS-NTA	1,2-Dioleoyl-sn-glycero-3-[(N-(5-amino-1-carboxypentyl)iminodiacetic acid) succinyl]
DiI	1,1'-Dioctadecyl-3,3,3',3'-tetramethylindocarbocyanine
DiD	1,1'-Dioctadecyl-3,3,3',3'-tetramethylindodicarbocyanine
DOPC	1,2-Dioleoyl-sn-glycero-3-phosphocholine
DTT	DL-Dithiothreitol
ECM	Extracellular matrix
E. coli	*Escheria coli*
eDHFR	*E.coli* dihydrofolate reductase
EDTA	Ethylenediaminetetraacetic acid
Erk	Extracellular signal–regulated kinases
FKF1	Flavin-binding, kelch repeat, F-Box 1 protein
FMN	Flavin mononucleotide
FRAP	Fluorescence Recovery after Photobleaching
FtsA	Filamentous temperature sensitive A
FtsZ	Filamentous temperature-sensitive Z

GFP	Green fluorescent protein
Gln	Glutamine
GSH	Glutathione
GST	Glutathione S-transferase
GUV	Giant unilamellar vesicle
His-tag	Protein tag from 6 to 10 Histidins
iLID	Improved light-induced dimer
IPTG	Isopropyl-β-D-thiogalactopyranoside
K_d	Dissociation constant
k_{off}	Dissociation rate
k_{on}	Association rate
LB	Luria-Bertani Medium
LED	Light-emitting diode
LID	Light-induced dimer
LOV	Light-oxygen-voltage-sensing domain
LUV	Large unilamellar vesicle
MBP	Maltose-binding protein
NIR	Near-infrared
NTA	Nitrilotriacetic acid
PCR	Polymerase chain reaction
PEG	Polyethylene glycol
PhyB	Phytochrome B
PIF	Phytochrome interacting factor
PMSF	Phenylmethylsulfonylfluorid
PNIPAM	Poly(N-isopropylacrylamide)
POI	Protein of interest

POPC	Palmitoyl-2-oleoylphosphatidylcholine
POPG	1-Palmitoyl-2-oleoyl-sn-glycero-3-phospho-(1'-rac-glycerol)
PVA	Polyvinyl alcohol
QCM-D	Quartz crystal microbalance with dissipation monitoring
Rac	Ras-related C3 botulinum toxin substrate 1
RGD	Arginine-glycine-aspartic acid motif
RhoA	Ras homolog gene family, member A
ROI	Region of interest
RT	Room temperature
SDS	Sodium dodecyl sulfate
SDS-PAGE	Sodium dodecyl sulfate–polyacrylamide gel electrophoresis
SLB	Supported lipid bilayer
SNAP	Protein tag derivate from the O^6-methylguanine DNA methyl-transferase
SNARE	Soluble N-ethylmaleimide-sensitive-factor attachment receptor
SUV	Small unilamellar vesicle
TEMED	N,N,N',N'-Tetramethylethylendiamine
TEV	Tobacco Etch Virus nuclear-inclusion-a endopeptidase
Tris	Trizma base
trisNTA-Suc-DODA	N-Succinyldioctadecylamine with three Nitrilotriacetic acid groups
TRITC	Tetramethylrhodamine
UV	Ultraviolet light
Vis	Visible light

Abstract

The aim of bottom-up synthetic biology is to use molecular building blocks to create synthetic cells and to mimic cell functions. In biological cells, many of their cellular functions arise directly from both the spatial and temporal control of fundamental processes. Examples of these controlled events are the formation of protein patterns at the cellular and multicellular scale and cell adhesion during motility and tissue development. When mimicking these functions in minimal synthetic cells, visible light can be used as a trigger to provide the required high spatiotemporal control with the added advantage of it being non-invasive, biocompatible and dynamic.

Dynamic protein patterns are fundamental in cell signaling, cell division, cell migration, and tissue formation and are tightly regulated. To replicate and control the formation of protein patterns in a minimal synthetic cell, I used the light switchable protein dimer iLID, which interacts with its binding partners Micro or Nano under blue light conditions and dissociates from them in the dark. For this purpose, iLID was immobilized on giant unilaminar vesicles (GUVs), which were used as a minimal cell model. Illuminating these GUVs with blue light leads to the recruitment of a Nano fused proteins of interest and their subsequent dissociation when the light trigger is turned off. The iLID-Nano interaction allowed for the patterning proteins over multiple cycles and on different scales, from sub-GUV level to a single vesicle and to tissue-like GUV assemblies.

During cell motility, the cell adheres asymmetrically to a surface with new adhesions forming at the front and adhesions that dissemble at the back. The iLID-Micro dimer was used to imitate motility in a minimal synthetic cell through the light-guided movement of GUVs. This was achieved by controlling adhesions both at the subcellular scale and over time with light. For this purpose, iLID was immobilized on a glass surface to mimic the extracellular matrix with Micro attached to a GUV to mimic the cell adhesion receptor. The iLID-Micro interaction was strong enough to induce GUV adhesion to the surface under blue light, which reversed in the dark, as witnessed by the changing adhesion energies and length of adhesion site. The high spatiotemporal control of light was used to create stronger adhesion in areas exposed to light and weaker adhesions in areas left in the dark. This asymmetry in adhesion led to movement of the vesicle towards the illuminated regions in a manner similar to cell migration. Displacement of the GUV over multiple cycles at a speed close to that seen in mammalian cell motility allowed guiding the GUV over tens of micrometers in different directions.

The interaction between cells through their adhesion is important for the building of larger tissues from single cells, for the organization of cells within their environment, and for communication between them. The blue light dependent interaction of iLID and Nano was employed to control cell-cell adhesions between two populations of GUVs functionalized with these proteins respectively. When mixed together in close proximity, blue light illumination triggered the adhesion of the different subpopulations of vesicles. The interaction was strong enough that the adhered vesicles withstood mechanical stresses like laminar flow, but not strong enough to induce fusion of the lipid bilayers.

Overall, the blue light triggered interaction of iLID with Micro and Nano, is a valuable new tool in bottom-up synthetic biology for mimicking cell functions where dynamic control in time and space is required. Not only does it provide a general way to pattern proteins of interest and control interactions between different minimal cells but it also allows for reproducing the dynamic asymmetry in adhesion observed during cell motility and guiding the movement of a vesicle with visible light.

Zusammenfassung

Das Ziel der „Bottom-up“-synthetischen Biologie ist es, minimale, synthetische Zellen aus molekularen Bausteinen zusammenzufügen, um Zellfunktionen zu imitieren. In der Biologie rühren viele zelluläre Funktionen von der räumlichen und zeitlichen Kontrolle von Zellprozessen her. Beispiele dieser streng kontrollierten Prozesse ist die Bildung von Proteincluster auf zellulärer und multizellulärer Ebene, die Zelladhäsion an Oberflächen während Zellmigration und Zell-Zellinteraktionen bei der Bildung von Geweben. Um diese Funktionen in einer synthetischen Zelle zu imitieren, bietet sichtbares Licht die benötigte Kontrolle, ist biokompatibel und dynamisch.

Dynamische, mikrometergroße Proteincluster spielen eine fundamentale Rolle in Signaltransduktion, Zellteilung, Migration und Gewebeaufbau und sind daher streng kontrolliert. Um solche Cluster in synthetischen Zellen mit derselben Kontrolle nachzuahmen, wurde die Interaktion des lichtschaltbaren Dimers iLID, welches in blauem Licht mit deinem Interaktionspartner Nano oder Micro interagiert, ausgenutzt. Diese Interaktion ist im Dunklen umkehrbar. iLID wurde dafür auf „Giant Unlimellar Vesicles“ (GUVs), ein oft genutztes Modell für minimale Zellen, immobilisiert. Aktivierung von iLID durch blaues Licht führt zur Rekrutierung von einem an Nano gebundenem Protein an das GUV und dessen Dissoziieren im Dunkeln. Die iLID-Nano Proteinrekrutierung kann nach Bedarf von einzelnen Vesikeln auf Vesikelteppiche übertragen werden.

Während einer Zellmigration adhäriert die Zelle asymmetrisch an das Substrat mit starker Adhäsion an der vorderen Seite der Zell und mit schwacher Adhäsion am hinteren Ende. Das Proteinpaar iLID-Micro wurde benutzt, um Zellmigration in einer minimalen synthetischen Zelle zu imitieren. Dabei wurde die Adhäsion auf subzelullarer Ebene kontrolliert, um das Vesikel mit Licht zu führen. iLID, welches immobilisiert auf dem Substrat ist, stellt dabei die extrazelluläre Matrix dar, Micro, welches auf dem GUV immobilisiert ist, dagegen die Zelladhäsionsrezeptoren. Die Proteininteraktion war stark genug, um Vesikeladhäsion an eine Oberfläche mit blauem Licht zu induzieren. Dies spiegelt sich in der Änderung der Adhäsionsenergie und der Adhäsionslänge wieder. Durch die Kontrolle, die Licht bietet, konnte ein definierter Teil des GUVs mit Licht aktiviert werden, um in diesem Bereich starke Adhäsion zu induzieren, während die unbeleuchteten Bereiche nur schwach adhäriert waren. Diese asymmetrische Adhäsion führte zur Migration des Vesikels in den beleuchteten Bereich. Die Migration war über mehrere Zyklen konstant mit einer Geschwindigkeit ähnlich der von

Säugetierzellen. Die Interaktion zwischen Zellen ist notwendig, um Gewebe aus Einzelzellen aufzubauen, sie ist aber auch nötig für die Zellorganisation und die Kommunikation zwischen Zellen. Um Zell-Zellinteraktionen zu induzieren, wurden zwei Populationen von Vesikeln mit iLID und Nano funktionalisiert. Wenn diese unter blauem Licht in engen Kontakt kommen, adhärieren die Vesikel und dissoziieren wieder im Dunkeln. Die Interaktion widersteht laminarer Strömung, ist aber nicht stark genug, um Fusion herbeizuführen.

Das lichtaktivierbare iLID hat sich als wertvolles Werkzeug erwiesen, welches zeitliche und räumliche Kontrolle über den Trigger bietet, um Zellfunktionen in eine synthetische Zelle zu implementieren. Es erlaubt nicht nur Proteincluster und kontrollierte Zell-Zell-adhäsion in synthetischen Zellen zu imitieren, sondern auch dynamische Asymmetrie zu generieren, wie sie in der Zellmigration vorkommt, um Vesikel durch Licht auf einer Oberfläche zu bewegen.

1 Introduction

“A cell is regarded as the true biological atom”

– George Henry Lewes (1817-1878)

The cell is the building block of all known organisms and the smallest form of what is commonly called “life”. Defining what is meant by „life“ seems easy at first glance, but what exactly it constitutes remains heavily debated by scientists. They can, however, agree that life started with a cell at some point in our earth’s history.

The cell as basic unit of life has been the focus of different areas of science for quite a long time, not only in the endeavor to define the origin of life but also as a model to understand our modern cells. Success here would not only increase our understanding of fundamental biological processes but it also opens up new possibilities in medical treatments such as new ways of drug delivery.[1] But up to date, the intricate workings of the cell are not fully explored.

1.1 Towards a minimal synthetic cell

Even in the simplest living organisms, the molecular complexity is too great to be fully understood.[2] Therefore, one of the challenges that the field of synthetic biology has taken on is to produce a programmable living system with reduced complexity.[3] This “minimal cell” can be defined as a system with a minimum of functions necessary to call the consortium of parts “living”.[4] It is believed that designing such a minimal cell would help to understand complex biological processes, making it possible to bend the functions of a cell to our will and to find insight into the origin of life.[5-7]

There are two distinct approaches for achieving minimal cell-like systems. The so called top-down approach reduces the complexity of cells to a minimum to find the simplest form which can be called living (Figure 1.1.1). This can be achieved through knockdown and knockout of genes as well as whole gene deletion and genome

modification. The most remarkable result is taking *Mycoplasma genitalium*, the organism with the smallest known genome of 525 genes that can be cultured in the lab, and reducing it to live with only 384 essential genes.[8] The assumption is that this "minimal genome" would be sufficient to sustain a minimal synthetic cell. Despite this success, the huge problem remains that the function of 28% of genes on this "minimal genome" are unknown, but none the less essential. This raises the question how a system can be fully programmable and controllable, a requirement for a minimal synthetic cell, if its components are not fully understood.

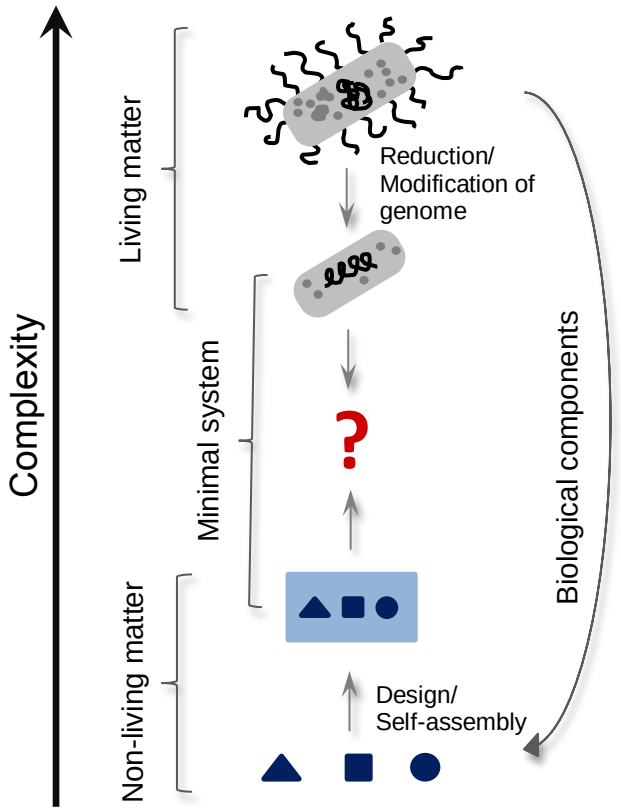

Figure 1.1.1 The two approaches to synthetic biology to reach a minimal synthetic system. The top down approach reduces the complexity of known organisms, whereas the bottom up approach uses non-living building blocks to create a living unite.[9] Copyright @ 1999 Elsevier. Reprinted with permission from Current Opinion in Colloid & Interface Science.

En route to developing minimal cells, a multitude of application for top-down synthetic biology have arisen. Biofuel production in yeast and *Escherichia coli*[10,11], and biological computers[12] are just some examples how such systems can be

+programmed. Genetic engineering of cells allows effecting the whole organism or just certain pathways to generate the desired function. The major limitations with this approach are, as mentioned, the complexity of modern organisms that have evolved over millions of years. As a result, there are multitudes of feedback loops and complex signaling pathways in a cell, which limit the programmed pathways and interfere in unpredictable ways. Maintaining oversight over what happens within the cell when even one single pathway is perturbed is already challenging, not mentioning multiple deletions or changes. Therefore, genome engineering can have unexpected and undesired effects in creating new functions and a "minimal cell".[1,13,14] This is also mirrored in that the creation of minimal organisms has only been truly successful in mimicking viruses and bacteria, which are far less complex than mammalian cells. Attempts to produce a minimal eukaryotic cell have failed so far.[1]

1.1.1 Bottom up synthetic biology

Even though the top-down approach to a minimal cell holds a lot of potential and has proven useful in multiple applications, in the last years a complementary approach has been on the rise: the bottom-up approach (Figure 1.1.1). Following the mould of Richard Feynman (1918-1988) "What I cannot create, I do not understand" (on his blackboard at the time of death in February 1988), the bottom-up approach tries to create the functions of a cell from molecular components and a self-sustainable living entity from not-living matter. Such a methodology would enable us to create an organism with a reduced complexity and fully characterized parts that are defined by the builder. To construct such a synthetic minimal cell, natural cells are deconstructed into building blocks and cell functions to obtain a road map.[4,15,16] The *de novo* assembly of systems that recapitulate basic cell functions from molecular building blocks of biological or chemical origin block by block allows increasing the amount of functions and complexity in the desired synthetic cell. This approach would give full, designed control over the minimal synthetic cell. Bottom-up synthetic biology can profit from the input of multiple established disciplines, methods from other scientific fields, most prominently among them polymer chemistry and biochemistry, and from synthetic or naturally derived systems to build up each of the modules.[4] This approach opens the possibilities to answer questions from drug delivery to the origin of life and gives the opportunity to define at which point a system can be called "alive".

A minimum of functions, called the proliferome, has to be fulfilled in a minimal cell: Energy supply, Metabolism, Growth, Replication and Division, Signaling and Motility.[17]

Adenosine triphosphate (ATP) is the universal unit of **energy** in the cell. A constant energy supply is needed for metabolism, motility, active transport, etc. to keep a living system out of equilibrium and sustain the highly ordered structures giving rise to emergent properties found in living cells.[18] Therefore, it is not surprising that reinstating an ATP-producing system into a synthetic cell was a focus of research in the effort to create an energy supply for the synthetic cell. The first major step into that direction was made by Choi et al. who developed a light-driven ATP-producing system. This study used an amphiphilic triblock copolymer as carrier material for proteins and as the model cell membrane.[18] Into this membrane the proteins bacteriorhodopsin and ATP synthase were reconstituted simultaneously. The purple bacteriorhodopsin is a blue light driven (absorption maximum 560 nm) proton pump[19], which allows for protons to be pumped into the compartment, creating a proton gradient between the surrounding and the inside of the compartment. The ATP synthase puts this proton gradient to use as driving force for ATP synthesis.[18] To increase the applicability and efficiency of this system new compartments that show more cell-like behavior were developed, such as copolymer/lipid hybrid vesicles[20] and droplet stabilized giant unilamellar vesicles (GUVs)[21]. Additionally, different ways of creating the necessary proton gradient were investigated. Otrin et al. showed that cytochrome bo3 quinol oxidase can be used to attain a similar proton gradient in a compartment inducing ATP-biosynthesis.[20]

Metabolism envelops all chemical reactions within a cell to maintain life. Implementing only parts of metabolism of a cell into a synthetic environment is a huge feat. Additionally, the drive to build up a whole metabolism for a synthetic cell provides the opportunity to model existing pathways to increase the efficiency of metabolism or create entirely new pathways with the help of metabolic engineering.[22] One example towards implementing an improved metabolic pathway into a synthetic surrounding is the fixation of carbon dioxide (CO_2) *in vitro*. Through computational design and genetic engineering as well as combining enzymes from different organisms, it is possible to create the so called CETCH cycle (crotonyl-CoA/ethylmalonyl-CoA/hydroxybutyryl-CoA) *in vitro*. This reaction network converts CO_2 into organic molecules at a rate comparable to that of the citric acid cycle in plants.[23] This shows what is possible to implement in a synthetic system, but is still far from the metabolism complexity of a cell.

Growth is the increase of surface area and volume of a cell or vesicle. In colloidal systems, like water droplets in an oil phase, this occurs through Ostwald ripening, when matter in a system moves from smaller colloids, particles or crystals to bigger

ones. In a colloidal system this leads to increasing sizes of the bigger droplets ("growth"), while the smaller droplets shrink even more.[24] In a giant vesicle this process is decidedly more difficult, as the inside of the vesicle is partitioned from the outside through a membrane. This membrane firstly reduces free diffusion as it is a barrier. Secondly, the membrane restricts the volume of the vesicles as membranes are flexible only to a certain degree, restricting growth except when replenishing the membrane with more lipids. There have been methods developed allowing for lipid vesicles to grow. Growth based on the fusion of multiple vesicles into one has been achieved by a multitude of triggers like synthetic fusogenic molecules[17,25], electroporation, Ca^{2+} and polyethylene glycol (PEG)[25]. A more sophisticated system was developed by adding membrane precursors to a buffer solution, which hydrolyze through addition of an amphiphilic catalyst and thus supplement the membrane, allowing for membrane growth.[26] Remaining problems include the lack of control over the growth process as the sizes of the resulting compartments are not homogenous and are not regulated. Moreover, the dynamic nature of the growth process as well as expanding the developed methods of growth from lipid-based systems to a broader range of microcompartments has proven to be problematic, as every compartment has their own physical properties needed to be considered in growth (see chapter 1.2).

Replication and **division** are important steps towards obtaining a growing and self-sustaining synthetic cell population. It is known that vesicles can undergo voluntary budding of lipid membranes due to spontaneous curvature and available excess membrane.[27] But there is a need for a controlled manner of division of synthetic cells. The incorporation of known eukaryotic division proteins into a synthetic cell has been shown to be functional and leads to induced division. Osawa and Erickson have shown that implementing the filamentous temperature-sensitive Z (FtsZ), a tubulin homologue, and its binding partner FtsA into vesicles leads to the forming of FtsZ-rings in a liposome. These FtsZ-rings can induce separation of the liposome into two distinct new liposomes.[28] A step further was taken when the amplification of DNA allowed the so-called self-reproduction of the cationic giant vesicle through addition of membrane precursor and a catalyst. DNA is replicated in a GUV by DNA polymerase. Through the interaction of the amplified, negatively charged DNA and the positively charged membrane the membrane is replenished. This leads to growth and sequentially to division of the vesicle giving rise to two equal daughter vesicles.[26]

Signaling is a complex and trigger dependent machinery inside a cell, which normally consists of a multitude of proteins, other biomolecules and molecular triggers working

together to transport information. The different pathways in a cell are connected to each other and are far from being linear, making it a challenge to implement even short signaling structures into a “minimal cell”. The first step in mimicking such a signal pathway was carried out recently by reconstituting integrin into a droplet stabilized GUV.[21] Integrins are one of the most prominent examples of cell adhesion proteins and bind to the arginine-glycine-aspartic acid-motif (RGD), present for example in fibrinogen, collagen and laminin.[29] It was shown that the GUV with reconstituted integrin interacts with a fibrinogen coated surface observable through spreading of the vesicle on the surface.[21] This represents a good first step towards building a signaling pathway as the cellular receptor, integrin, interacts with an external stimulus, fibrinogen. However, an internal signaling unit to transduce the interaction signal within the cell is still missing.

These are just a few examples of the work that has been done towards creating a minimal synthetic cell out of non-living molecular building blocks. It shows not only the recent progress that has been made, but also gives a glimpse into the complexity that is present in a modern cell. A lot of work remains to be done to understand the intricacies of the cell’s pathways and to introduce them into a synthetic system, steps necessary in the creation of a fully functioning, living cell.

1.2 Synthetic cell models

Towards the aim of building a minimal synthetic cell, it is important to produce systems that mimic cell functions. Hence, what is the most minimal cellular system? If one would take a mammalian cell and take everything out and clean it up a little, you would be left with a shell.

This outer membrane is one of the most important organelles of a cell: it is not only responsible for giving the cell a boundary; it is also responsible for the mechanical stability of the cell and protecting intracellular molecules from external stresses. Through the clear division of “out-“ and “inside” an out-of-equilibrium state can be achieved and maintained, which is used for example in ATP production (see chapter 1.1.1). As an organelle the outer membrane is important for passive transport as well as scaffolding for transport and pore proteins, controlling the transport of waste to the outside and nutrients to the inside. The membrane and the associated proteins

are also the only connections a cell has to the surrounding and are responsible for detecting changes in the environment and adjusting to them. Last but not least, the physical properties of the outer shell has an influence on many cell processes especially adhesion, migration, and growth.[1,30] Therefore, the outer shell is one of the most important building blocks of a cell. In a mammalian cell the membrane is made in general from lipids, cholesterol and functional proteins, but the nature, composition and properties of the membrane have immense influence on the properties. The size of the compartment has significant influence as well, as the physical dimension of a cell has an exponential impact on surface-to-volume ratio and diffusion time of molecules within the compartment.[3] It has to be semipermeable, structurally sound and capable of the encapsulation of molecules. This makes the cell membrane, hereafter referred to as the cell model, the most important point in creating a functioning synthetic cell.[31]

In synthetic biology a multitude of approaches have arisen, inspired by both natural and artificial structures, to provide a wide variety of model membranes with differing characteristics.[1] Here, the most important and promising cell models and their benefits are highlighted.

1.2.1 Fatty Acids

Fatty acids are single chain amphiphilic molecules.[1] When introducing them into an aqueous surrounding they will spontaneously form bilayers with their hydrophobic tails towards the inner part of the layer and the hydrophilic heads outwards to the buffer. Already in 1973 Gibick and Hicks demonstrated that fatty acids form spherical vesicles, named ufasomes, with one or more layers of membrane with an aqueous interior, when resuspended in a buffered solution.[32]

They have been considered as a cell model due to their stability and chemical simplicity.[30,32] Additionally, in research about the origin of life, it is believed that under prebiotic conditions fatty acids were formed, while higher forms of lipid-like molecules have probably evolved later. Therefore, fatty acids have become a focus for studies of protocells on early earth.[1,33] To encompass the functions mentioned above, the membrane must be dynamic, to allow for growth and permeability.[30] Fatty acids provide this dynamic, as the acid chains can flip freely between the two leaflets of the bilayer.[33] In a growth process, additional molecules that are built into the outer leaflet of the membrane can flip easily to the inner leaflet and allow for uniform growth of the vesicle.[33-35] Moreover, fatty acids show permeability for small polar molecules as well as nucleotides and ions, which implies that these cell models would be able to have

functional transport between the cell and the environment.[34,35] Fatty acids provide a very simple and also cheap system to provide a homogenous, synthetic cell membrane.[32]

One problem arises from the lacking control over the distribution in size and amount of layers of a vesicle derived from the forming method, which makes it hard to create a reproducible and faithful representation of a natural cell membrane.[32] Despite this drawback, the amount of work that has been done in fatty acid membrane vesicles makes it clear that this very simplified model of a cell membrane has been important to answer questions on the origin of life.[1]

1.2.2 Proteinosomes

A relatively new cell model has been designed by the Mann lab: proteinosomes, protein based microcompartments. Proteins unify many beneficial qualities when acting as building blocks for membranes as they are biocompatible, biodegradable and have multiple chemical functionalities.[31]

In proteinosomes, proteins with primary amine groups, such as bovine serum albumin (BSA), are crosslinked to temperature responsive poly(*N*-isopropylacrylamide) (PNIPAM) to create “giant amphiphiles”, which self-assemble at a water/oil interphase into vesicles with sizes in the tens of micrometer range.[31] Different sizes of the compartment can be achieved by different preparation methods, like microfluidics[36] and controlled concentration of building blocks with defined applied shear stress. The tight size control allows for the assembling of hierarchical structures ranging from an assortment of compartments to tissue-like structures.[37] A great advantage of proteinosomes is that their structure and function can be defined by controlling the chemistry of the protein building blocks.[38] In theory a whole variety of proteins with different functions and physical properties can be utilized to modify the vesicles, as long as there are primary amine groups available.

The encapsulation capacity of proteinosomes has been demonstrated for a wide range of molecules, from fluorescent dyes to enzymes and a cell free gene expression system. The use of the thermo-responsive polymers as part of the membrane structure permits the control of permeability according to size with temperature.[31] Pore size can furthermore be regulated by differential crosslinking as well as enzyme-mediated disassembly. Additional work demonstrated the protection of these protocells from proteosomal degradation by building an outer hydrogel wall. This hydrogel wall does not restrict the permeability and yet provides sufficient protection against

degeradation.[39] Proteinosomes provide a very robust cell model, especially for very harsh conditions such as dehydration and elevated temperatures, (e.g. 70 °C) as needed for example for a Polymerase Chain Reaction (PCR).[31] The crosslinking chemistry though limits the application for more dynamic processes like cell model division.

1.2.3 Polymersomes

Vesicles made from purely chemically synthesized amphiphilic polymers are called polymersomes. As early as 1964 they were proposed for use as a cell mimic.[40] Amphiphilic block co-polymers have the same basic architecture as lipids (hydrophilic head, hydrophobic tail) and thus show the same self-assembly behavior, making it easy to form vesicles.[41-43]

Owing to decades of research, the biggest advantage to this system is the diversity of the block coploymers available for use. As such, polymersomes allow for tunable properties including electrical charge and hydrophobicity, making it possible to truly design the compartment towards its ultimate purpose. The different polymers also allow different surface chemistry to functionalize or immobilize the surface with a variety of molecules from dyes to adhesion proteins thus tuning their behavior.[41,42,44] One prominent example is that immobilized polyethylene glycol (PEG) chains on a polymersome in the blood stream show a “stealth effect” increasing the circulation time compared to the pure polymersome.[41] Further stability (e.g. towards pH, temperature and solvents), fluidity, and intermembrane dynamics can be greatly influenced by the choice of the polymer.[41,42]

The methods to produce polymersomes are as multifold as the building blocks available; from easy bulk methods[40] to highly sophisticated microfluidic set ups.[44,45] And it is possible to have great control over size and hierarchal cells, multiple smaller polymersomes encapsulated by a bigger host polymersome[46]. Even shape changes in polymersomes have received great interest, as the shape of the cell has influence over the functionality. An example for the shape-function relationship is the bowl-like shape of red blood cells to increase the surface area for gas exchange, which was mimicked in a poly(ethyleneglycol) polystyrene polymersome.[42,47] Further, thermodynamic and kinetic approaches towards controlled shape change have been developed[42] but are beyond the scope of this thesis.

One disadvantage of using block copolymers is their high molecular weight as this increasing the thickness of the formed bilayer. As such the polymersome membrane is,

in general, several times thicker than a lipid vesicle membrane.[42] This greatly enhances stability, but also opens up the question if transport across such a membrane is possible to serve as a versatile cell model. For example, transmembrane proteins have a defined transmembrane domain of a defined size that has been evolutionary adjusted to conform to the thickness of a cell membrane, which is much closer to that of a lipid vesicle than a polymersome.

Early on it was shown that polymersomes have great encapsulation capabilities[40] but the thickness of the membrane has limited the permeability of even small molecules.[42,48] One of the very few successful attempts at creating semipermeable polymersomes was the reinstitution of Aquaporin Z into a ploymersome allowing for water exchange between the cell model and its surrounding.[43,49] Another approach to increase and control permeability of polymersomes was to include stimuli responsive block copolymers, similar to the thermo-responsive PNIPAM into the proteinosomes (see chapter 1.2.2), to generate pores in response to increased temperature.[50] A completely different idea was developed by Cheng et al., who incorporated small amounts of lipids into a polymersome, which were extracted after crosslinking yielding defined pores in the vesicle membrane.[51]

Polymersomes show great potential for a wide range of cell mimic applications, with a diversity of functions, but also have their drawbacks. They are made purely of chemical blocks that need chemical treatment, which can itself be harmful to sensitive proteins that need to be attached to or encapsulated in the membrane. Additionally, the organic solvents that can be necessary in the production of polymersomes makes a thorough clean-up process necessary before introducing them into a biological system, resulting in low yields. Even though the membrane thickness can be regulated through the use of block copolymers with a lower molecular weight, these can still pose a problem for the incorporation of transmembrane proteins into the system.

1.2.4 Inorganic cell model

Microcompartments from inorganic colloidal particles with an aqueous core and a monolayer membrane can be easily produced by Pickering emulsion.[52] The particles spontaneously self-assemble at the interface of a water-in-oil-emulsion into tens of micrometer sized compartments, driven by the degree of free energy in the system.[53] Colloidosomes are by default semipermeable through the gaps between the nanoparticles[1] and provide a wide range of possibilities for modification and functionalization.[1,53]

Their use as biomimic for cell membranes was only highlighted recently when Li et al. described the encapsulation of multiple active biomolecules of an *in vitro* cell-free gene expression system for the green fluorescent protein (GFP) into a colloidosome.[54] One of the biggest challenges in the use of colloidosomes as a cell mimic is the transfer of the assembled microcompartments into bulk water, as it induces immediate disassembly.[55] This was overcome by the crosslinking and grafting of a copolymer that would create an outer polymer shell to protect the colloidosome from disassembly.[55-57] As mentioned before inorganic microcompartments are semipermeable. The degree of permeability is determined by the size of the colloids forming the microcompatments, as bigger colloids will lead to bigger gaps in between particles. Smaller colloids allow for tighter packing on the water-oil interface and thus allow for smaller spaces between molecules.[55] This permeability can be further fine-tuned by using thermo-responsive polymers or pH-responsive cross-linkers or even by creating electrostatically gated membranes.[43,55] These systems are neither very plastic nor dynamic meaning creating growth in the assemblies is difficult. Moreover, it would be hard to recreate a fatty acid-like growth process in this system. Advancements towards mimicking growth have been made by swelling of the microcompartments through organosilane-mediated methanol formation. The methanol increases the volume of the aqueous core, which leads to an increase in size up to bursting.[38]

Even though inorganic membranes seem on the first glance as a rather farfetched way of establishing a cell model, it was shown that a multitude of characteristics of a natural lipid membrane can be mimicked and thus inorganic membranes supplement the available possibilities for cell mimics. They provide an alternative to the lipid-like cell models and offer the opportunity to extend the technological scope.[55]

1.2.5 Lipid vesicles

Over all modern organisms, from bacteria to humans, the cell membranes are comprised of a mixture of phospholipids, glycolipids, cholesterol and functional proteins. They form a nanometer thin membrane that prevents free diffusion between inside and outside.[6,41,58] It seems an obvious choice for a proliferome to use phospholipids as cell membrane, because it is a main component of the cell membrane. Therefore, it would be expected to entail similar physical properties, namely flexibility, softness, fluidity and semi permeability. A membrane composed of lipids would still keep to the simplicity synthetic biology is aiming for[58], while presenting

relatively high pH and temperature stability[6]. Thus, it is not surprising that most synthetic cell compartments have been produced using phospholipids.[6,14,15,59,60]

Phospholipids form vesicles in aqueous solution, so called liposomes. They are categorized according to the amount of layers into unilamellar (one bilayer) and mulitlamellar (multiple bilayers in one vesicle) and according to their size from SUV (small unilamellar vesicles, <50 nm) to LUV (large unilamellar vesicle, <1 µM) and GUV (giant unilamellar vesicles >1 µM).[58] GUVs are of special interest as they are comparable to cells in size, they are unilamellar, and the encapsulation volume is similar to that of a cell.[15]

Currently GUVs, in comparison to other cell mimics, provide the closest replication of a cell membrane in a synthetic system. There have been a number of methods describing how GUVs can be formed, from very simple methods like film hydration[61,62], gel assisted hydration[63] and double emulsion[35] to more intricate methods like electroformation[64] and microfluidics[65]. With the emergence of more sophisticated methods the complexity of lipid mixtures has increased significantly, as well as the throughput and homogeneity of the vesicles. This also allows for the addressing of more complex questions regarding the function of the membrane and allows for the creation of more sophisticated cell models. GUVs can easily be modified by using different lipid compositions and cholesterol proportions, which changes their mechanical and physical properties.[14] This enables research into the physical properties of a membrane specifically regarding the insertion and folding of membrane proteins.[14,66]

A definite advantage that lipid membranes have over other membrane mimics is the nature of membrane organization and segregation. It is known that lipid membranes have a very fluid and dynamic structure.[67] Lipids within a membrane can rotate, wobble, laterally diffuse, undergo *trans*-gauche isomerization, and do a flip-flop motion.[34] In mixtures of lipids with a high and a low melting temperature the lipids separate into distinct domains, so called lipid rafts.[68] In nature, such lipid rafts are presumed to be involved in a multitude of cellular functions, like protein clustering in signaling processes, modulation of membrane fluidity and protein trafficking inside the membrane.[69] Consequently, the investigation of these rafts has increased in importance, as the nature and function of the rafts could shed light on the influence of the lipid organization on protein function and liposomes are the only membrane platform capable of mimicking their actions.

The closeness to nature in thickness and composition presents the opportunity for relatively easy integration of functional transmembrane proteins[34,70,71] and precursors of signaling pathways in form of integrins[72,73]. With the semipermeable nature of lipid membranes being quite similar to fatty acids, where neutral molecules can cross the membrane passively, the integration of transport proteins could provide a platform to study active transport. Active transport is important in creating and maintaining concentration gradients, e.g. proton gradient needed in ATP production.[18,34] The encapsulation efficiency for active biocomponents like enzymes, proteins and other biomolecules has been described and is similar to other cell models.[74] Moreover, lipid vesicles can be used as bioreactors, enabling whole reaction cascades to be done in one compartment as well as using the membrane itself as a scaffold for reactions.[75-78]

Lipid membranes are, as mentioned earlier, quite fluid, but have a reduced dynamic compared to fatty acid membranes. Therefore, the controlled induction of growth and division is not as easy as in fatty acid vesicles. One step towards tackling this issue has been made, by introducing the bacterial Min system into lipid vesicles. The Min proteins are responsible for the positioning of the division site in the middle of *Eschericha coli*, by oscillating from pole to pole inside the bacteria placing the divisome protein FtsZ in the middle of the cell.[79] The formed protein gradient can be regulated in velocity and shape.[79,80] These results hint that liposomes can work as a platform for the investigation of division and reconstituting a divisome.

Lipid vesicles have received substantial attention, as it is the closest model to a cell membrane and is consequently an obvious choice as cell model in synthetic biology. This is reflected in the number of publications and the amount of work in terms of applications for medicine[81] and as bioreactors[75,77,78]. The increased amount of GUV preparation methods will ensure that lipid vesicles remain in focus for cell membrane models for the near future.

All of the above described membrane models are suitable as a synthetic cell model for the proliferome. The advantages and disadvantages of every model have to be carefully evaluated before choosing and finding the best option for the research goal. It is possible that within the next years even more models will emerge, increasing the pool of functions mimicked and enabling them to be as close as possible to the natural membrane or possibly even exceeding its characteristics.

1.3 Protein clusters and patterning

Protein patterns and clusters play a role in many cell functions and make the membrane an important organelle in the cell as the major platform for pattern and cluster formation. At that protein patterns can differ in shape and size, can span distances of up to several micrometers and are assembled in a dynamic and spatiotemporally controlled manner from different proteins thereby having diverse functions.[82]

1.3.1 Protein patterns in nature

Notably, protein clusters are involved in signaling. One of the most prominent examples is the T-cell receptor clustering. When an immune cell binds to its target various receptor-ligand pairs, prominent among them the T-cell receptor, sort themselves into spatially exact patterns. These patterns attract and recruit signaling molecules to the membrane, initiating signaling pathways to react to the invasion. Further experiments into T-cell receptor clustering emphasize the importance of spatial control, as it determines the effect of the signal.[83]

Bacterial division is another process defined by protein patterns. Key to this process is the spatiotemporal control of FtsZ clustering in the middle of the bacteria, which defines the division site *E.coli*. The inhibitory Min proteins oscillate from pole to pole in the bacterium, inhibiting the binding of FtsZ to the bacterial membrane at the poles, driving the FtsZ to the middle. Thus, the FtsZ polymerizes in a ring formation in the middle of the bacterium inducing division. If the Min proteins do not cluster properly at the poles, the division does not take place directly influencing the bacterium and the overall bacteria population.[80,84,85] The control over the cluster is therefore responsible for the outcome of the process.

Another example is integrin clustering in cell adhesion and migration. This will be discussed in more detail in a following chapter (see chapter 1.4.1). In short, upon binding of integrin to the extracellular matrix (ECM) supplementary integrins diffuse from the other parts of the membrane to build up clusters at the site of contact, which determines the adhesion strength.[86,87] As adhesion and migration are involved in a multitude of cell functions, protein clusters and patterns also influence development and tissue formation. Additionally, protein patterns in the ECM have an influence on the cell behavior. For instance, RGD nanoclusters (RGD is the major binding motif for Integrin, see chapter 1.4.1) define cell adhesion and motility dependent on the spatial conformation of the RGD ligand.[88]

1.3.2 Light controlled mimics of protein patterns

The importance of protein clusters and patterns in such key processes demonstrates that it is also important to mimic such clusters and patterns in minimal synthetic cells.[89-91] In the optimal case the mimicked patterns and clusters show the same high spatiotemporal control and dynamic as displayed in cells. Due to the influence protein clusters have on cell behavior and signaling, techniques to pattern proteins have been intensely researched.[89,92-95] Especially, for medical application and their use in synthetic biology, the protein patterning should be done under physiological and biocompatible conditions to preserve protein function and integrity. Many procedures though are based on unspecific adhesion to substrates, which can cause denaturation and thus a loss of function.[95,96] The focus here will be on protein patterning platforms that provide required high spatiotemporal control observed in nature through the use of light. As also detailed in chapter 1.6 light provides noninvasive and better control than most other stimuli.

Azobenzenes are one class of light responsive molecules that are commonly used for protein patterning taking advantage of the *trans* to *cis* isomerization under UV light irradiation. The azobenzene conformational change is reversible in the dark, which makes the patterning reversible.[97] In rudimentary way, a monolayer of azobenzenes on a substrate can be used to tune the wettability under UV light and hence decrease the protein absorption.[91] To pattern a specific protein such as α-Chymotrypsin, an inhibitor for it was coupled to an azobenzene group. Through UV-light illumination the azobenzene changes conformation and therefore the accessibility of the inhibitor for the binding of α-Chymotrypsin, letting α-Chymotrypsin bind only to the illuminated area.[89] Unfortunately, the need to use UV light renders the azobenzene based systems not biocompatible and protein patterns either rely on unspecific absorption or are only achieved for a limited number of POI, as they rely on defined protein interactions.

The nitrobenzyl photoremovable group and its derivates are commonly used to cage protein binding groups or motives and can be removed through cleaving by UV light illumination. In a number of approaches nitrobenzyl allows to introduce temporal and spatial control to protein patterning.

Biotin has been caged with a nitrobenzyl group as cleaving moiety to allow for photoactivated avidin patterning.[98] The avidin-biotin interaction is a very well characterized interaction and one of the strongest known in nature.[99] The protein

binding can either be used to pattern proteins of interest by binding avidin in a sandwich-like manner between the biotinylated surface and a biotinylated protein or directly link the POIs to avidin.[94]

Another protein that can be photocaged with a nitrobenzyl moiety is benzylguanine. Benzylguanine binds to the so called SNAP-tag, a protein tag derivate from the O^6-methylguanine DNA methyltransferase. The SNAP-tag can be attached to a huge variety of proteins. Upon UV light illumination of the caged benzylguanine the tagged protein can be recruited to the surface in a defined manner. As benzylguanine can easily be bound to lipids, this approach allows recruiting lipids not only to a two dimensional surface but also the surface of vesicles either from the out- or inside.[90]

A similarly renowned protein tag is the so called His-tag, a repetition motif of usually six to ten histidine residues that complexes with Ni^{2+}-Nitrilotriacetic acid (NTA). This interaction can be blocked with a NTA-headgroup with a Φ-His peptide, which is attached to a PEGylated surface. Incorporating a nitrobenzyl derivate renders the His-peptide UV light cleavable, freeing the NTA groups after illumination for His-tagged proteins. This can be repeated on different sections of the same sample multiple times, recruiting different proteins to each section.[92] Transferring this approach into a Hydrogel allows for protein patterning in three dimensions.[100]

A reverse approach to use the photoliable group was used to remove already bound proteins from a surface in a spatial controlled manner. Linker constructs that can be covalently bound to a surface contained a nitrobenzyl group and a binding motif as head group, e.g. cRGD.[101,102] After binding of the protein of interest the surface can be illuminated in a spatially controlled manner to cleave away the bound protein, leaving protein only in parts that where not illuminated as patterns.[102]

Protein patterning in hydrogels affords the luxury of being able to pattern in three dimensions. DeForest et al. developed a photocleavable hydrogel based on *ortho*-nitrobenzyl esters, where bioactive proteins can be introduced and sequentially released from the illuminated areas, leaving the protein patterns. This process can be done simultaneously with multiple proteins and through the whole gel in defined space in x,y and z direction.[103]

Constructing photoliable groups with nitrobenzyl allows great spatial and temporal control over protein patterning. UV light though is not biocompatible and is therefore not useful in a physiological setting. To overcome this problem approaches have been developed that use biocompatible wavelengths.

Nitrodibenzofuran can be cleaved upon two photon excitation (wavelength 730 nm). Gluthatione (GSH) fused to nitrodibenzofuran renders it inactive. After nitrodibenzofuran cleaving glutathione S-transferase (GST), the natural interaction partner of GSH, can bind. This can be done in a two dimensional setup over multiple cycles recruiting fluorescent GST-fused proteins. To model this approach in three dimensions the photoactivatiable GSH can additionally be incorporated into a hydrogel.[93]

A blue light photliabale caging group is 6-Nitroveratroyloxycarbonyl (Nvoc). Caging a binding partner of *E. coli* dihydrofolate reductase (eDHFR) allows for controlled patterning of proteins fused to eDHFR. The benefit of this system is that it has been shown to work even in a living cell, providing a biocompatible system.[104]

Upconverting nanoparticles in combination with blue light cleavable ruthenium complexes are another reversed protein patterning approach without the use of UV light. Nanoparticles grafted with PEG and ruthenium complexes will bind proteins. After illumination, globally or through a mask, the ruthenium complex is cleaved off with the proteins still attached to it. The residual proteins on the surface form the pattern.[96]

Light as an energy source can be used in an indirect way to pattern proteins by creating heat. PNIPAM, a thermoresponsive polymer, is extended in its native form and collapses when heated. This conformation change is reversible through cooling. Spatially controlled heating of the light-to-heat-converting surface collapses the PNIPAM letting proteins unspecifically absorb from a buffer to the surface, while the unheated, extended PNIPAM chains protect the surface from protein adsorption. Multiple cycles of this process allow patterning of multiple proteins.[95] Unfortunately this approach loses spatial and temporal resolution losing the advantages of light and only unspecifically absorbs proteins.

Obviously there have been a lot of methods developed to pattern proteins with different advantages and disadvantages. In general, many of the approaches utilize ultraviolet light, which is not biocompatible and subsequently is not useful for physiological conditions. Visible or near infrared light would provide more physiological environments and would allow for the same high spatial, temporal control as UV light does. Each of the discussed approaches provides a different way to answer a defined question in fundamental research or medicine, on different time and space scales.[105] Yet there is still a need for a very dynamic patterning approach with the desired dynamic and tight

control over time and space. To create protein patterns close to nature, they have to form, dissolve and form again.

1.4 Cell adhesion

Cells interact with their environment in multiple ways; cell can adhere to the ECM around them or other cells in their proximity. This is why cell adhesion is fundamental to cell biology and cell adhesion is dynamically regulated during vital processes like growth, differentiation[106], cell-cell communication, development[107], immune response, hemostasis[108] and trafficking[86,109]. It is not surprising therefore, that the missregulation of cell adhesion is at the heart of a lot of diseases. The two forms of cell adhesion: cell to ECM adhesion and cell to cell adhesion, have distinct roles in cell biology. Nonetheless, there is cross-talk between these two forms of adhesion due to the intracellular coupling of these adhesive interactions to cytoskeleton and overlapping signaling pathways.[110,111]

In the following, the two main protein families, integrin and cadherin, that mediate cell-matrix and cell-cell adhesions, respectively, will be discussed. It should be noted that in nature the mentioned processes are much more complex and many more proteins are involved creating complex clusters and machineries than are depicted here. But to understand the principles the overview given here should suffice.

1.4.1 Cell-matrix adhesions

The integrin receptor family is responsible for cell adhesions to the ECM.[109] Integrins are a family of heterodimeric transmembrane receptors containing a α- and β-subunit (see Figure 1.4.1A). The head regions of the dimers are exposed to outside and contain the binding sites to the ECM.[112] An important motif that integrins recognize is the RGD peptide sequence, which occurs in important ECM proteins including fibronectin and fibrinogen. The binding of integrins to the ECM leads to a conformational change and a connection of the cytosolic integrin tail of the β-unit to the cytoskeleton through adapter proteins (see Figure 1.4.1A).[87]

Activation of adapter proteins leads to clustering of integrin at the adhesion point. The receptor diffuses from other regions of the membrane to the adhesion site, leading to more ligand binding at the adhesion site and the generation of integrin clusters also named focal adhesions.[86,87] The focal adhesions are not only influenced by

posttranslational modifications, protein-protein and protein-lipid interactions, but also by exogenous signals like mechanical stress and presentation of ligands on the ECM.[87,109]

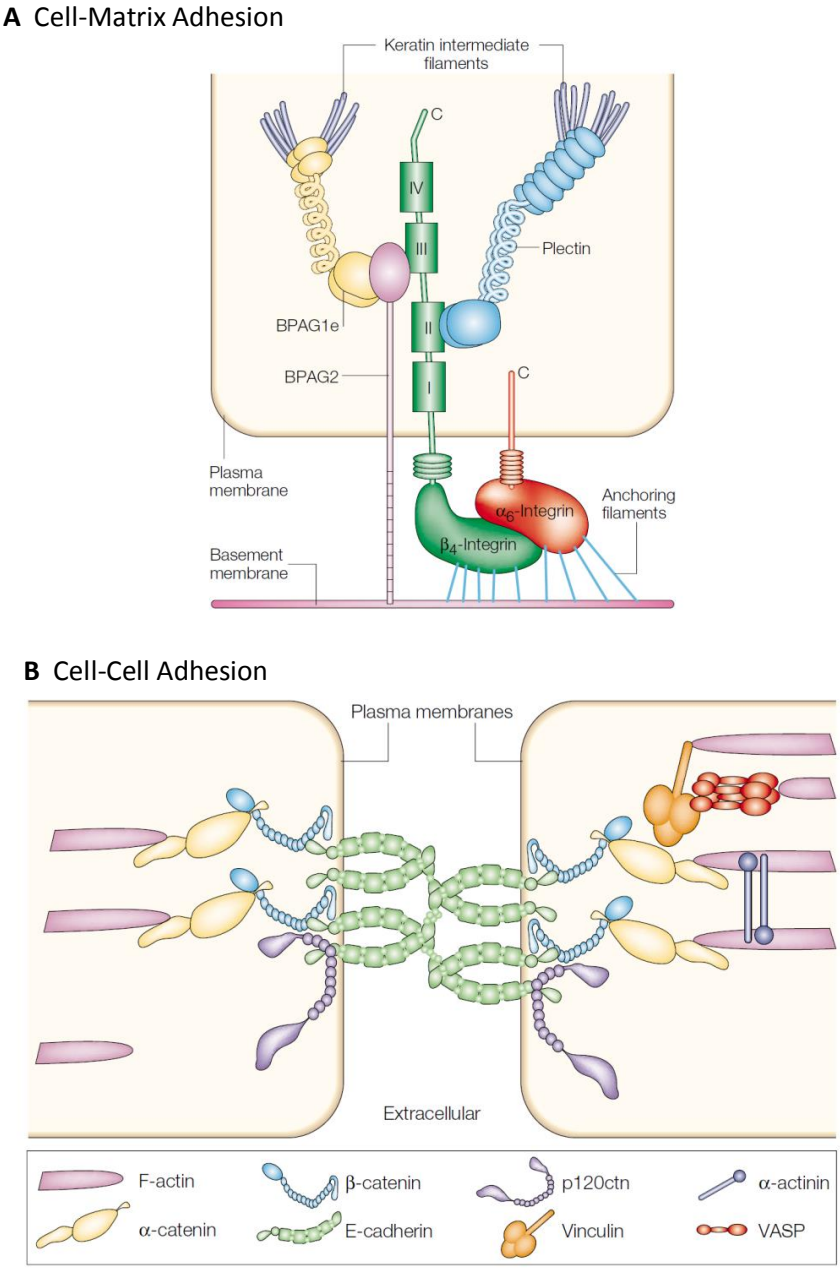

Figure 1.4.1 Overview over protein complexes occurring during cell-matrix adhesion and cell-cell adhesion. A) The key protein in cell-matrix adhesion is integrin which connects the information from the ECM to the cytoskeleton inside the cell. B) Cell-Cell adhesion is mainly mediated through cadherins. Also cadherins are connected to the inner cytoskeleton via catenin and is involved in signalling pathways. They also give mechanical stability to cell organisation.[113] Copyright @ 2002 Springer Nature. Reprinted with permission from Nature Reviews Genetics.

Integrins have both an inside-out- and outside-in-signaling function, connecting the inner workings of the cell with the outside reacting to exogenous signals. The conformational changes in integrins as well as their clustering have an influence on the signaling pathways of a cell.[114] Integrins work as an allosteric switch, meaning the extracellular changes in conformation lead to activation inside the cell.[112] During outside-in-signaling the exogenous signals lead to activation of intracellular pathways that arise from the cytoplasmic domain of integrin.[115] One example would be the integrin dependent activation of Akt through the integrin linked protein kinase B. This stimulation of signaling pathways also has the function of giving the signal for maturation and disassembly of the adhesion.[87] The inside-out signaling is mainly induced by Talin and Kindlin, which bind with the PTB-domain to integrin and are directly connected to actin.[87,112] The regulation of this process is very complex and full account exceeds the scope here.

1.4.2 Cell-cell adhesions

The most important cell-cell adhesion molecules are the family of cadherins. Cadherins are expressed on the surfaces of adjacent cells and thereby the interaction of cadherins on different cells leads to the formation of cell-cell adhesions. The family of cadherins comprises of a multitude of proteins. In general, cadherins have a single transmembrane domain and five extracellular cadherin domains that are linked through calcium, which makes them stiff and rod-like structures (Figure 1.4.1B, green). The cadherins are connected to the actin skeleton, similar to integrins, through catenins (Figure 1.4.1B, blue and yellow).[112,116] Cadherins bind homophilic to each other, the exact mode of binding is still disputed though. Interestingly this could hint that also cadherin has different conformational stages that regulate adhesion.[112] The complexes of cadherins and catenins haven been shown to be regulators of multiple signaling pathways of extensive width: they are involved in epithelial-mysenchymal transition and mesenchymal-epithelial transition, cell sorting, cell rearrangements and collective cell motility to name but a few.[116]

The signaling in cadherin mediated cell-cell adhesions work in a homologues way to integrin mediated adhesions showing outside-in and inside-out-signaling with a multitude of signaling pathways attached. Homophilic binding of cadherins leads to a conformational change in the cadherins or a change in physical organization, which leads through catenin to a signal transfer. Cadherins additionally have been shown to

cluster at the cell surface upon activation at cell-cell junctions, also similar to integrins.[112,117]

1.4.3 Spatiotemporal regulation of adhesions

As hinted before, the two forms of adhesion are designated to different kinds of proteins, but are linked to each. They have several things in common, namely the binding to actin filaments, same signaling pathways, their function as mechanical sensors and even some structural components are similar.[118] There is a constant "cross-talk" between integrins and cadherins up- and downregulating each other depending on the conditions.[110,118] The activation of integrins can lead to an upregulation of cadherin expression or activity, activation of cadherin and integrin activation can lead to a common signal in the cell. Additionally, adaptor proteins can induce association between the two adhesion molecules to form a so called adhesive network. Noteworthy, though is that the two adhesion complexes are often spatially separated. To allow for a spatial separation there, evidence suggests to be local downregulation mechanisms in place. It was shown that activation of integrin locally in cancer cells has shown to be able to decrease the cadherin complexes.[119] Also in epithelium remodeling the downregulation of cadherins seems to activate cell-to-matrix adhesion to promote cell migration.[118] It is clear that the crosstalk between these types of adhesion is important for the behavior of the cell. Moreover, the crosstalk helps to transport signals globally over a tissue from cell to cell.[111] This is the reason why the control and dynamics of adhesion are so important.

Cell adhesions have to be temporally and also spatial very finely controlled. Of utmost importance is the control of adhesions in developmental processes like cell differentiation or branching morphogenesis. For example, the integrin mediated activation of Rac and the resulting increase in cadherin expression is necessary for myogenesis. However, this type of activation needs to only happen in a defined number of cells (spatial), at the right time point in development (temporal). Adhesion and signaling of cadherin also have an influence on cell intercalation and cell sorting behaviors in morphogenesis. In branching morphogenesis, which is a crucial step in lung, liver and kidney development, decrease of cadherin expression at the branching site leads to a precisely localized cleft formation.[106,111] Also, in a fully developed organism controlled adhesion is of the utmost importance. Vascular endothelial cells have to withstand considerable amounts of mechanical stress, needing tight adhesion, while red blood cells should not adhere to other cells especially not vascular

endothelial cells, except when building a blood clot in wound healing. If blood clots form at the wrong time and place they can lead to thrombosis, stroke or heart attack.[108] This is one extreme example where the spatiotemporal control of adhesion is of critical importance to an organism. Cancer metastasis is one of the examples of missregulated adhesion. In ovaricarcinoma, for example the expression of cadherins is downregulated, meaning lower cell-cell adhesion forces. This allows the cells to disperse and migrate resulting in metastasis.[111] Deletion of integrin leads in mammary gland cancer to rapid tumor initiation and progression.[107] Overall, these examples give an impression of the importance of spatiotemporal control of adhesions in cell biology and how missregulation can lead to disease.

1.4.4 Adhesion in minimal synthetic cells

The crucial function of cell adhesions in nature makes it clear that in a minimal cell adhesion will be of great importance. On one hand minimal synthetic cells can contribute to the precise understanding of the mechanisms behind cell adhesions and on the other hand are important for building up higher multicellular systems from different minimal synthetic cells. This is why researchers are constantly developing new methods to mimic or control adhesion processes with the needed precision.

Synthetic biology strives for simplistic systems to mimic and control complex cell functions. Vesicle adhesion to a surface or to each other can be driven by the electrostatic interactions of lipids[60,120] and if strong enough can be used to build up large vesicle assemblies[121]. Due to the different charges a negatively charged vesicle adheres to a surface after application of an external potential.[120] This process can be controlled in time, but not in space. Additionally, the needed negative charged vesicles that are necessary do not provide a physiological surrounding.

Lipophilic ligands induce vesicle aggregation. When incorporated in vesicles they form the complexes between the ligands in presence of metal ions leading to fusion of vesicles. The addition of metal ions provides a limited temporal control. Thus, they provide a minimal molecular system to introduce synthetic fusion.[122]

Stereoisomers of phosphatidic acid show different aggregation behavior according to their stereoisomers. They have along hydrophobic tail and can form vesicles similar to natural lipids. They show that vesicles made from (*R,R*) and (*S,S*) isomers undergo fusion while vesicles from (*R,S*) isomers show only fission.[123] This is a perfect example of the simplicity synthetic biology strives for, but offers no precise control over the interaction of the vesicles.

To provide a more physiological way to induce adhesion, a series of natural occurring protein interactions have been used to induce and control adhesion.

Integrin, as one of the best understood adhesion molecules, has been a focus in attempting to reconstitute adhesion in a synthetic cell. For this purpose, integrins have been incorporated into GUVs as active transmembrane receptors (see chapter 1.1.1). Streicher et al. showed that the integrated integrins bind to surfaces coated with RGD, the integrin binding motif.[73] In a later study, they showed that in the presence of activators like Mn^{2+} or DL-Dithiothreitol (DTT) the lateral diffusion coefficient of integrins in the GUVs did not change, whereas when integrins bind to the the ECM protein fibrinogen the coefficient decreases significantly, consistent with the clustering of integrin, as observed in cells.[72] Also the detachment of integrin from fibrinogen has been studied, looking into different peptides to initiate the detachment, helping understand the mechanisms behind integrin.[124] This provides not only a model for adhesion but also allows insights into the workings of the natural adhesion machinery.

Likewise cadherins have been functionally integrated onto lipid droplets and GUVs.[59,125] In these synthetic systems, cadherin can, without connection to the cytoskeleton, still induce adhesion and even fusion of membranes.[125] When GUVs functionalized with cadherins adhere to likewise functionalized supported lipid bilayer (SLB), cadherins cluster at the adhesion sites, again mimicking the observations in cells.[59]

The binding of avidin to biotin (including avidin analogs like neutravidin and streptavidin) has also been used to study the adhesion of GUVs to SLBs. Avidin functionalized GUVs bind to a biotin-functionalized SLB and tethering the vesicle to the SLB inducing vesicle to surface adhesion.[59,126,127] To mimic the effects of the glycocalyx, a polysaccharide rich protective layer occurring around the cell in nature, on adhesion, PEG chains were grafted onto biotin containing SLBs. These PEG chains sterically blocked the adhesion of avidin functionalized GUVs to biotins on the SLB in a concentration dependent manner.[128]

Complementary DNA fragments induce adhesion and fusion of lipid vesicles. Two families of lipid vesicles were modified with cholesterol bound to complementary DNA strands. Upon mixing the two populations the DNA strands form duplexes with each other pulling the vesicles together and leading to fusion. Due to the specificity of the Watson-Crick Base pairing this adhesion and sequential fusion is highly defined.[129,130]

Thanatin, an antimicrobial peptide, binds to bacteria membranes and tethers vesicles together. Mimicking the gram positive and gram negative bacteria membranes with different compositions of lipids allows for thantin to agglomerate these vesicles.[131] Thanatin allows for agglomeration of big amounts of vesicles at once, but does not provide control over the adhesion.

Lectins are another class of proteins that can be used to induce vesicle adhesion either to other vesicles or a surface. Glycan-functionalized GUVs can be crosslinked by adding of lectin. Due to the carbohydrate specificity of different classes of lectin, the interaction between vesicles can be controlled by adding different lectins. This leads to the forming of complex vesicle architectures that show stability against laminar flow.[127]

SNARE (soluble N-ethylmaleimide-sensitive-factor attachment receptor) proteins are the most prominent natural fusion proteins. Not surprising therefore, that they were introduced into vesicles and proved to be a powerful tool to research adhesion event between vesicles and vesicle-ECM.[132]

Light is the perfect trigger to control the adhesion of minimal synthetic cells in space and time as it is observed between natural cells. Towards this end, Kong et al. developed cholesterol with a photocleavable PEG chain in order to control the interactions between liposomes. For demonstration this new cholesterol was incorporated into liposomes functionalized with the SNARE inspired peptides, peptide E and K. Upon UV-light illumination, the nitrobenzyl linker between the PEG chains and the cholesterol was cleaved away and the coiled-coil interactions between peptide E and K induced adhesion between the liposomes and sequential fusion. Longer PEG chains were able to hide the two peptides from the other, while shorter chains could not stop the peptide and subsequent vesicle interactions. In the same study the light-controlled adhesion and fusion of the liposomes was used to spatiotemporally control the transfection of cells.[133]

These synthetic systems show that it is not simple to exactly divide between cell-ECM adhesion and cell-cell adhesion and fusion, as the same or similar systems can be used to mimic these adhesion forms. Where very strong adhesion is implemented or needed (e.g. to overcome the energetic barrier of repulsive forces), uncontrolled fusion can occur instead of adhesion of vesicles. There have been multiple approaches with very different objectives toward this subject, and accordingly many different methods.

Yet, there is still the need for controlled adhesion with a clear differentiation between cell-cell and cell-ECM adhesion.

1.5 Cell motility and its minimal synthetic cell models

A cell function closely related to adhesion is cell motility. In nature motility is involved in similar processes as adhesion such as wound healing, immune response and embryonic and tissue development.[134]

Reconstituting movement into non-living objects has proven to be quite a challenge. Locomotion and taxis of bacteria could be mimicked with nano- or microswimmers.[135] This form of active diffusion can be controlled through external fields such as chemical gradients[135] or magnetic fields[136]. Mammalian cell motility though is much more complex. In mammalian cells the movement of the cells depends on complex cellular machinery including the adhesion complexes and actin-myosin networks that together create traction forces and directed movement.[134]

Mammalian cell motility follows four steps: protrusion forming, adhesion at the leading edge, detachment at the following part and contraction of the cell body.[134]

In the first step cells form membrane protrusions into the direction of movement. They define the leading edge of the cell (Figure 1.5.1). Mimicking such deformations in minimal synthetic cells is possible by a multitude of methods like extrusion[137], optical tweezers[138] and the local and global addition of anchoring polymers that lead to protrusion[139,140]. The incorporation of the cytoskeleton proteins actin and tubulin also leads to deformation of lipid vesicles. Fygenson and coworkers showed that the incorporation of tubulin in GUVs and its temperature-induced polymerization leads to the forming of microtubules and thereof gradual tube formation of the vesicle.[141] This provides an internal stimuli to introduce protrusions in difference to the former named outer stimuli induced shape change. The introduction of cytoskeletal proteins like actin also leads to shape changes and blebbing.[142,143] The amount of the protein and the architecture of the actin network influences how the GUV shape changes[144] but the biggest challenge is to spatially control the deformation of the synthetic cell to create the leading edge.

In another approach, actin has been used as an outer force generator to induce motility and to pull a vesicle from the outside. Liposomes coated with actin polymerization

factors form an actin shell, when surrounded by an actin mesh. Dependent on the membrane curvature, the actin exerts propulsive forces causing the liposome to move through the actin mesh. But in this setup actin is an outer force to propel vesicles and requires a surrounding actin mesh, which does not mirror physiological conditions and gives very limited control over the movement.[139,140]

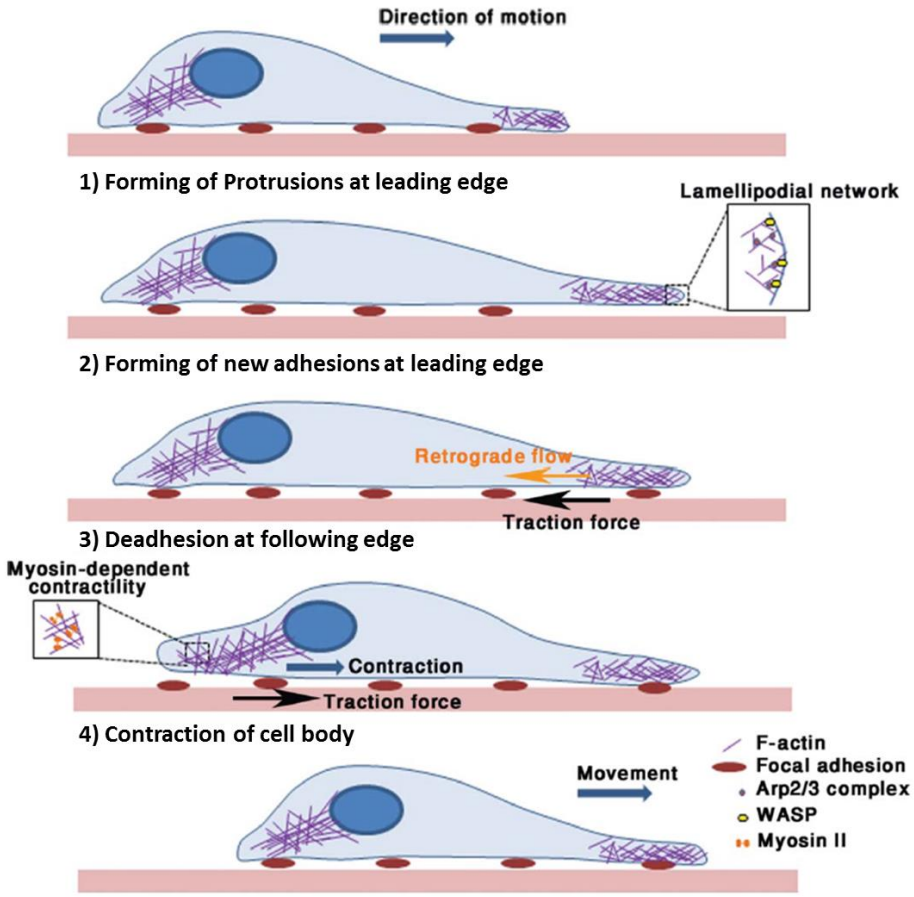

Figure 1.5.1 Schematic of mammalian cell migration. Cell migration is a 4 step process that involves transmembrane proteins as well as the actin-myosin-network: Protrusion forming, adhesion, deadhesion and contraction. This process is very precisely controlled especially in space, as adhesion is asymmetric in migration.[134] Copyright @ 2016 Taylor and Francis. Reprinted with permission from Cell Adhesion and Migration.

In the second step during migration, the cell adheres to the substrate at the leading edge. (Figure 1.5.1 (2)) This is the crucial step as the strength of the adhesion defines if motility occurs and the speed of movement. In the third step, the adhesions at the trailing edge have to disassemble (Figure 1.5.1 (3)). The coordinated interplay of these

two steps leads to an asymmetry in adhesions during motility: stronger and more adhesions form at the front, as weaker adhesions disassemble the back of the cell. In addition, this asymmetry in adhesions is also dynamic as the cell moves forward and is also temporally controlled. Only the coordinated spatiotemporal control of the adhesions leads to directed motility of the cell.[134]

Adhesion of synthetic minimal cells can be formed with different proteins and molecules as explained before (see chapter 1.4.4). Yet, the critical point is that none of these systems offer the spatiotemporal control observed during cell migration and cannot reproduce the dynamic asymmetry of adhesions.

In the last steps of cell motility, myosin contracts, which works against the adhesion. If the adhesion is strong enough the cell will follow the leading edge. If the adhesion is too weak, the contraction of the actin-myosin filaments leads to stalling of movement or even retraction of the protrusion.[145]

Striving to create a model of the contraction, parts of this protein machinery have been introduced into liposomes and GUVs. Even though myosin motors were implemented into GUVs with actin to create an active cytoskeletal vesicle, they show deformation, but no active contraction, as observed in a moving cell. When actin is introduced to GUVs, GUV deformation, filipodia-like protrusion, and oscillatory motion is observed.[146-148] The actin skeleton conformation within the GUV can be controlled through an actin related molecular motor and addition of energy in form of ATP.[149] This research gives insight in the working principles of actin, but does not induce motility of a vesicle.

These four steps are dependent on each other and need to be controlled precisely both spatially and temporally in order to lead to cell migration. In the cell a myriad of proteins are involved in the regulation these steps, like actin regulators for protrusion formation, integrin adaptor and associated signaling proteins for adhesion forming and branching proteins for myosin dependent contractions. This complexity leads to only a partial understanding of how these processes are coordinated and minimal synthetic cells provide a simplified model for these processes. But up to date, there have been no synthetic systems that were able to mimic mammalian cell motility. This is in part because of the low spatiotemporal control that currently have over different steps in cell motility, which are dynamically and asymmetrically taking place in the cell.

1.6 Light as tool to control cell functions

Using light as tool in biological, physical and chemical research is not a new concept. Without the research of Ernst Abbe (physicist, 1840-1905), Carl Zeiss (optician, 1816–1888) and Otto Schott (chemist, 1851-1935) bending light to our needs, microscopy might not be of the foremost importance as it is today. Optical fibers allow us to transfer light and thus images in an endoscope camera or information in telecommunication cables. In chemistry, light can be used as catalyst[150] and in biology it is used to produce energy via photosynthesis.

Light has a lot of advantages over traditional approaches of manipulating biological systems, which predominantly rely on chemical stimuli. First, light gives high spatial control.[151,152] Light can be applied in a defined area of the sample, even at a subcellular resolution under a microscope and the spatial resolution of photoactivation is only limited by the diffraction limit in optical microscopy.

Light also provides high temporal control; it can be turned on at a defined time point of the experiment and the trigger is immediately delivered. Both the spatial and the temporal control are important characteristics to manipulate events in biology where spatiotemporal control is important as detailed for the formation of protein patterns, cell adhesions, and cell migration in sections.[153]

An important asset of light control is also its reversibility, which means that the trigger can be cut off immediately. When coupled to photosensory domains that have the capability to reverse back to the dark state without continuous photostimulation, associated protein interactions are rendered reversible (see chapter 1.6.1).[154] The dynamics of light also make it easy to create patterns of light pulses, modulating the duration of light and dark phases.[155]

Light can be used as a real continuous trigger when kept at the same intensity. Chemical triggers are restricted by diffusion or degradation making the actual concentration of chemical trigger at its intended destination almost impossible to exactly predict and control. To keep any kind of control over such a trigger, it has to be added continuously, which also means disturbing the system continuously. Light provides this control with the addition that it can be shut off practically instantly. Light can be held at the exact same intensity over an experiment. But it can further be applied in different, modulated dosages in terms of power. So, reactions can be varied by changing the intensity to the desire of the researcher.[156]

Additionally, light is a noninvasive trigger as it can be applied remotely without disruption of other processes.[153] In contrast, invasive triggers, such as chemicals, can have unpredictable side effects in the system by interacting with not only the targets but other biomolecules. In addition, as they have to overcome membrane barriers commonly quite radical methods have to be applied to a cell when using such triggers, such as injection or change of membrane permeability. This can lead to a multitude of problems. First as mentioned above, it makes the exact amount of trigger for the target hard to calculate. The interactions can render biomolecules useless through oxidation or reaction with non-target molecules impeding the viability of a cell or impeding the pathway of interest, which can lead to wrong conclusions.[157]

Visible light is not just non-invasive but also biocompatible, meaning that the influence on a living organism is minimal, where as many chemicals put stress on cells impeding their viability.[158] An exception to this is UV radiation, or any high energy radiation, which is known to interact in particular with DNA, inducing changes such as single and double strand breaks. Therefore response to visible light is preferred and will be the focus of further work discussed in this thesis.[159]

Colloquially, “light” is referred to as a single entity, but white light contains distinct wavelengths with different colors. That makes it possible to address and trigger multiple targets at once with different wavelengths. Tools that distinctly react to different parts of the spectrum controlled at the same time, without influencing each other.[160,161] Also, through choosing the system carefully different wavelengths can be used to both simultaneously induce and image a process allowing for simultaneous control and observation.[155]

One major restriction in using light as a trigger can be its penetration depth. When it comes to controlling processes in tissues or when thinking of medical applications, short wavelengths will not be able to penetrate more than a few micrometers below the surface.[162] But there have already been ambitions to get around this limitation by increasing the range of light triggers to near-infrared and radio waves. The longer wavelengths penetrate tissues better as the interaction with the tissue is decreased compared to shorter wavelengths, increasing the penetration depth markedly.[163-165]

Light is a versatile tool and is established as a useful trigger in biology and other research areas. It overcomes many disadvantages of chemical triggers in order to control biological systems and allows for tunable control with high spatiotemporal

resolution opening the door for new approaches on how and when to apply triggers, thereby increasing the scope of research.

1.7 Optogenetic tools

The use of light on a subcellular level to control the function of genetic modified cells is a relatively novel concept, called optogenetics.[166-168] Optogenetics have been exploited to investigate dynamic process in the cell, like signaling pathways and gene regulation[169], to control functions like migration and the action of enzymes[153,167] and has been used as a biological engineering tool.[156,157,160] Optogenetics has been proven to be a powerful tool in the fundamental study of biological systems.[166,168]

These light-dependent protein-protein interactions are known from plants and photosynthetic organisms, where they control vital functions: chloroplast motility, growth regulation and stomatal and leaf opening.[154,170] The photosensory domain of the relevant proteins will undergo conformational changes upon illumination. This is mediated either by a chromophore or through the intrinsic residue tryptophan.[167] The field of optogenetics uses light-dependent protein-protein interactions and conformational changes of proteins to control cell functions with light.[161] In the last years, a number of optogenetic dimers have been developed for the manipulation and control of cell functions. They exploit a different wavelength as well as different dimerization modes, hetero and homodimerization. The most prominent to be named are: The red/farred light responsive heterodimer PhyB-PIF[171] and homodimer Cph1[172], the blue light responsive homodimer Vivid[173] and Cry2olig[174] and the hetrodimers pMag-nMag[175] and Cry2-CIB[176]. In the context of this thesis, the blue light dependent interactions between the iLID (improved light induced dimer) protein and its interaction partners will be discussed.

1.7.1 The iLID system

The iLID protein is based on the LOV2 domain of phototropin 1 from *Avena stativa.* The key for molecular switches to convert a stimulus or trigger into a signal are the sensory domains. The light-oxygen-voltage-sensing (LOV) uses flavin mononucleotide (FMN) as its chromophore converting, making them blue light responsive.[154] The mechanism of the photocycle of the LOV domain has been of great interest, as they gained increasing importance as optogenetic tools and subjected to an improvement process including molecular engineering.[169,177,178]

There are three critical parts in the photoreceptor LOV2 domain: FMN as the chromophore, the LOV2 core protein domain with a conserved cysteine (Cys) and glutamine (Gln) and the so called Jα-Helix, an about 20 amino acid long helix with a conserved pattern of hydrophobic and hydrophilic residues.[154] The mechanism is proposed to work in three steps: the FMN is excited by blue light, which leads to a change from the singlet to the triplet state (Figure 1.6.1A). A covalent bond between the conserved cysteine and FMN is formed, simultaneously breaking the hydrogen bond between FMN C4=O and the conserved Gln. This process occurs within 10 µs (Figure 1.6.1B). The breaking of the hydrogen bond allows the Gln to flip and β-Sheets of the protein to move (Figure 1.6.1B, marked grey), which in turn leads to the first phase of Jα-Helix unwinding (Figure 1.6.1B, marked green). Finally, the helix unfolds completely within 240 µs.[154,170,179] The cysteine-FMN bond stays stable for tens of seconds before it is broken and the protein returns to the ground state.[154]

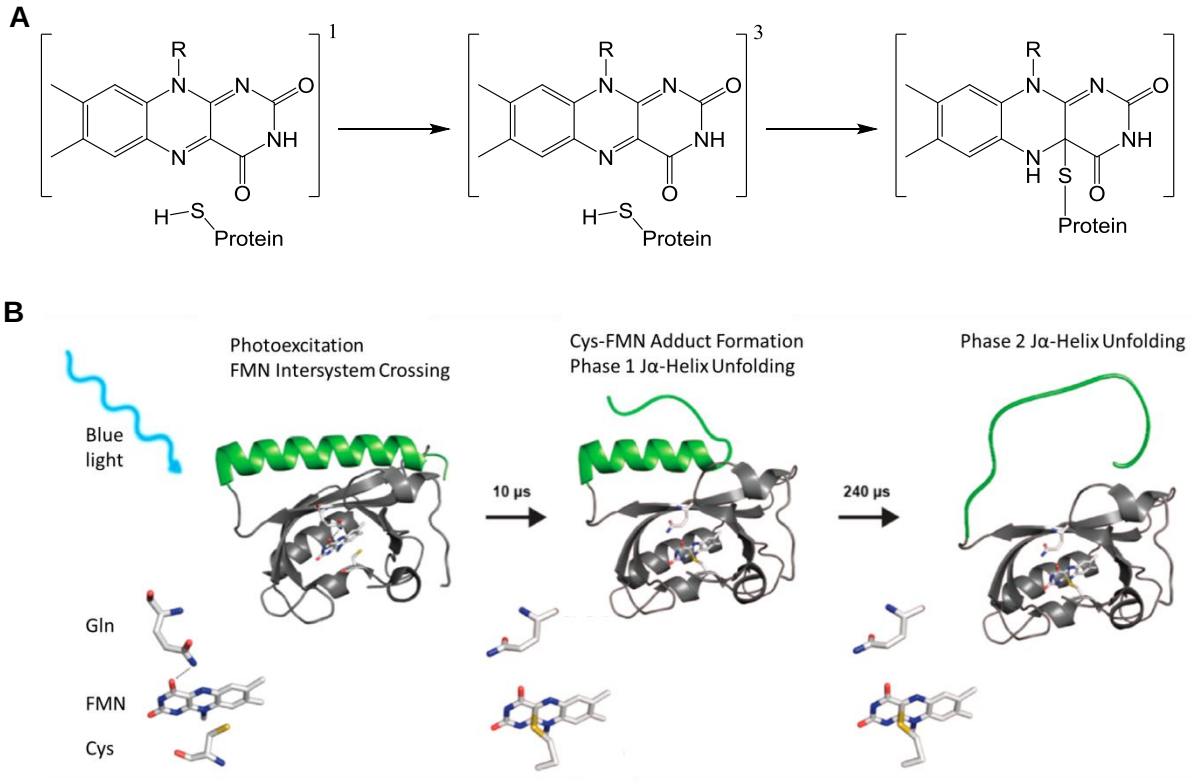

Figure 1.6.1 Three-step mechanism of the LOV2 domain of iLID. A) FMN activation through blue light leads the FMN to change into the triplet state, forming a covalent bond with the cysteine of the LOV2 domain.[170] B) The mechanism of the Jα-helix unwinding (green) upon blue light activation. Through forming of the Cys-FMN bond the hydrogen bridge with Gln is broken which leads to movement of β-Sheets (grey) and unwinding of the helix (green). In the lower part depicts the according states of FMN.[179] Copyright @ 2016 American Chemical Society. Reprinted with permission from The Journal of Physical Chemistry Letters.

To create a LOV2 based dimer a binding domain was hidden in the Jα-helix. The bacterial SsrA peptide was incorporated into the helix and is named light induced dimer (LID). Its binding partner, the peptide SspB, is recruited in a light dependent manner to the SsrA.[177] To expand this system for the use in optogenetics, an improved version of this light induced dimer (iLID) was developed by combining computational design and phage display screening. They found that SspB R73Q as biding partner showed a change in affinity for iLID from 800 nM in light to 47 µM in dark. Therefore, they called the dimer pair iLID-Micro. Another binding partner wild-type SspB showed binding affinities between 130 nM (light) and 4.7 µM (dark), called therefore iLID-Nano. iLID-Micro and iLID-Nano devise molecularly small heterodimerizing systems which associate under blue light within seconds to the unwound Jα-helix and dissociate in the dark again within minutes.[169] Further tuning of this system revealed that the binding partner can be designed to have even broader binding affinities, making it possible to choose the right binding partner for the application. The so called iLID-Milli dimer shows 42-fold change in affinity from blue light (3 µM) to dark (125 µM) by introducing the point mutation A58V into SspB. Moreover, they also showed that a mutation of iLID (N414L) changes the kinetics of the reversion, making the lit state of iLID last longer. This system provides a versatile, reversible protein dimer system that is specific for its interaction partner, can be genetically encoded, and readily usable in multiple organisms.[177,178]

These dimers have already been used for the recruitment and control of proteins within living cells, mainly to and from membranes. One of the interaction partners is attached or incorporated into the cell membrane; the other partner is free to diffuse in the cell, typically fused to a Protein of Interest (POI). Proteins that have been fused to one of the interaction partners can be recruited to the illuminated area, as light gives not only temporal but also spatial control.

This strategy has been used to control multitude of situations: fluorescent proteins fused to Micro in a cell can be recruited to a membrane bound iLID with high precision in a proof of principle.[169,178,180] Of greater interest is to recruit guanine nucleotide exchange factor (GEF) domains to the membrane, which can in turn activate multiple kinases including RhoA, Rac and Cdc42[169,181,182], kinases that play a role in cell migration. Activation of Rac and Cdc42 under spatial control of iLID leads to cell migration towards the illuminated area[182,183], whereas activation of RhoA kinase leads to migration away from the light, as RhoA controls the contractility of actin and myosin.[181] This can be done by either recruitment of an activation factor to the

illuminated area[182,183] or through fusing RAC to a LOV domain rendering it inactive in the dark and after light illumination free to interact with its effector.[184]

The ability to spatially control the protein location is also used in developmental research and to model signaling pathways, e.g. the Erk pathway. To activate the Erk pathway in *Drosophila* Johnson et al. fused Micro to a Rac activator, son-of-sevenless (SOS), which was then recruited to membrane bound iLID, spatially controlling the Erk pathway activation.[153] They could show that within the first four hours of *Drosophila* embryogenesis, ectopic signaling of the Erk pathway, induced through blue light, leads to significant changes in morphology and patterning formation in the embryo. In later developmental phases the importance of the Erk signaling seems to recede as ectopic signaling appears to be buffered. Induced signaling at this late state does not show the morphology changes.[153]

A similar approach was used to investigate the role of phosphatidylinositol-4,5-bisphosphate ($PI(4,5)P_2$) in vesicle tethering and docking in insulin secreting cells. Here Micro was used to recruit a phosphatase to the membrane, which led to a local decrease in $PI(4,5)P_2$ concentration through dephosphorylation. With this system it was proved, that $PI(4,5)P_2$ plays a significant role in vesicle tethering as the removal of $PI(4,5)P_2$ leads to vesicle undocking from the plasma membrane.[185]

The iLID system can act as tool in bioengineering from connecting proteins to compartments. Nitrilase, when fused with multiple iLIDs, can assemble in blue light in the presence of Micro to form multimeres, as the micro is sandwiched between the iLIDs.[186] On a subcellular level it can be used to bring cell compartments together. Shi et al. showed that iLID attached to the outer mitochondrial membrane and Micro attached to the endoplasmic reticulum could tether those compartments together following blue light activation. This provides a completely new way of addressing scientific questions of contact areas between compartments and their influence as signaling interfaces.[157] An engineering approach on the level of the cell showed that these interactions are strong enough to bring microcompartments together. This allows for a defined reversible assembly of cell-like compartments into “prototissues”. Two different populations of polystyrene beads, one functionalized with iLID and one with Nano, build clusters under blue light and disassemble in the dark, allowing the building of synthetic cell contacts and form huge tissue-like assemblies. This system is orthogonal to other blue light switchable systems, and the stoichiometry defines the arrangement ratio.[160]

The iLID dimer has already shown potential as an investigative tool for answering questions that could not be previously addressed due to a lack of control, dynamic or tightness and its further potential remains to be unlocked, especially with the open possibilities of changing the binding affinities easily by changing the binding partner. Moreover, it has been applied as an engineering tool, but not all possibilities have been exploited yet. In synthetic biology it could be applied as controlling unit for metabolism or signaling pathways or to create contacts and information exchange between cells, allowing to make full use of the benefits of light as trigger.

2 Results and Discussion

2.1 Dynamic blue light-switchable protein patterns on giant unilamellar vesicles

Aim

Synthetic biology aims to reduce the complexity of cell functions like protein patterns and introduce new tools that allow one to mimic these functions. Here, the optogenetic protein pair iLID-Nano is established and characterized as a tool to mimic protein patterns and cluster on a lipid vesicle platform. This provides the first visible light-based platform to pattern proteins in a dynamic and spatiotemporal controlled manner under physiological conditions.

Contributions

The recruitment at different wavelengths, all QCM-D measurements and analysis, recruitment to multiple GUVs and the recruitment to differently fluid GUVs was performed by me. The experiments “Proof of principle”, “recruitment to a region of interest” and “recruitment so a single GUV in presence of other GUVs” were performed by me and Elizaveta Chervyachkova in close collaboration in equal measures. Experiments to “recruitment to surfaces”, “reversion” and “laser intensities” were performed by Elizaveta Chervyachkova. Jan Steinkühler helped in questions of GUV formations and patterns. Julia Riecken synthesized the PEG molecules for the surface functionalization. Robert Wienecke synthetized the tris-NTA-Lipids. Rumiana Dimova, Robert Tampé and Seraphine V. Wegner supervised.

Copyright

Abstract

Protein patterns and local protein clustering are essential during many biological processes, such as cell signaling, division, and migration as well as during all stages of tissue formation and development.[82,84] These patterns are highly dynamic and yet precisely regulated in space and time.[80,83,103] It is of great interest to produce such dynamic protein patterns in vitro to understand and control the underlying processes, however our ability to do so is restricted. Classical approaches to pattern molecules, such as lithography, micro-contact printing and chemical vapor deposition require multiple steps, harsh conditions (e.g. UV light, high temperature, non-physiological pH) and chemicals, which are not biocompatible.[90,95,187]

Introduction

Light responsive approaches to protein patterning are particularly promising as visible light provides the desired high spatiotemporal control and is biorthogonal (see chapter 1.3). Visible and near infra-red light has been used to photopattern proteins by locally heating the thermoresposive polymer poly(N-isopropylacrylamid)[95] or decomposing ruthenium complexes with upconverting nanoparticles.[96] Subsequently, the changes in surface chemistry allow proteins to unspecifically adsorb on the substrates following the photopattern. In these approaches all proteins in solution absorb indiscriminately and the protein integrity is not assured. Photocleavable nitrobenzyl caging groups are useful to photopattern proteins through specific interactions. Nitrobenzyl groups have been used to control the interaction between Ni^{2+}-NTA (N-nitrilotriacetic acid) groups and His-tagged proteins[100,102], biotin and streptavidin[98] as well as glutathione and glutathione S-transferase.[93] In particular, photocaged lipids allow recruiting proteins with high spatial and temporal control to phospholipid membranes, which are important cell models to study protein function. [90,104] Yet, the decaging of nitrobenzyl groups is irreversible, which does not allow to alter protein patterns dynamically and requires cytotoxic UV light.[188] Reversible protein photopatterns can only be produced with azobenzenes, which change surface properties when they undergo *cis-trans* isomerization.[89,91] However, the unspecificity of the protein interaction, the requirement of UV light for the *trans* to *cis* isomerization, and in particular the photodynamic equilibrium limit this approach. Overall, there is still a need for a highly specific, biocompatible, and reversible way to pattern proteins with the desired spatiotemporal control that operates in the presence of other biomolecules under physiological conditions. To achieve this goal, we suggest using photoswitchable protein heterodimers recently developed in the field of optogenetics. In particular, we utilized the

proteins iLID (improved light-inducible dimer, based on the photoswitchable LOV2 domain from *Avena sativa*) and Nano (wild-type SspB), which specifically interact with each other under blue light (488 nm) and dissociate from each other in the dark. These proteins have been used to reversibly control various processes in live cells.[169,177]

In this study, we anchor purified iLID to the outer membrane of giant GUVs (giant unilamellar vesicles) and recruit proteins fused to Nano to the outer GUV membrane in situ with blue light (Figure 2.1.1A). Since the binding of Nano to iLID is reversible in the dark, we will be able to form reversible and dynamic protein patterns with precise control in space and time. The high specificity of the iLID-Nano interaction and the response to blue light will allow patterning a specific protein in the presence of other biomolecules including lipids and without damaging them.

Results and Discussion

To demonstrate this concept, we immobilized His-tagged iLID on GUVs with Ni^{2+}-NTA groups on their surface (lipid composition: POPC with 10 mol% POPG + 0.1 mol% DGS-NTA-Ni^{2+} + 1 mol% DiD dye). When we transferred these GUVs into a solution of Nano-mOrange (orange fluorescent protein fused to Nano), upon blue light illumination over 15 min we could observe a gradual increase in mOrange fluorescence on the GUV membrane (Figure 2.1.1B). We quantified this increase by comparing the fluorescence intensity on the membrane before and after illumination (Figure 2.1.1C). Subsequently, when we placed the GUVs in the dark, the fluorescence intensity at the membrane decreased, proving that the recruitment of the Nano-mOrange is reversible. In the dark after 15 min approximately 70% and after 30 min approximately 95% of the recruited Nano-mOrange had dissociated from the iLID-decorated GUVs (Figure 2.1.1D). Additionally, Nano-mOrange can be recruited to the GUVs multiple times. After renewed blue light illumination for 15 min, the fluorescence at the GUV membrane reached the same level as after the first blue light illumination. Hence, the photoswitchable interaction between iLID and Nano can be used to reversibly and repeatedly recruit proteins fused to Nano onto an iLID-decorated GUV. This interaction can in principle also be used to pattern on different types of surfaces. As an example, we have immobilized iLID on glass surfaces coated with Ni^{2+}-NTA terminated PEG (polyethylene glycol) chains. Also in these samples we observed more Nano-mOrange recruitment to the surface under blue light illumination than in the dark (Figure 2.1.2).

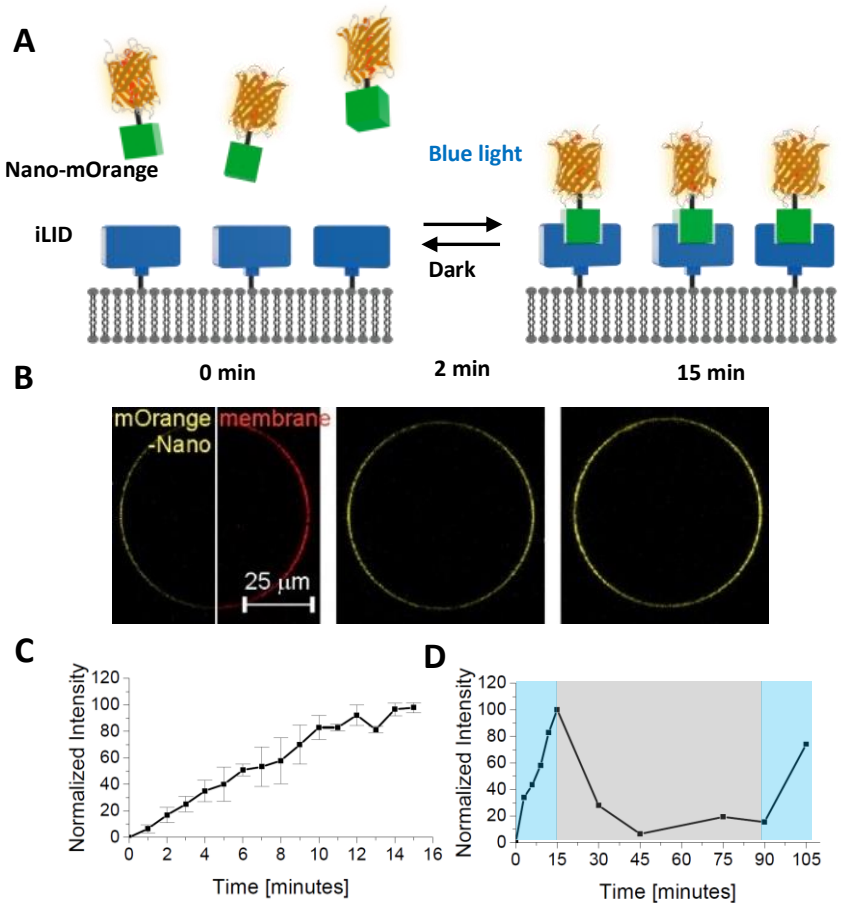

Figure 2.1.1 Proof of principle. A) Schematic representation of Nano-mOrange recruitment to iLID-functionalized lipid bilayer under blue light but not in the dark. B) Fluorescence images of iLID-decorated GUVs (red) in the presence of Nano-mOrange (yellow) under blue light illumination (5% laser power: 575.5 ± 21 nW, 488 nm). C) Nano-mOrange recruitment to GUV membrane under blue light. Error bars show the standard deviation from 3 independent experiments. D) Change in fluorescence intensity under blue light (coloured in blue) and in the dark (coloured in grey).

The amount of the protein that recruits to a membrane is one of the key parameters to control protein activity. Using the iLID-Nano interaction, we can easily adjust how much protein recruits to the GUV through the intensity of the blue light (Argon laser, 488 nm). Already light powers as low as 70 nW through a 63x water objective, which corresponds to 1% of the laser power, are sufficient to partially activate iLID and recruit Nano-mOrange to the membrane (Figure 2.1.3A). Higher light powers up to 6.3 µW (20% laser power) increased both the rate and the amount of protein recruitment. Further, intensity increase led to no additional recruitment. This can either be due to the full activation of iLID achieving the photostationary state or the bleaching of the fluorescent protein.

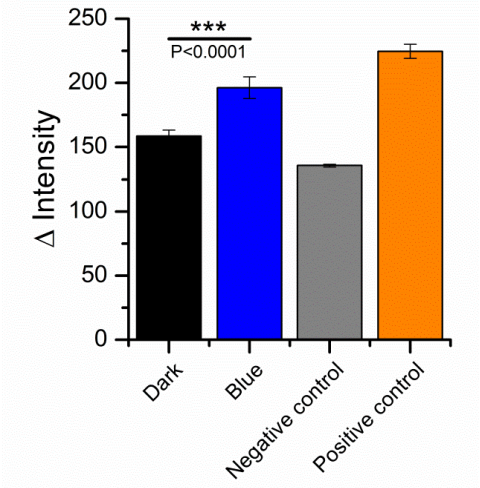

Figure 2.1.2 Protein recruitment to iLID immobilized Ni^{2+}-NTA PEG functionalized glass surfaces under blue light and in the dark. Surfaces without immobilized iLID incubated with Nano-mOrange and Nano-mOrange with a His6-tag were used as negative and positive controls, respectively. A non-parametric Mann-Whitney test was performed to analyse the statistical difference. The error bars are the standard error from 3 technical replicates.

We also investigated if the iLID-Nano interaction is selectively induced exclusively under blue light and not with light of different wavelengths. In the absence of blue light illumination, we observed that Nano-mOrange is not recruited to the iLID-modified GUV membrane (Figure 2.1.3B). During our experiments, we excited mOrange with green light (561 nm) for fluorescence imaging, and prepared the samples under red light (633 nm) (labelled as dark). Similarly, far-red (750 nm) light illumination fails to induce Nano-mOrange recruitment to the membrane.

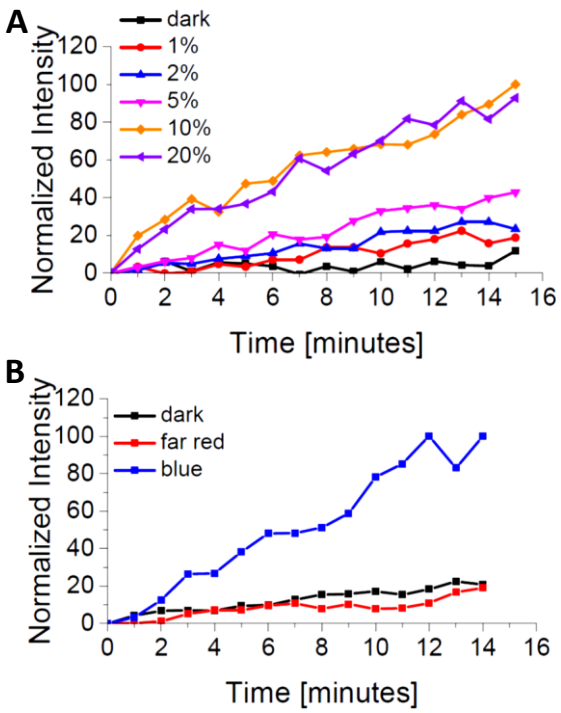

Figure 2.1.3 Nano-mOrange recruitment to iLID-functionalized GUVs depending on A) the blue light intensity and B) the illumination wavelengths.

The lack of protein recruitment in the absence of blue light illumination, despite the use of green, red and far-red light, confirms the selectivity for blue light. The orthogonality to other wavelengths allows combining the iLID-Nano protein interactions with red light-dependent protein interactions to specifically pattern two different proteins, as it has been achieved in optogenetic studies.[176,189]

We further quantified the changes in kinetic and thermodynamic parameters for immobilized iLID and Nano under blue light and in the dark. The reasons to utilize the QCM-D (Quartz Crystal Microbalance with Dissipation Monitoring) for these measurements are twofold. First, QCM-D allows to measure protein surface interactions with high sensitivity in real time. Second, it is a non-spectral technique, so that the measuring process does not interfere with the light sensitive proteins and allows performing the measurements in either complete darkness or under blue light. For the measurements we immobilized His-tagged iLID on supported lipid bilayers (SLB) (lipid composition: DOPC + 5 mol% DGS-NTA) and subsequently titrated increasing concentrations of Nano on these surfaces under blue light or in the dark (Figure 2.1.4).

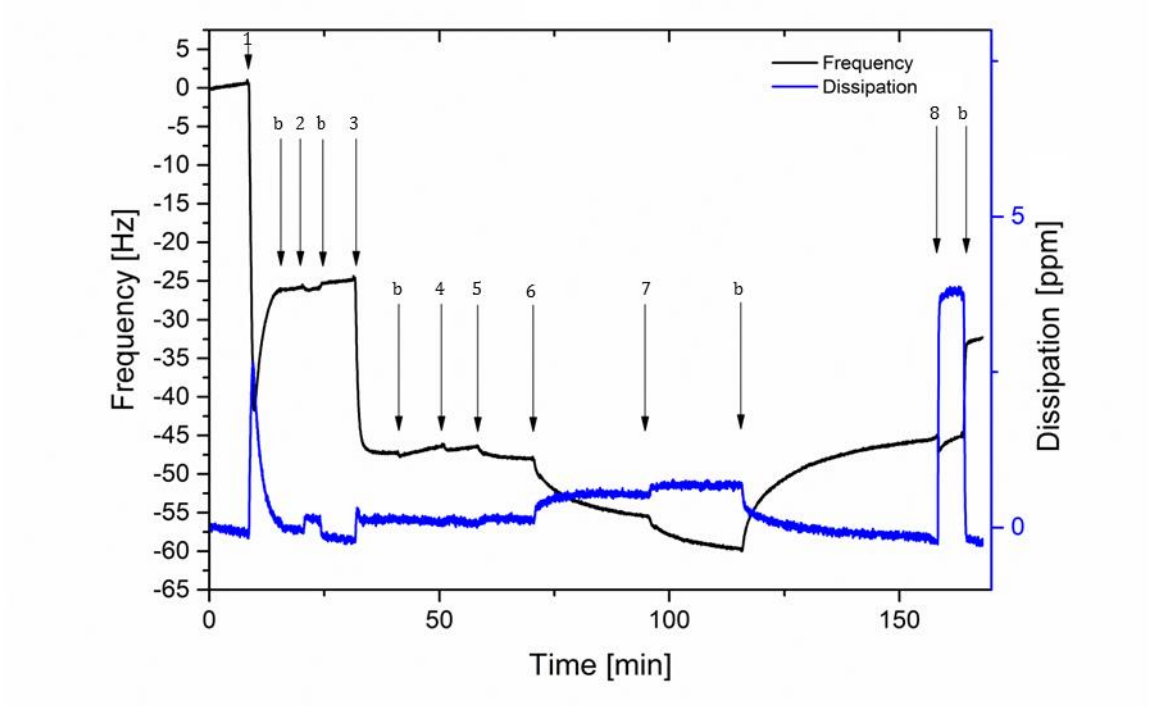

Figure 2.1.4 Exemplary changes of frequency and dissipation (7th overtone) in a QCM-D measurement. Arrows indicate the start of addition of the following components in buffer (150 mM NaCl, 10 mM Tris, pH 7.4). 1) 10 mg/mL Lipids (DOPC + 5 mol% DGS-NTA) with 5 mM $CaCl_2$, 2) 10 mM $NiCl_2$, 3) 1 µM iLID, 4) 250 nM Nano, 5) 500 nM Nano, 6) 1 µM Nano, 7) 2 µM of Nano, 8) 250 mM imidazole. b indicates washing steps with buffer.

From decrease in frequency, which is proportional to the amount of protein bound to the surface, it is evident that Nano binds to immobilized iLID better under blue light than in the dark. For example, already at 500 nM Nano efficiently binds to iLID under blue light but there is very little binding at the same concentration in the dark. Yet, it should be noted that the two proteins interact under both conditions. We modelled the QCM-D data to obtain the thickness of the adsorbed protein layer and to calculate K_d (dissociation constant) as well as k_{on} and k_{off} (association and dissociation rate constant, respectively) under blue light and in the dark (Table 2.1.1, Figure 2.1.5).

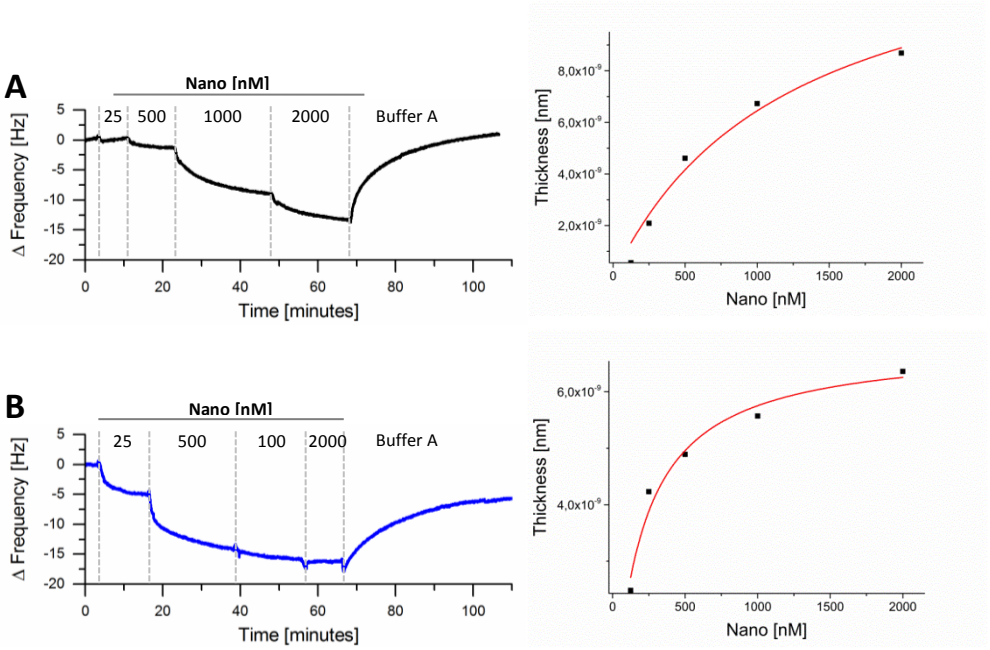

Figure 2.1.5 Thermodynamic study of the iLID-Nano interaction A) in the dark and B) under the blue light using QCM-D. Increasing concentrations of Nano are binding to an iLID-functionalized supported lipid bilayer shown by decreasing frequency. From the fit of the concentrations to the layer thickness the thermodynamic and kinetic constants can be calculated.

Table 2.1.1 Thermodynamic and kinetic constants of the iLID-Nano system.

Constants	Blue light	Dark
K_d [µM]	0.28 ± 0.14	1.20 ± 0.40
k_{off} [min^{-1}]	$5.4 \times 10^{-2} \pm 0.8 \times 10^{-2}$	$11.0 \times 10^{-2} \pm 5.0 \times 10^{-2}$
k_{on} [$\mu M^{-1}s^{-1}$]	$3.3 \times 10^{-3} \pm 0.8 \times 10^{-3}$	$1.6 \times 10^{-3} \pm 0.7 \times 10^{-3}$

From the modelling we derived the K_d values for the interaction of Nano with immobilized iLID to be 280 nM under blue light and 1.2 µM in dark (Table 2.1.1). This equals more than 4-fold difference in binding affinity between the active state and the dark. In the literature the affinity between the two proteins in solution changes from 132 nM under blue light to 4.7 µM in the dark, which is a 36-fold change.[169] This shows, that the immobilization of iLID on a lipid membrane significantly influences the light dependent change in affinity to Nano. Investigating the recruitment of Nano-mOrange to GUVs with different lipid composition (DOPC vs. POPC) and fluidity (POPC + 20-40 mol% cholesterol), we observe that these parameters do not affect Nano-mOrange binding under blue light (Figure 2.1.6). Hence, we propose that the steric hindrance imposed by the immobilization of iLID results in a lower change in affinity from the dark to the lit state.

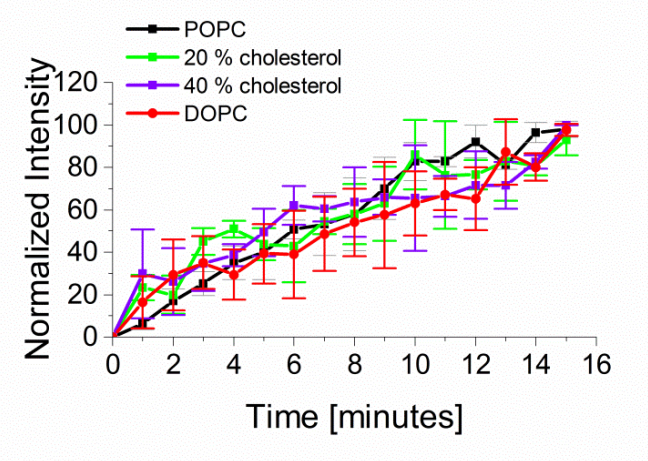

Figure 2.1.6 Protein recruitment to GUVs with different lipid composition and membrane fluidity. POPC-GUVs (used in all other the protein recruitment experiments to GUVs) are shown in black, POPC-GUVs with additional 20 mol% cholesterol are shown in green, POPC-GUVs with additional 40 mol% cholesterol are shown in purple and DOPC-GUVs are shown in red. All GUVs contain 0.1 mol% DGS-NTA to immobilize iLID on the GUVs. The error bars show standard deviation from 3 different experiments.

As in many optogenetic studies one interaction partner is localized to a membrane this effect is of major importance.[169,176] The k_{off} can be computed from the washing off of Nano from the surface in the QCM-D measurements. The calculated k_{off} values are 5.4 x 10^{-2} min^{-1} (half-life 12.8 min) and 11.0 x 10^{-2} min^{-1} (half-life 6.3 min) under blue light and in the dark, respectively (Table 2.1.1). The dynamic range of the protein unbinding is on the order of minutes to hours, which is in agreement with our findings of enrichment and depletion of proteins to the GUV membrane (Figure 2.1.1C-D). Also in literature, the interaction between iLID and Nano is reported to reverse within minutes in optogenetic

studies.[169] The affinity range of nano- to micromolar and the time range of minutes, which the iLID-Nano interaction can cover to form dynamic protein patterns, are highly relevant to the affinity and time scale observed for protein patterns in nature.[190,191]

We sought to use the high spatiotemporal control that the iLID-Nano interaction provides to locally control protein enrichment on a GUV membrane. Towards this end, we illuminated a small region of interest (ROI) on one side of an iLID-decorated GUV, while continuously imaging to observe Nano-mOrange recruitment (Figure 2.1.7A). Despite the high fluidity of the lipid membrane, the fluorescence intensity increases locally in the ROI (Figure 2.1.7B). For a more quantitative analysis, we compared the local fluorescence increase in the ROI to the mirrored area on the other side of the GUV. The illuminated ROI showed consistently higher fluorescence intensity compared to the area on the opposite side of the GUV (Figure 2.1.7C). The local illumination overt time led to gradual increase in fluorescence over the whole GUV. The high lipid membrane fluidity leads to diffusion of the recruited protein from the ROI at one pole of the GUV and allows forming transient protein gradients on the GUV. Presumably, fixed patterns can be achieved on membranes in the gel phase where diffusion is hindered, but the biological relevance of gel-phase membranes is limited.

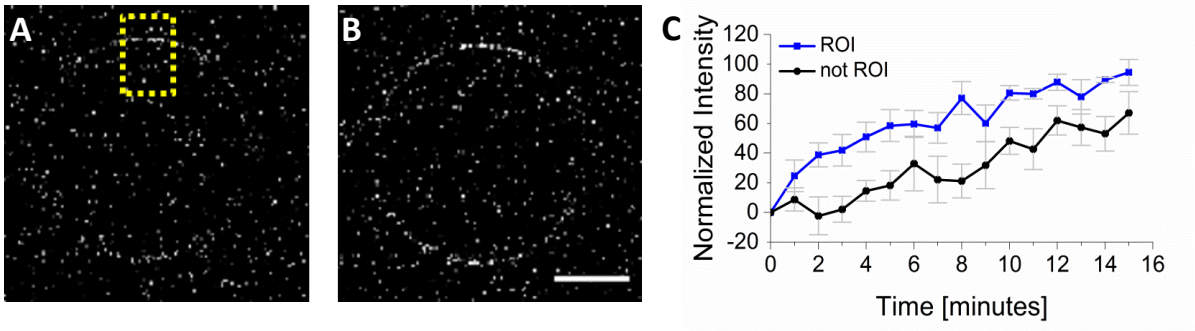

Figure 2.1.7 Local recruitment of Nano-mOrange to a ROI on a single GUV. Fluorescence images of iLID-decorated GUVs in the presence of Nano-mOrange A) before and B) after local illumination with blue light (488 nm Argon Laser, 15 min) at the ROI (yellow rectangle). Scale bar is 15 µm. C) Normalized intensity vs the time shows that in the illuminated RO the fluorescence is constantly higher, while in both areas the illumination increasesover time.

We also are able to spatially control the recruitment of proteins to one specific GUV in the presence of another. To achieve this, we have locally illuminated only one iLID-decorated GUV with blue light in the presence of another GUV (Figure 2.1.8A-B). Indeed, we observe recruitment of Nano-mOrange just to the illuminated GUV but not the other.

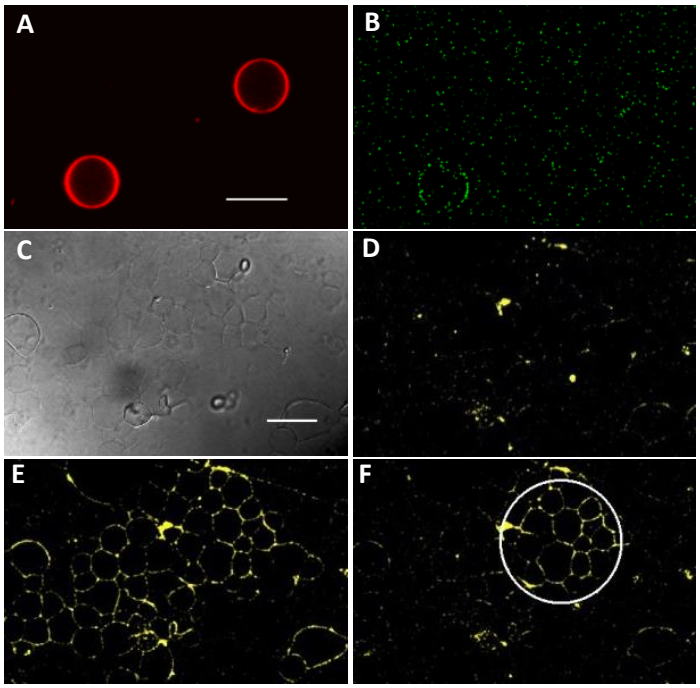

Figure 2.1.8 Selective GUV activation. A) Fluorescent image of two GUVs. Scale bar 25 µm. B) Local Nano-mOrange recruitment to a single GUV by local blue light illumination. (C-F) Patterning of Nano-mOrange on an iLID-functionalized GUV carpet. C) DIC image of the immobilized GUVs. Fluorescence images of the GUV carpet D) in the dark, E) fully activated with blue light and F) locally activated in a ROI with blue light (488 nm) for 1 min. The circle approximately indicates the irradiated region. Scale bar 25 µm.

During tissue formation, protein patterns emerge over many cells and we would like to mimic this by recruiting proteins at the scale of multiple GUVs.[192] As a tissue-like substrate, we created a carpet of GUVs (lipid composition: POPC + 10 mol% POGP + 1 mol% trisNTA-Suc-DODA[193]) on a PVA (polyvinyl alcohol) substrate so that the GUVs remained supported by it (Figure 2.1.8C-D). As in previous results, we could recruit Nano-mOrange to a whole carpet of GUVs under blue light illumination within minutes (Figure 2.1.8E) and reverse it (Figure 2.1.9).

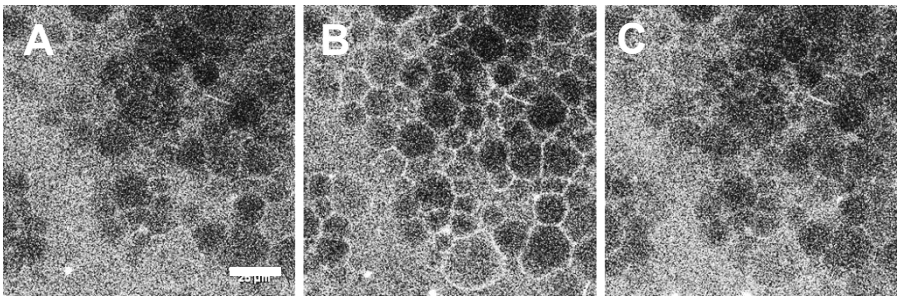

Figure 2.1.9 Reversibility of patterns. GUV carpet A) before illumination, B) after blue light illumination for ca. 1 s and C) after approximately 3 minutes in the dark. Scale bar is 25 µm.

By only illuminating a ROI on the GUV carpet, we locally recruited Nano-mOrange onto multiple GUVs (Figure 2.1.8F). Interestingly, the membrane fluidity also leads to protein recruitment to connected membranes of neighboring GUVs.

Additionally, we demonstrate that depending on the size of the ROI, the protein recruitment can range from a few to many GUVs (Figure 2.1.10).

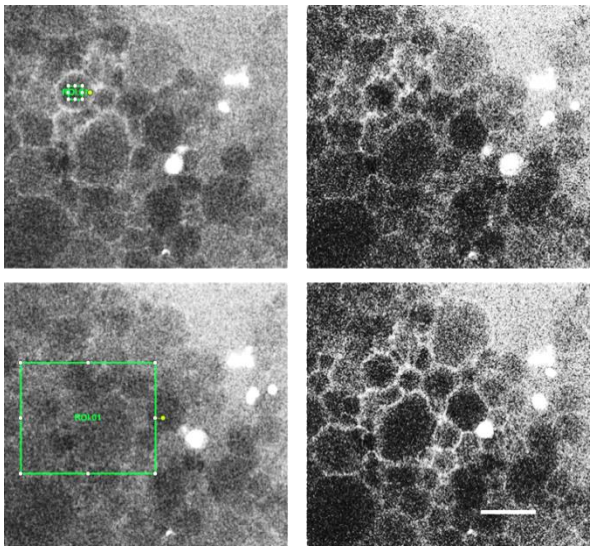

Figure 2.1.10 Illumination of regions of interest in different sizes on a GUV carpet. Left panel indicates the area and size of illuminated region. Right panel shows the respective area with Nano-mOrange recruited to the GUV membrane. The scale bar is 25 µm.

Overall, it is possible to sequentially pattern proteins and to dynamically reverse these patterns according to the needs with great flexibility in size and shape.

Conclusion

In summary, the photoswitchable interaction between iLID and Nano can be used to photopattern proteins of interest with blue light. Unlike existing protein patterning methods, the iLID-Nano interaction is reversible and dynamic, non-invasive, operates under physiological conditions and is very specific, which allows using it in complex environments with multiple biomolecules. Most importantly, the protein patterns can be formed with high spatial and temporal resolution in affinity and time scales relevant to biology. The detailed characterization of thermodynamic and kinetic parameters for iLID-Nano provides insight into the protein interaction, reversion and pattern dynamics. In this study we broaden the application of iLID and Nano from optogenetics, where they are

used to control intracellular processes, to photopattern proteins on materials. Here, we have focused on protein recruitment onto lipid bilayers as they mimic the physiological surrounding proteins operate in. However, this is not limited to lipid interphases and extendable to any substrate functionalized with Ni^{2+}-NTA to immobilize the His-tagged iLID and to any protein of interest fused to Nano. This patterning approach is also scalable from subcellular to the level of a single GUV and a GUV carpet providing exceptionally versatility. As the protein pair iLID-Nano only responds to blue light, it would be possible to combine it with other light responsive interactions to simultaneously pattern multiple proteins with high complexity and yet exquisite control.[169,176,177,189]

2.2 Light guided motility of a minimal synthetic cell

Aim

To increase the scope of processes mimicked in synthetic biology, this study focuses on inducing light guided motility of a lipid vesicle. After confirming that the iLID-Micro protein pair can induce precisely controlled dynamic adhesion this protein dimer was used to guide the vesicle over a two dimensional surface with light. Therefore, the iLID-Micro pair is a versatile tool and for the first time a system provides a tool to guide a vesicle by light freely over a surface.

Contributions

I performed all GUV experiments including the analysis of the cell motility and all QCM-D experiments with analysis. Jan Steinkühler analyzed the adhesion energy and performed the time-adhesion area analysis. Rumiana Dimova and Seraphine V. Wegner supervised the work.

Copyright

Abstract

Cell motility is an important but complex process; as cells move new adhesions form at the front and adhesions disassemble at the back. To replicate this dynamic and spatiotemporally controlled asymmetry of adhesions and achieve motility in a minimal synthetic cell, we controlled the adhesion of a model giant unilamellar vesicle (GUV) to the substrate with light. For this purpose, we immobilized the proteins iLID and Micro, which interact under blue light and dissociate from each other in the dark, on a substrate and a GUV, respectively. Under blue light the protein interaction leads to adhesion of the vesicle to the substrate, which is reversible in the dark. The high spatiotemporal control provided by light, allowed partly illuminating the GUV and generating an asymmetry in adhesions. Consequently, the GUV moves into the illuminated area, a process that can be repeated over multiple cycles. Thus, our system reproduces the dynamic spatiotemporal distribution of adhesions and establishes mimetic motility of a synthetic cell.

Introduction

Motility is a key feature of living cells and is at the core of complex life processes including immune response, development and the progression of diseases.[145] Mammalian cell motility on a 2D substrate is a complex multistep event, which requires 4 synchronized steps: (1) formation of membrane protrusions, (2) new adhesions to the substrate at the leading edge, (3) contraction of cell body and (4) detachment at the trailing edge (see chapter 1.5).[134] To orchestrate these processes the cell relies on complex molecular machinery including the actin cytoskeleton to form protrusions, integrins, which mediate adhesion to the substrate, myosin-dependent contractions and a multitude of other regulatory proteins to coordinate different steps. In a moving cell the symmetry between the back and the front is broken and different events, which span different time and length scales, have to be spatiotemporally controlled and synchronized, which adds another layer of complexity (Figure 2.2.1A).

To understand the underlying complexity of cell motility, minimal synthetic cells provide simplified models and give mechanistic insight into how different machinery contributes to the process.[194] Towards this goal different machinery required for cell motility to form cell protrusions, contraction and adhesion have been introduced in GUVs (giant unilamellar vesicles), which are frequently used as a cell-like compartment.[58] In GUVs the polymerization of actin in the presence of motor proteins leads to the deformation of the vesicle, formation of membrane protrusions and oscillatory motion of the

vesicles.[139,148] Adding myosin and coupling the actomyosin network to the membrane generates tension and results in symmetry breaking during the contraction of the network but does not lead to GUV movement. Furthermore, the cell adhesion receptor, integrin, has been functionally incorporated into GUVs and can prompt adhesion to substrates functionalized with the adhesion peptide RGD and extracellular matrix proteins.[72,73,124,195,196] Likewise, other interactions such as biotin-streptavidin[197], E-cadherin[59], lectin-sugar[127] and electrostatic interactions[120,198] were used to understand GUV adhesion to substrates. Despite all these studies, which provide great molecular insight into key players in cell motility, none of them have achieved the ultimate goal of replicating cell motility.

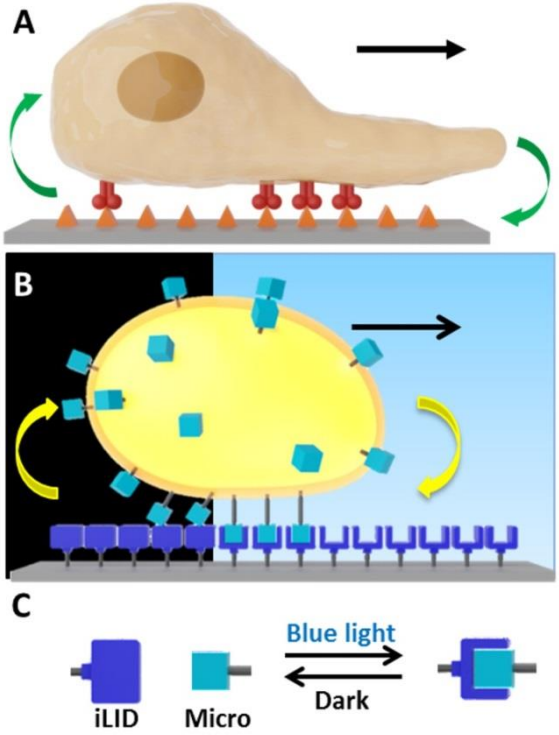

Figure 2.2.1 Cell vs. GUV motility. A) Simplified scheme of cell motility. Cell motility requires new adhesions to form at the leading edge, whereas adhesions have to disassemble at the trailing edge for the cell to move forward. The adhesion receptor integrin, is shown in red and the adhesion motif on the substrate in orange. B) The light-controlled adhesion of a GUV allows to spatiotemporally control adhesions by partially illuminating the GUV. This mimics the dynamic asymmetry of adhesions in a minimal synthetic cell and leads to movement of the GUV. C) The proteins iLID and Micro interact under blue light and dissociate in the dark.

Part of the challenge in mimicking cell motility in a minimal synthetic cell is that in a migrating cell there is an asymmetry in terms of adhesion between the leading and the trailing edge. More and new adhesions form at the front to generate high traction forces

coupled to the actin network and adhesions at the back, which disassemble enabling the detachment and retraction of the cell rear. Overall this asymmetry in adhesions is dynamically maintained and results in a directional cell movement. Replicating this dynamic spatiotemporal distribution of adhesions in a minimal synthetic cell requires a trigger that induces asymmetry in adhesions between the front and rear of a GUV and hinders the system to reach an equilibrium state. Such a trigger must provide spatial control at the sub GUV scale (typical diameter ca. 20 µm) and temporal control at a time scale that is relevant for a migrating cell (typical speed between 0.1 to 4 µm/min[199]). In addition, like in a cell, these triggered adhesions must be reversible and have matching formation and reversion kinetics so that the trailing edge can detach as new adhesion are formed in the front. Current synthetic cell models based on integrins and synthetic interactions neither provide such spatiotemporal control nor the required reversibility and dynamics.

Results and Discussion

To reproduce cell motility in a minimal synthetic cell and create dynamic asymmetry in adhesions, we established reversible GUV adhesions with high spatiotemporal control and matching on/off dynamics. For this aim, we propose to control the adhesion of GUVs to a substrate with visible light by using photoswitchable protein interactions as adhesion mediators (Figure 2.2.1B). Photoswitchable proteins provide reversible remote control at µm spatial resolution and down to second timescales with visible light.[178,200] Some photoswitchable protein interactions have already been used to control the interactions of mammalian and bacterial cells with substrates using light.[156,201] A critical parameter in selecting the photoswitchable protein interaction is that it has comparable on and off switching dynamics, so that the front and the rear of the GUV move at the same speed. In particular, we picked the photoswitchable protein iLID (improved light induced dimer protein, based on the LOV2 domain), which binds to the protein Micro under blue light and dissociates from it in the dark (Figure 2.2.1C).[169] Our choice for this couple is based on the fact that interaction between iLID and Micro reverses quickly in the dark within seconds to minutes, which matches the fast photoactivation with blue light. Other photoswitchable protein interactions like those between the PhyB and PIF6 under red light as well as CRY2 and CIBN or nMagHigh and pMagHigh under blue light activate much faster with light than they reverse in the dark.[156,201] The rapid deactivation of the PhyB/PIF interaction is possible with far-red light but is technically more complex as it would require the co-illumination with a second far-red light source.

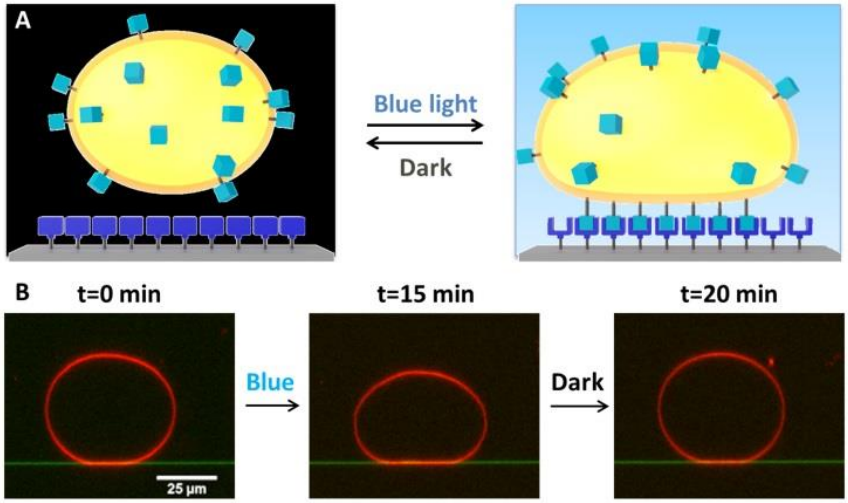

Figure 2.2.2 Light-dependent adhesion of a GUV to a substrate. A) Light-dependent adhesion of a GUV decorated with Micro to a substrate functionalized with iLID. Upon light illumination the GUV adheres to the substrate and detaches in the dark. B) Fluorescence microscopy images of a GUV over a time line being illuminated with blue light for 15 min adhered (compare first and second image). After further 5 min in the dark the GUV detached (last image). Micrographs represent (x,z) side-views. Red channel is membrane dye and green channel is the reflection of the 561 nm laser at the glass-water interface.

As the first step to establish photoswitchable adhesions, we immobilized His-tagged iLID as the adhesion ligand onto a polyethylene glycol (PEG) coated glass substrate with Ni^{2+}-NTA end groups (Ni^{2+}-NTA end groups ca. 40 pmol/cm^2)[202] through the His-tag-Ni^{2+}-NTA interaction and His-tagged Micro as the adhesion receptor onto deflated GUVs (POPC + 10 mol% POPG + 0.1 mol% DGS-Ni^{2+}-NTA, Ni^{2+}-NTA end groups ca. 0.25 pmol/cm^2) including a lipid with a Ni^{2+}-NTA head group (Figure 2.2.2A). The GUVs were osmotically deflated by partially evaporating the outer buffer. Deflation leads to excess membrane allowing for membrane fluctuations and various vesicle morphologies including spherical-cap-like adhering states.[203] In addition, the GUVs were loaded with a solution (100 mM sucrose) of higher density compared to that of their surrounding so that they sunk onto the substrate. The vesicles were labelled with a red-shifted fluorescent dye (1,1'-Dioctadecyl-3,3,3',3'-tetramethylindodicarbocyanine) to observe them with confocal microscopy in x,z direction without activating the photoswitchable protein interaction. In the dark, Micro-functionalized GUVs settled on the iLID functionalized substrate but did not exhibit significant adhesion, i.e., the GUVs were free to displace by diffusion and convection and the weak membrane-substrate interactions were also witnessed by thermal membrane undulations in the vicinity of the substrate (Figure 2.2.2B, t=0 min). Only upon activation of the iLID-Micro interaction with blue light (Laser

at 488 nm), the GUVs adhered strongly to the substrate, as observed from the deformation of the GUV expressed in an increase in adhesion area and suppression of optically resolvable membrane fluctuations in the adhesion segment (Figure 2.2.1B, t=15 min, Figure 2.2.3).

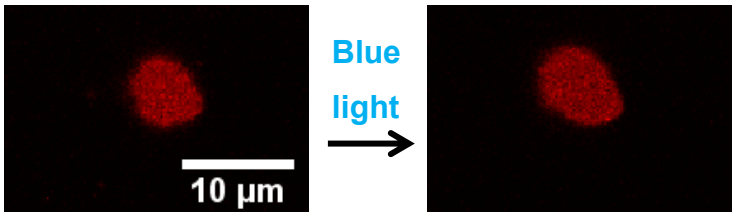

Figure 2.2.3 Adhesion area increase of a GUV after 10 min irradiation with blue light. Adhesion area was detected from x,y-scans at the surface of the substrate. A clear increase in adhesion area was visible upon blue light illumination.

This adhesion was reversible in the dark. After turning off the blue light, the adhesion area decreased approximately to the initial dark state (Figure 2.2.2B, t=20 min). The adhesion of the GUVs could be turned on and off repeatedly over 4 blue light/dark cycles (Figure 2.2.4).

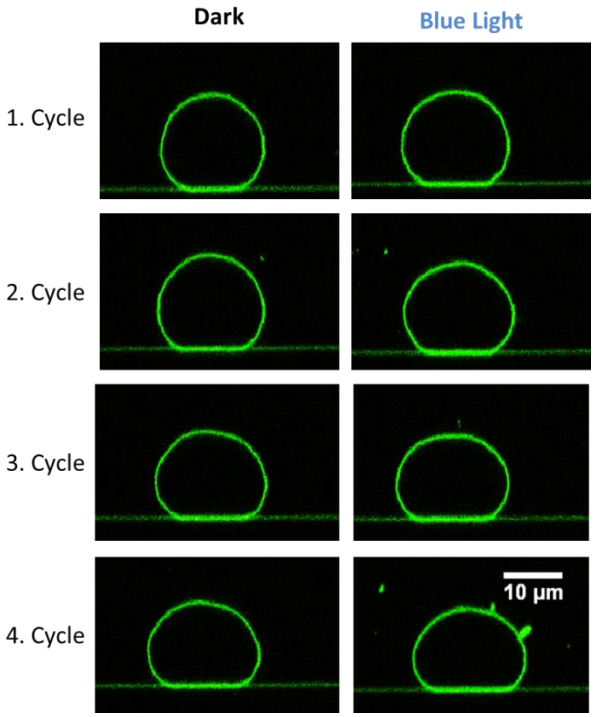

Figure 2.2.4 Adhesion of a GUV over multiple dark/blue light cycles. Images of the GUV were acquired in the x,z plane after each 5 min. period in the dark and 5 min. under blue light over 4 cycles. The adhesion site of the GUV increased after each blue light exposure and decreased each time illumination with blue light was stopped.

Additional control experiments showed that the GUVs do not adhere to the iLID-functionalized substrate in the dark over time or if the GUVs were not functionalized with Micro (Figure 2.2.5).

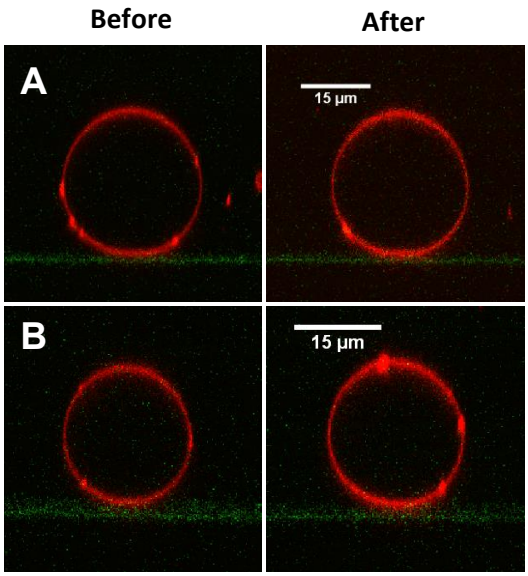

Figure 2.2.5 Negative controls of adhesion. Images of the GUV were acquired in the x,z plane. (A) iLID-functionalized substrate (green) with Micro functionalized GUVs (red) observed over a 10 min period in the dark; before (left image) and after 10 min (right). No change in adhesion was observed. (B) mOrange functionalized substrate (green) with Micro functionalized GUVs (red) under blue light illumination observed over 10 min; before (left) and after 10 min (right). No change in adhesion was observed.

Similarly, GUVs also adhered light-dependently if the position of the iLID and Micro proteins are swapped, i.e. immobilizing iLID on the GUV and Micro on the substrate (Figure 2.2.6).

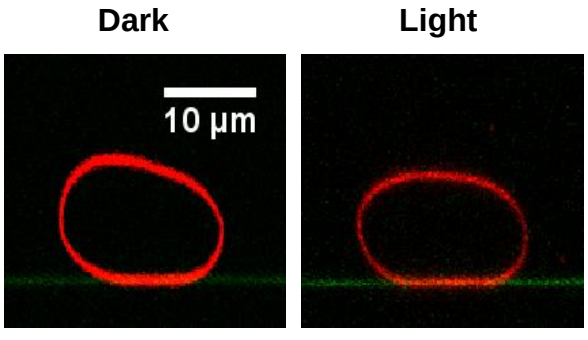

Figure 2.2.6 Images of an iLID-functionalized GUV on a Micro functionalized substrate were acquired in the x,z plane before and after 10 min blue light illumination. Swapping the positions of the proteins resulted in similar blue light dependent GUV adhesion to the substrate as observed through increased adhesion site and GUV deformation.

Nonetheless, in all following experiments we immobilized the light activated protein partner iLID on the PEG coated glass substrate; so that iLID is not mobile and its spatially controlled photoactivation is not wiped out by diffusion in the GUV membrane.

When the membrane stiffness of the GUVs was increased by adding cholesterol, the light-triggered GUV deformation was less pronounced, showing only reduced formation of an adhered membrane segment (20 mol% cholesterol) or adhered membrane segments that were below the optical resolution (40 mol% cholesterol) (Figure 2.2.7).

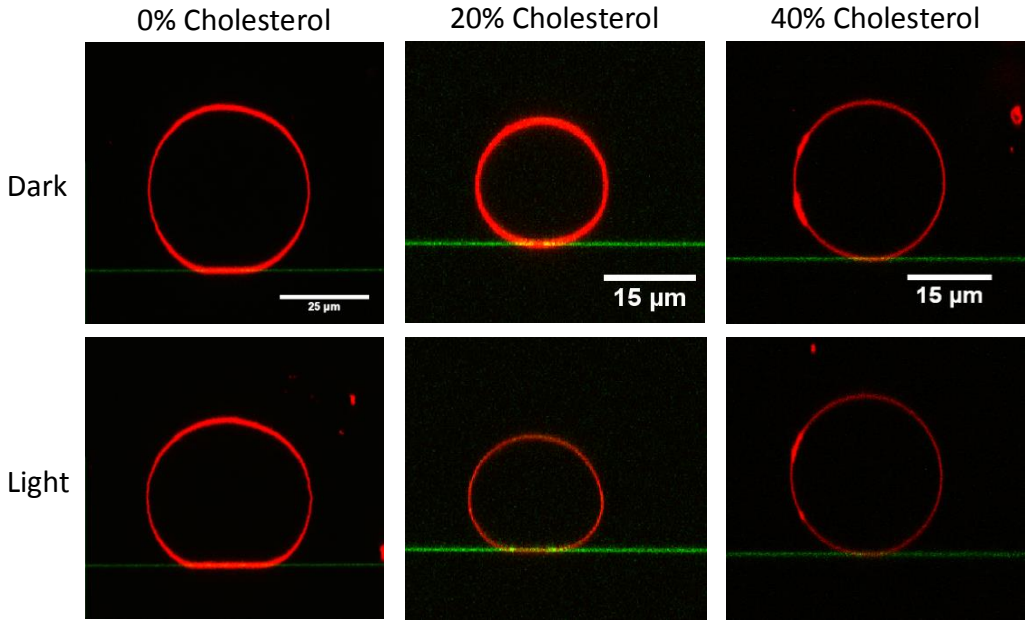

Figure 2.2.7 Effect of GUV membrane stiffness induced by different cholesterol concentrations (0-40 %) on the adhesion of deflated GUVs. Images of the GUVs in the x,z-plane were acquired in the dark and after 10 min blue light illumination. The GUV without cholesterol showed clear adhesion under blue light in form of deformation, increase in adhesion site and clear change in apparent adhesion angle, showing that membrane is clearly attached to the surface. The GUV with 20% cholesterol also changed its morphology upon blue light illumination, but the deformation was less pronounced and the GUV contact curvature between membrane and substrate stayed above the optical resolution. The GUV with 40% cholesterol did not change its shape upon light illumination. These differences in adhesion showed that membrane flexibility and fluidity are important for light dependent adhesion. High concentrations of cholesterol impede the flexibility of the membrane reducing the deformation due to adhesion to a degree that adhesion is below the optical resolution.

Likewise, when the GUVs were not osmotically deflated, the light-dependent GUV adhesions only led to minor deformation of the GUV (Figure 2.2.8). Hence, lower bending rigidity of the deflated GUVs is a critical requirement to observe light-dependent

GUV deformation and membrane fluctuations to mimic the protrusions formed in migrating cell.

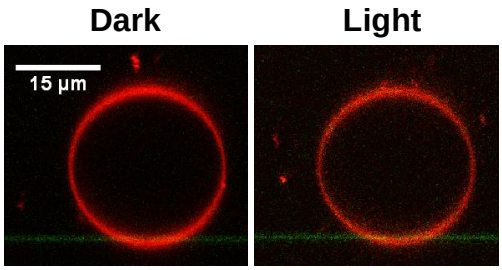

Figure 2.2.8 Adhesion of a fully inflated GUV in dark and after 10 min light exposure. Images were acquired in the x,z plane. Through the stiffness of the fully inflated GUV and the lack of excess membrane there were no obvious signs of adhesion like deformation and only a very small increase in adhesion site, if at all.

Kinetics of the light-induced adhesion and unbinding were quantified by time-resolved imaging and analysis of the GUV-substrate contact area (Figure 2.2.9, Figure 2.2.10A). The GUVs showed an increase of adhesion region to about double the size within the first 10 minutes of blue light illumination (Figure 2.2.9, Figure 2.2.10A, Light). Subsequently, when the GUVs were placed in the dark, the adhesion area of the GUVs decreased back to about its initial value within 5-6 min (Figure 2.2.9, Figure 2.2.10A, Dark). However, the exact kinetics did vary between individual GUVs, presumably reflecting the complex relationship between membrane adhesion and iLID light activation, membrane dynamics, vesicle tension and size (Figure 2.2.9).

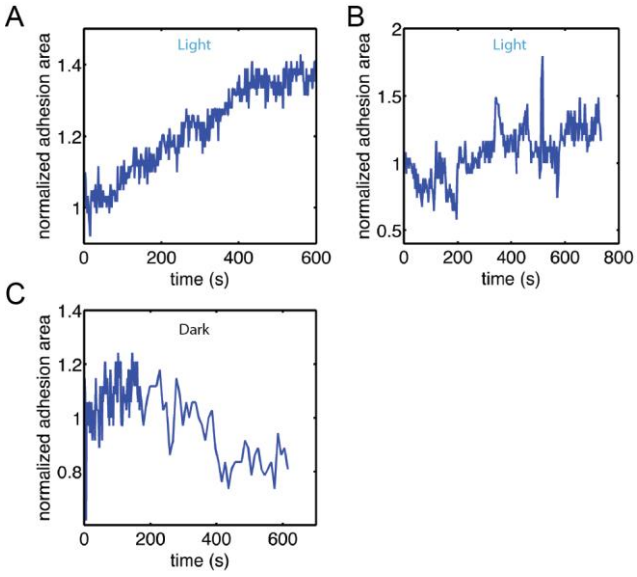

Figure 2.2.9 Additional examples of light induced (A) adhesion and (C) reversion kinetics of the adhered GUVs. Apparent noise in the normalized adhesion area traces is partly due to unprecise quantification of the adhesion segments but also reflects movement or membrane fluctuations of the vesicles themselves.

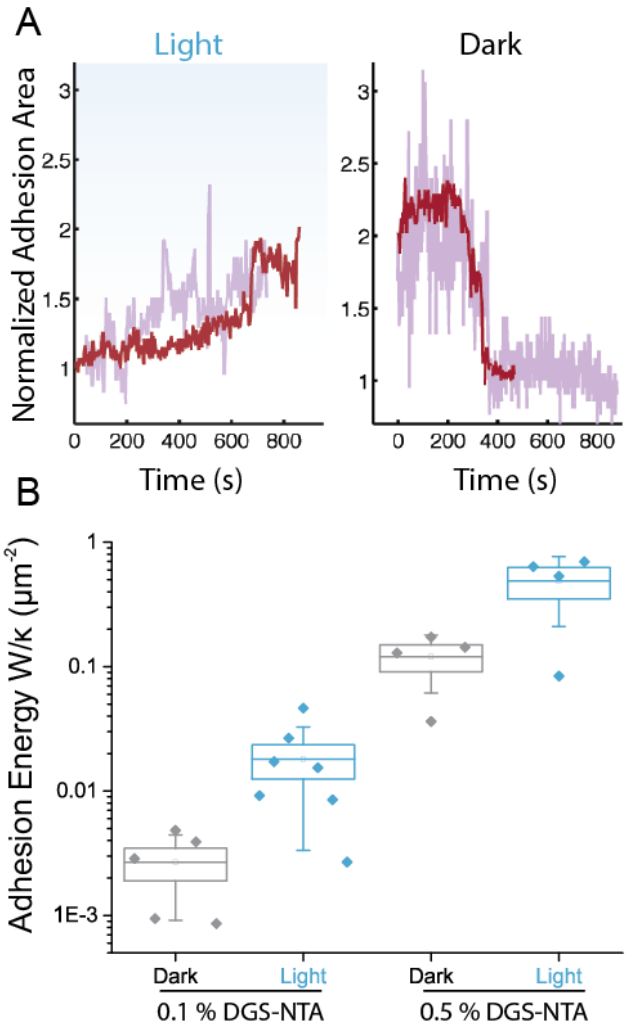

Figure 2.2.10 Quantification of adhesion. A) Examples of time-dependent evolution of the normalized adhesion area vs time under blue light illumination and in the dark of 2 different GUVs (red and pink traces). Under blue light, an increase to about 1.8 times of the initial adhesion area was observed and subsequently in the dark the adhesion area decreased back to its initial value. Note that changes in adhesion area were related to adhesion energy, see equation (1) in SI. B) Adhesion energies for GUVs functionalized with different Micro concentrations (0.1 mol% and 0.5 mol% DGS-NTA lipid for Micro immobilization) in the dark or under blue light. The adhesion energy W (rescaled by the GUV bending rigidity $\kappa \approx 20\ k_BT$ [204]) for the 0.1 mol% DGS-NTA containing GUVs under blue light activation corresponds to about 0.4 $k_BT/\mu m^2$, which was used in the following light guiding experiments. All populations were found to be significantly different from each other ($p < 0.05$ Student t-test).

The fact that the adhesion under blue light and detachment in the dark take place at a similar and at minute time scale is important as the kinetics of attachment in the front and of detachment in the back of the GUV should match so that the cell can move in one piece. Notably, in a migrating cell adhesion and detachment also takes place on this time scale. When cells adhere, integrins enrich/cluster at the adhesion site and are depleted

from other parts of the cell membrane. We used mOrange tagged Micro to observe whether Micro also enriched at the adhesion site upon photoactivation but could not detect significant Micro enrichment at the adhesion site (Figure 2.2.11).

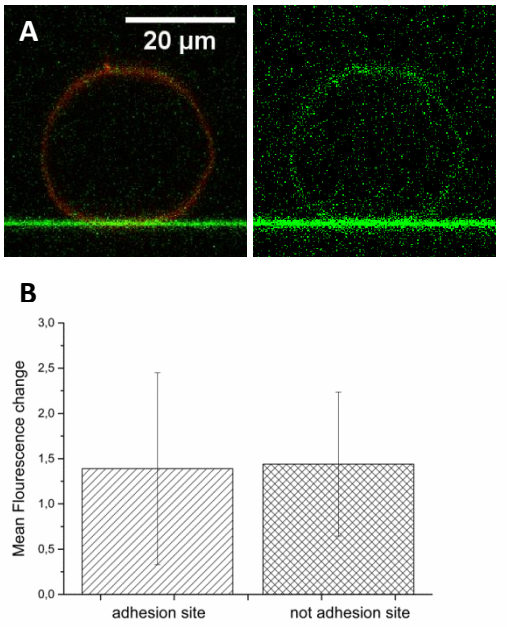

Figure 2.2.11 Micro-mOrange distribution over on an adhered GUV. A) Fluorescence image of the lipid membrane (red) and the mOrange (green of an adhered vesicle) were acquired in the x,z plane. The mOrange signal was homogeneously distributed over the whole GUV. B) mOrange fluorescent intensity analysis of six GUVs at the adhesion site and the top of the GUV (not adhesion site). The contribution of from the reflection at the substrate was subtracted. The change in fluorescence before and after adhesion is expectedly small. The error bars, which are the standard deviation, indicate that change in fluorescence intensity before and after blue light activation were not significantly different in different parts of the GUVs. Hence, within the sensitivity of this method the adhesion did not result in enrichment of Micro at the adhesion site.

It is also interesting that in some cases upon reversing GUV adhesion in the dark, excessive membrane shedding in the form of small vesicles from the GUVs is observed (Figure 2.2.12). This observation supports the idea that upon light activation the excess membrane of the deflated GUVs contributes to the increase in adhesion area, whereas upon decrease in adhesion this membrane can spontaneously bud off. Yet, it should be noted that such loss of membrane over repeated light/dark cycles will be a limitation for motility over long distances. The budding may be an indication of a change in the membrane spontaneous curvature because of local asymmetry induced by protein interactions in the vicinity of the adhesion zone.[27]

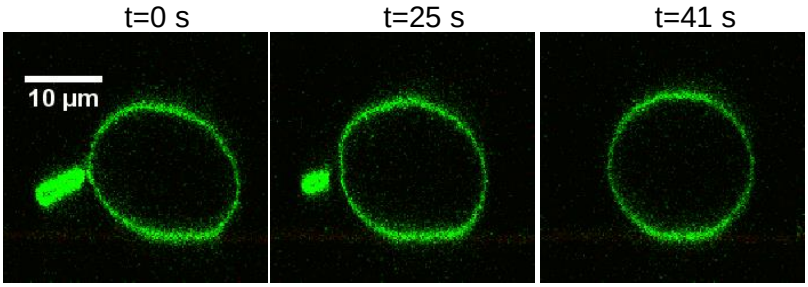

Figure 2.2.12 Fluorescence images in the x,z plane, of membrane shedding of a GUV adhered under blue light after placing back in the dark. During reversion of the GUV adhesions in the dark in some cases (ca. 30-40% of observed GUVs) membrane shedding was observed in the form of bud release accompanying the GUV stabilization and the detachment of the GUV over a timespan of seconds to minutes.

For this study it is critical that there is a difference in binding strength in the dark and under blue light and that adhesion and detachment kinetics match, which led us to determine kinetic and thermodynamic parameters for the iLID and Micro interaction under blue light and in dark. In the QCM-D (Quartz Crystal Microbalance with Dissipation monitoring) studies, iLID was immobilized on a supported lipid bilayer (DOPC+ 5 mol% DGS-NTA) formed on a SiO_2 crystal. 5 mol% DGS-NTA was required in QCM-D measurements for the reliable detection of His-tagged iLID binding. Subsequently, increasing concentrations of Micro were passed over the QCM-D crystal either in the dark or under blue light illumination and both the binding and unbinding kinetics were monitored (Figure 2.2.13).

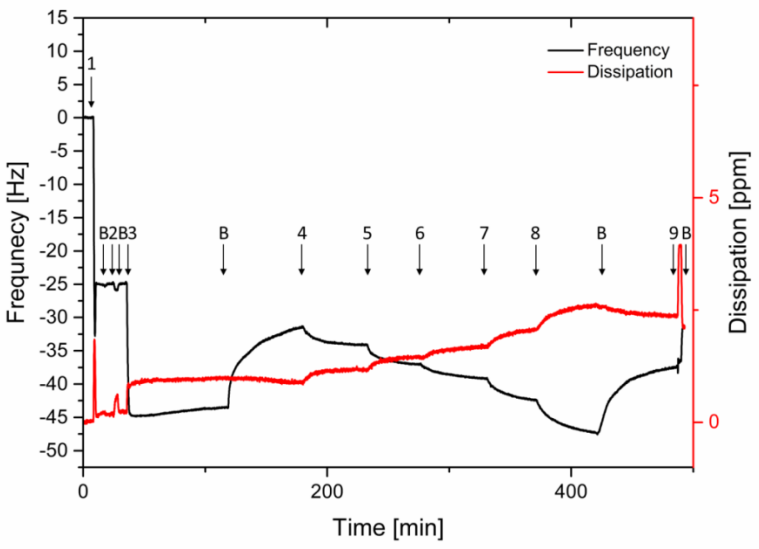

Figure 2.2.13 Exemplary changes of frequency and dissipation (7th overtone) in QCM-D measurements. Arrows indicate the start of addition of the following components in buffer (150 mM NaCl, 10 mM Tris, pH 7.4). 1) 10 mg/mL Lipids (DOPC + 5 mol% DGS-NTA) with 5 mM CaCl2, 2) 10 mM NiCl2, 3) 1 µM iLID, 4) 125 nM cutMicro, 5) 250 nM cutMicro, 6) 500 nM cutMicro, 7) 1 µM cutMicro, 8) 2 µM cutMicro, 9) 250 mM imidazole. 'B' indicates washing steps with buffer.

We observed that Micro binds to iLID both in the dark and under blue light, however the binding is more prominent under blue light. The analysis of the QCM-D curves showed that the K_d (dissociation constant) for the iLID-Micro interaction is 2.6 µM in the dark and 952 nM under blue light, which equals a 2.7-fold increase in binding affinity under blue light (Figure 2.2.14).

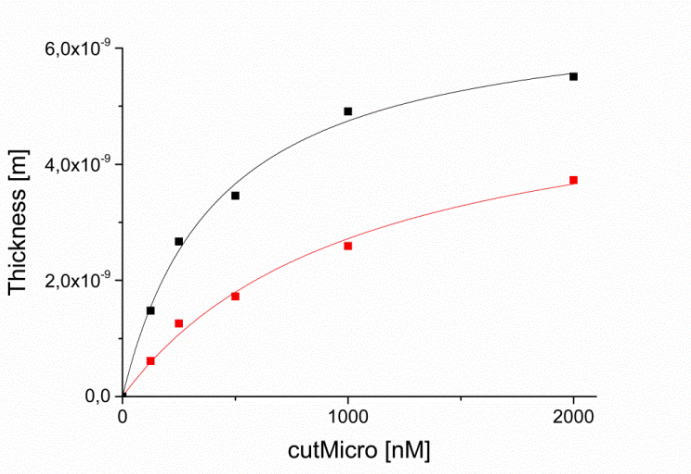

Figure 2.2.14 Film thickness as fitted to the QCMD measurements vs. cutMicro concentrations in dark (red) and under blue light illumination (black). The curves show Hill-fits.

While a 2.7 fold difference in interactions seems small, it is notable that this difference is enough to trigger light-dependent adhesion of the GUVs. Further, these values are significantly different from the reported K_ds of 47 µM in the dark and 800 nM under blue light (58-fold change) of the proteins in solution[169], showing that the immobilization of the iLID to a membrane affects the binding significantly. The k_{off} for the iLID-Micro interaction is similar in dark and under blue light ($k_{off,dark}$=8.5x10^{-4} s^{-1}, $k_{off,blue}$=1.1x10^{-3} s^{-1},) but the k_{on} increases significantly under blue light ($k_{on,dark}$=3.2x10^{2} M^{-1}s^{-1}, $k_{on,blue}$=1.2x10^{3} M^{-1}s^{-1}). These ranges of k_{off} and k_{on} are similar to those measured for integrin-extra cellular protein binding (Table 2.2.1)[115,205]. This is an additional aspect in which the iLID-Micro interaction is similar to cell-matrix interactions of the cell in terms of dynamics but without coupling them to intracellular machinery.

Table 2.2.1 Thermodynamic and kinetic constants of the iLID-Micro protein pair compared to natural adhesion proteins.

Constants	**Blue light**	**Dark**	**αvβ3-fibrinogen** [205,206]	**αvβ3-vitronectin** [205,207]	**α1β1-collagen** [205,208]
K_d [μM]	0.95 ± 0.47	2.63 ± 1.78	0.055	0.12	0.023
k_{off} [s^{-1}]	$1.1 \times 10^{-3} \pm 2.2 \times 10^{-4}$	$8.5 \times 10^{-4} \pm 4.4 \times 10^{-4}$	2.8×10^{-3}	9.2×10^{-4}	1.3×10^{-3}
k_{on} [$M^{-1}s^{-1}$]	$1.2 \times 10^{3} \pm 0.2 \times 10^{3}$	$3.2 \times 10^{2} \pm 0.2 \times 10^{3}$	5.1×10^{4}	7.9×10^{3}	5.6×10^{4}

The light-dependent adhesion of the GUVs was quantified by measurement of the membrane-substrate adhesion energy, which depends on the concentration of Micro on the GUV and number of light activated iLID on the substrate. In turn, the contact area and global shape of adhering GUVs depends on the adhesion energy, the membrane tension (or excess area) and the bending rigidity.[203] The osmotically deflated GUVs exhibited varying membrane tension and, as expected, areas of the adhered membrane segments were found to be heterogeneous within a population. To estimate the interaction energy between the GUV and substrate, the GUV area and volume were estimated from three dimensional reconstructions obtained by confocal microscopy.[120,209] In the dark, when Micro surface concentration was kept low (0.1 mol% DGS-NTA lipid for anchoring His-tagged Micro to the GUV), the adhesion energies between GUV and substrate were found to be smaller than 10^{-1} $k_BT/\mu m^{-2}$ and GUVs were essentially unbound (Figure 2.2.10B left).

In contrast, light activation increased the adhesion energy to about 0.4 $k_BT/\mu m^{-2}$. The change of adhesion energy between the dark and blue light activated state is about 6-fold and, interestingly, exceeds the change in iLID-Micro binding affinity of 2.7 fold. Presumably, this effect is at least partly due to the cooperative and non-linear dependence between membrane adhesion energy and receptor-ligand complex formation through suppression of membrane fluctuations.[210,211] As expected, an increase in Micro surface concentration (0.5 mol% DGS-NTA lipid, Figure 2.2.10B right) increased both adhesion energies in the dark and light-activated state substantially but the adhesion energy remained higher under blue light. Notably, the GUVs with 0.5 mol% DGS-NTA lipid significantly adhered in the dark, which is not desired for the light guided migration. It was not possible to increase the DGS-NTA lipid and hence the Micro

concentration on the GUVs further because the GUVs with higher DGS-NTA lipid significantly aggregated. On the substrate side, if the iLID density was reduced by decreasing from 100% to 10% the PEG-NTA, the GUVs no longer adhered even under long blue light illumination (Figure 2.2.14).

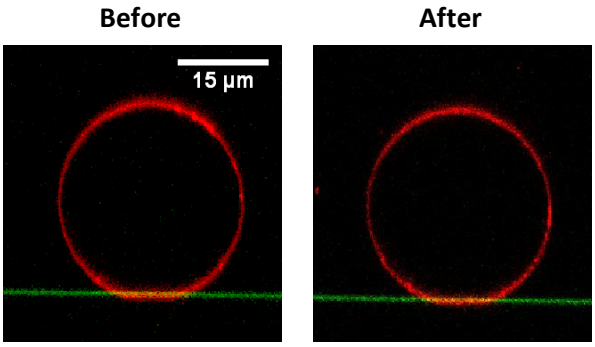

Figure 2.2.14 Adhesion of a Micro-functionalized GUV (0.1 % DGS-NTA) on a 10 % PEG-NTA substrate functionalized with iLID before and after 10 min blue light illumination. Images were acquired in the x,z plane. The GUV did not significantly adhere under blue light to the substrate with low iLID functionalization density.

Nonetheless, the adhesion energies between the GUVs and the substrate could be tuned over 3 orders of magnitude using the blue light triggered interaction between iLID and Micro allowing for different applications. In the context of light guided motility, we used 0.1 mol% DGS-NTA lipid and 100% PEG-NTA to immobilize Micro on the GUVs and iLID on the substrate respectively, as this combination resulted in low adhesion in the dark and significant adhesion under blue light.

Even though cell motility is thoroughly studied, there are no minimal synthetic systems that are able to reproduce this behavior. A key feature of cell motility is the dynamic asymmetry in cell adhesions, which are forming at the leading edge and disassembling at the trailing edge as the cell moves forward. To mimic this dynamic asymmetry of adhesions in a synthetic minimal cell, we used light-controlled GUV adhesion. For this purpose, we observed the GUV (0.1 mol% DGS-NTA lipid) from below at the interface between the glass substrate and the GUV (x,y direction) on a confocal microscope to see the adhesion area of the GUV on the iLID functionalized substrate and locally illuminated half of the GUVs adhesion area as well as a free region in front of it (Figure 2.2.15A-B).

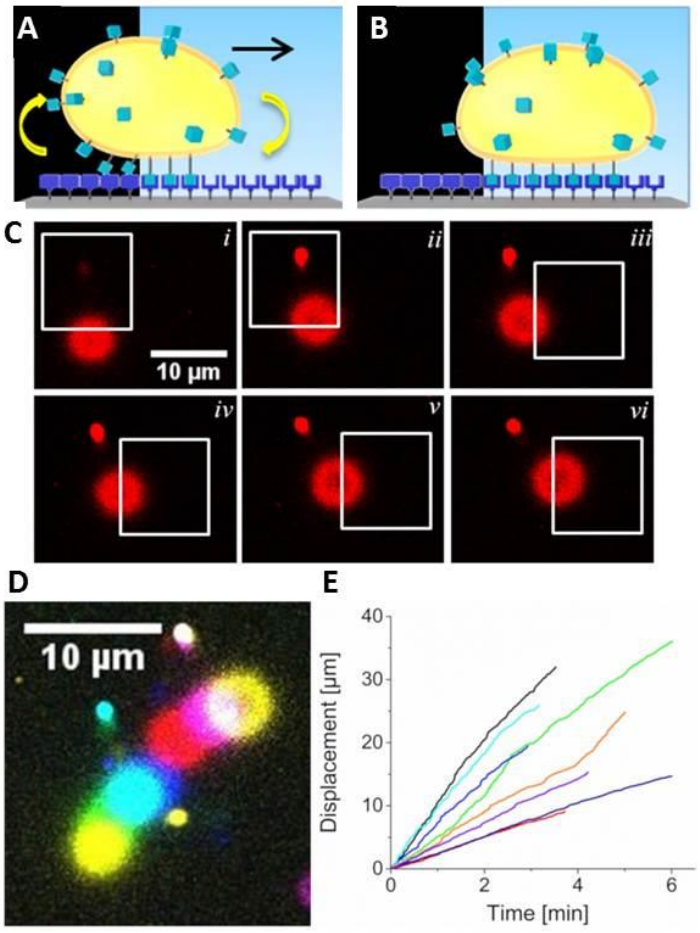

Figure 2.2.15 Light guiding. A) Asymmetric illumination of the GUV leads to stronger adhesion in the illuminate area and weaker adhesion in the dark area. B) This leads to migration of the GUV into the illuminated area. C) Fluorescence microscopy images (x,y scans at the substrates surface z=0) of a GUV (ca 20 µm in diameter) from below at the adhesion site to the substrate as it moves into the blue illuminated area (shown as white square). D) Overlay of the GUV at every illumination step (1 step ca. 1 min) to show GUV movement over time. E) Displacement of GUVs vs. time. 8 different GUV traces were analysed.

The illumination led to spatiotemporally controlled imbalance in adhesions; more and new adhesions formed in the illuminated half of the GUV compared to the half in the dark, where adhesions disassembled. Consequently, the GUV moved into the illuminated region, formed new adhesions in the illuminated area of the substrate and detached from the dark part of the substrate (Figure 2.2.15 C-D, Figure 2.2.16).

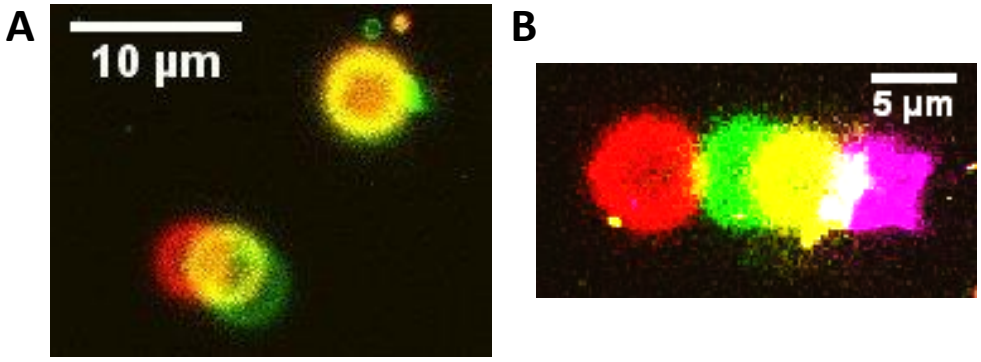

Figure 2.2.16 Light guided of GUVs. A) Overlay of GUV adhesion sites at different time points. The different colors correspond to different time points (red start, green end) spaced by ca 1.5 min. The movement of the GUV in the bottom-left corner was guided by illuminating half of the GUV, while the GUV in the upper-right corner was not exposed to light and thus did not move (Movie S1). B) Another example of a light guided GUV by illuminating half of the GUV and moving the illumination region as the GUV moves forward.

Further, if the illuminated area was moved again so that only half of the GUV resides in it, the GUV followed and displaced into the new illumination area. This process could be repeated 3-7 times, the GUV could be guided over tens of micrometers. This was also possible in multiple circuits like around a corner or back and forth (Figure 2.2.17-2.2.18).

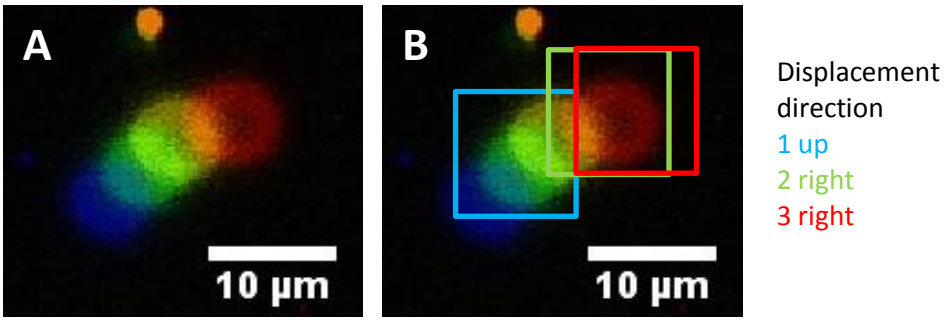

Figure 2.2.17 Light guiding of a GUV around a corner. A) Overlay of movement of GUV at different time points and with different guiding directions around a corner. B) Illumination areas indicated at different steps and the intended guiding direction. Blue is the initial illumination area moving the GUV upwards. Green indicates the 2nd und red the 3rd step guiding the GUV to the right.

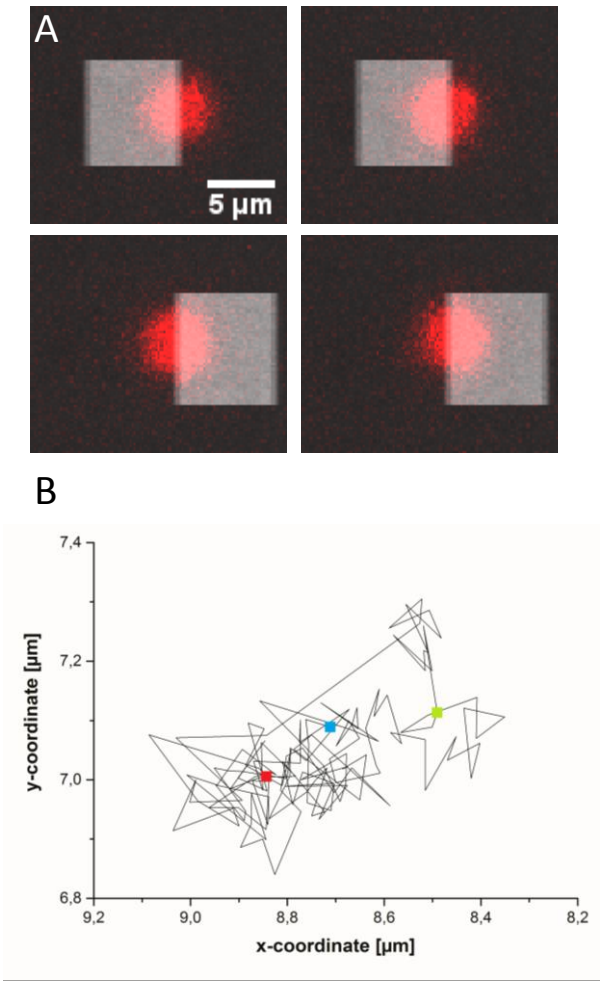

Figure 2.2.18 Back and forth light guiding of a GUV. A) The light areas show the illuminated areas and the movement of the red GUV into the illuminated area. Number 1-4 indicate timely sequence of events. (Movie S3). B) Direction map of GUV movement was generated by following the center of the GUV. Blue indicates the starting point, red indicates endpoint of the illumination to the left and green indicates endpoint of illumination to the right.

In addition to the light-triggered asymmetry in adhesions, it was also essential to use deflated GUVs during light guided motility, so that the adhesion area of the GUV was large enough (ca. 5 µm radius) to be able to partially illuminate the GUV and to create a significant imbalance in adhesions in space and time. Moreover, the fluctuations and excess membrane in the deflated GUV might be a compensation for protrusions observed during cell motility. During light guiding, we observed cases of visible membrane shedding and also a trail of membrane (Figure 2.2.19).

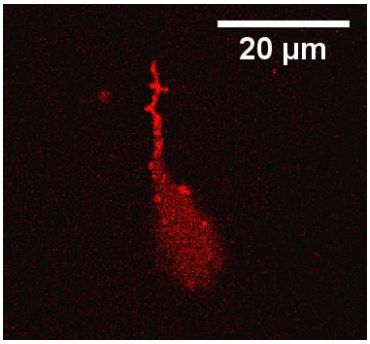

Figure 2.2.19 Membrane shedding during light guiding of a GUV. Some GUVs produce membrane tails during movement.

This loss of membrane is probably the reason why GUVs can be guided over only a couple of steps and not indefinitely. While the speed of the GUVs depended on many factors including the size of the adhesion side, the GUV size and the membrane tension, the average speed of eight representative GUVs was 4.9 µm/min (Figure 2.2.15E). This speed is reasonably fast and is comparable to a fast moving mammalian cell.[199]

Conclusion

Overall, we mimic cell motility in a minimal synthetic cell, assembled from molecular components. To achieve this, we dynamically and reversibly control the adhesion of a GUV to a substrate in space and time using the light-dependent interaction between the proteins iLID and Micro. This makes it possible to guide the migration of a GUV with light by forming new adhesions at the front of a GUV through local illumination and disassembling adhesions at the back placed in the dark. The provided examples show that it is sufficient to reproduce the dynamic and spatiotemporally controlled asymmetry in adhesions between the front and the back of a migrating cell, to move cell-sized objects. In the cell this requires complex molecular machinery but in a minimal synthetic cell this can be achieved with photoswitchable adhesions.

2.3 Light-controlled lipid-vesicle to vesicle adhesion

Aim

To build up tissue-like structures from synthetic cells and to creating communications between cells cell-cell adhesion has to be highly controlled. The light activated iLID-Nano dimer provides the control to bring single cells together to allow for defined interaction in a reversible manner. The interaction can be used in a bulk set up as well on single vesicles.

Abstract

Cell-cell contacts are necessary to build up multicellular organisms from cells and are dynamically regulated to control cell and tissue functions including tissue development and cell-cell communication. In synthetic biology, contacts between different synthetic cells are important to mimic multicellular tissues and achieve tissue-like functions with the same intricate control as provided by nature. Here, we introduce the iLID and Nano proteins on the surfaces of vesicles in order to dynamically control vesicle-vesicle adhesion using visible blue light. For this purpose, we separately immobilized the individual proteins of the pair on the surface of giant unilamellar vesicles (GUV) through NTA-Ni^{2+}-His-tag binding, thereby creating two distinct GUV populations. Under blue light illumination GUVs from the different populations will exclusively adhere to each other and subsequently can be detached in the dark. The light-controlled GUV-GUV interactions provide the possibility to build up vesicles into tissue-like structures dynamically. Therefore, the GUV-GUV interactions can be controlled with high spatiotemporal control and be used to control signal exchange between different minimal synthetic cells.

Introduction

Cell-cell adhesions are important to form tissues from cells and are involved in most major processes in cells and organisms amongst which are differentiation, communication, tissue development, and the immune response.[86,106-108] Adhesion not only provides mechanical stability to a cell assembly, but is also needed for cells to communicate with each other. A complex machinery of proteins enforces and controls adhesion between cells with the most prominent cell-cell adhesion protein family being the cadherins. These proteins are connected to the cytoskeleton through the binding with

catenins. This binding translates adhesion forces into the cell and stimulates signaling pathways; their feedback controls adhesion strength and communication between cells.[86]

The regulation of cell-cell adhesion is fundamental to their function as interactions have to be both mechanically stable and dynamic at the same time. This allows for creating defined tissue structures as well as reacting to changes in their external conditions. The degree of cell-cell adhesion has to be adjusted in processes like cell organization, embryogenesis, cell rearrangements in adult tissues, and cell migration.[112] Especially during embryonic development, cell adhesion needs to be precisely controlled in time and space for proper and functional tissues to form in the right place at the right time. For example, in branching events, such as occur in kidney and lung development, cadherin expression is decreased in a defined number of cells and at a predetermined time, leading to defined cleft formation.[106,111]

To mirror the formation of tissues with synthetic cells and recapitulate the dynamics of cell-cell adhesions, controlling interactions between synthetic cells is important. Most commonly used are GUVs as cell mimics due to their similarity to mammalian cells in both size and membrane structure. To gain precise spatiotemporal control over the interactions between these vesicles, light-inducible systems have been developed. For example, PEG chains can be rendered light responsive by the introduction of a nitrobenzyl group, which is cleaved under UV light illumination. Attaching these cleavable PEG chains to a vesicle can shield adhesive peptides from their binding partner until subsequent photocleaving induces adhesion and sequential fusion.[133] Another example of light-controlled adhesion is the development of an azobenzene-based surfactant that can be incorporated into a lipid membrane. Upon UV light illumination the azobenzene shifts from its *trans* to *cis* conformation changing its lipophilicity. The surfactant then extracts itself from the membrane into the aqueous surrounding taking lipid molecules with it inducing strain on the vesicle membrane. When in contact with other vesicles this then leads to adhesion and fusion of the membranes.[212] In both of these examples, UV light is the activating trigger. However, UV light is not biocompatible. More importantly, both interactions are irreversible, leading to fusion of the lipid vesicles and lack the dynamic control observed in natural cell-cell adhesion. Therefore, there is still a demand to create a synthetic cell-cell-adhesion model that not only provides precise spatiotemporal control but also the necessary dynamics.

To achieve this, we propose using the blue light responsive protein pair iLID-Nano to induce reversible, biocompatible and finely controlled GUV-GUV adhesion (Figure 2.3.1A). iLID binds to its interaction partner Nano under blue light illumination

with subsequent disassociation in the dark. These interaction dynamics occur in a time scale of seconds to minutes and have been shown to be strong enough to induce GUV to surface adhesion (see chapter 2.2).

Results and Discussion

To create a model for cell-cell adhesion His-tagged proteins iLID and Nano were immobilized on two separate GUV populations containing 0.1% of Ni^{2+}-NTA-DGS, a lipid with a Ni^{2+}-N-nitrilotriacetic acid (Ni^{2+}-NTA) head group. To differentiate the two populations of GUVs, two different dyes were integrated into the membrane: DiD for iLID-functionalized vesicles (depicted in red) and DiI for Nano-functionalized vesicles (depicted in green). Both populations were mixed in 1:1 ratio in the dark and GUVs settled onto the substrate due to the higher density solution (100 mM sucrose) within the vesicles, than the surrounding buffer. Statistically GUVs of opposite populations came into close proximity but did not interact strongly. Upon turning on the blue light, activating the iLID-Nano protein interactions, vesicles adhered to each other within a few minutes (Figure 2.3.1B), as evidenced by an increased overlap of vesicle membrane and deformation of one of the vesicles. Close proximity of the vesicles is required as the adhesion is dependent on the proteins being able to interact. Additionally, it was important that one of the vesicles was deflated; meaning one GUV has excess membrane. The excess membrane allows for the largest possible interaction surface between the GUVs therefore increasing the number of protein interactions that can form. The strength of this interaction is demonstrated by the resistance of the vesicles to laminar flow over the duration of the illumination. Another advantage of using deflated GUVs in one GUV population is that adhesion is observed more obviously through the significant deformation of the GUV membrane (Figure 2.3.1B). The adhesion once formed was stable over the duration of the blue light illumination of over 10 min, without showing apparent fusion. Thus, the process is controlled and restricted to adhesion.

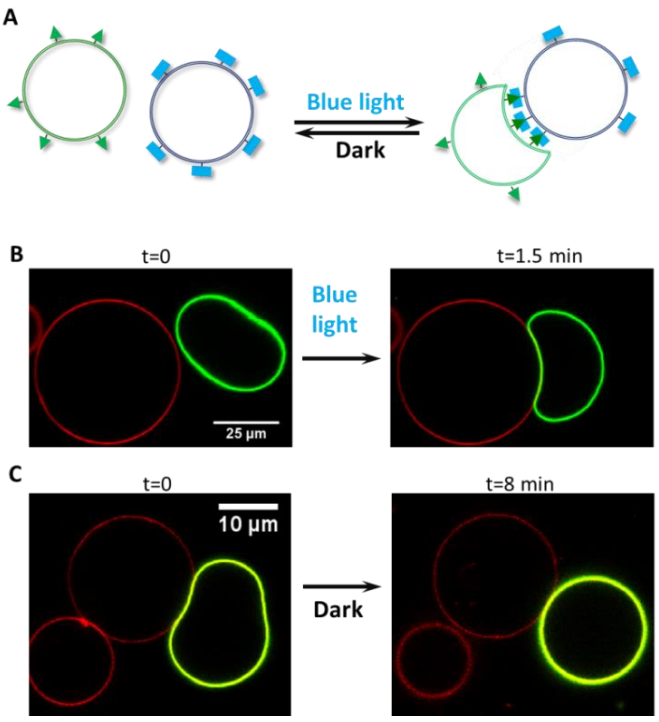

Figure 2.3.1 Vesicle to vesicle adhesion. A) Scheme of vesicle to vesicle adhesion with the use of photoswitchable proteins. The proteins decorate GUVs, creating two different populations. When mixed they adhere to each other under blue light. B) Red vesicle decorated with iLID, green vesicle decorated with Nano. Upon blue light illumination the deflated green vesicle adheres to the fully inflated red vesicle, visible through the adhesion site and the deformation of the vesicle. C) Reversion of adhesion. Full reversion of the adhesion of a green Nano-functionalized GUV from a red iLID-functionalized GUV within 8 minutes of darkness.

The observed adhesion was due to the specific interaction of the iLID and Nano proteins under blue light. This is witnessed by the exclusively interactions between differently functionalized GUVs. There are initial contacts between GUVs of the same type, but these do not show strong adhesion with strong deformation of the GUV. Moreover, they detach without any additional stimulus (Figure 2.3.2). In addition, the strong adhesions observed between opposite types of GUVs are not observed in the dark.

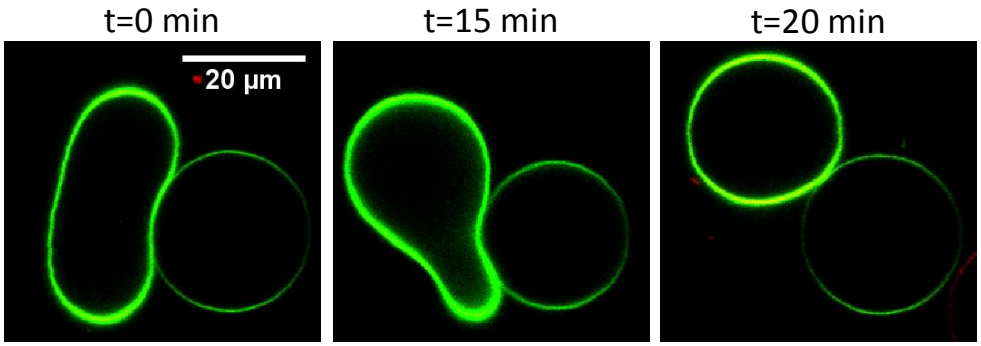

Figure 2.3.2 Time line of two Nano functionalized vesicles interaction under blue light over 20 min. The vesicles interact, constantly changing adhesion site length up to detaching from each other but do not adhere efficiently to each other.

As the iLID-Nano protein interaction is reversible, the vesicle adhesion based on it is, therefore, also reversible. In the dark, the vesicles show a relaxation of the adhesion up to complete detachment within a few minutes, observed as a decrease in overlay of the membranes of the two interacting vesicles and in relaxation of the deformation from a bowl shape back to spherical shape (Figure 2.3.1.C).

Whether reversion occurs, depends on how much the GUVs were deflated and deformed upon interaction. It appears that if the vesicle deforms extensively into a bowl shape that the energy barrier becomes too high for the reversal of the deformation, and these vesicles show no active separation from the other GUV (Figure 2.3.3). When detachment of vesicles following a return to dark conditions is observed, the detachment often goes hand in hand with a shedding of membrane. A similar phenomenon has been observed during the dark reversion for blue light dependent vesicle-surface adhesion (see chapter 2.3). This suggests that, when the strain resulting from the interaction between the GUVs is removed, the deflated GUV releases excess membrane in the form of small vesicles as this membrane is no longer required to form a stable GUV.

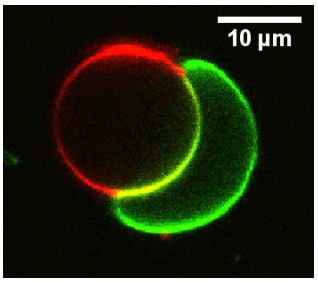

Figure 2.3.3 Example of adhered Nano functionalized GUV that is too far bend to a bowl shape reverse to a spherical shape in the dark.

The kinetics of the light triggered adhesion between the GUVs and the reversion in the dark were analysed by measuring the length of adhesion between the two GUVs over time under both blue light illumination and in the dark. (Figure 2.3.4)

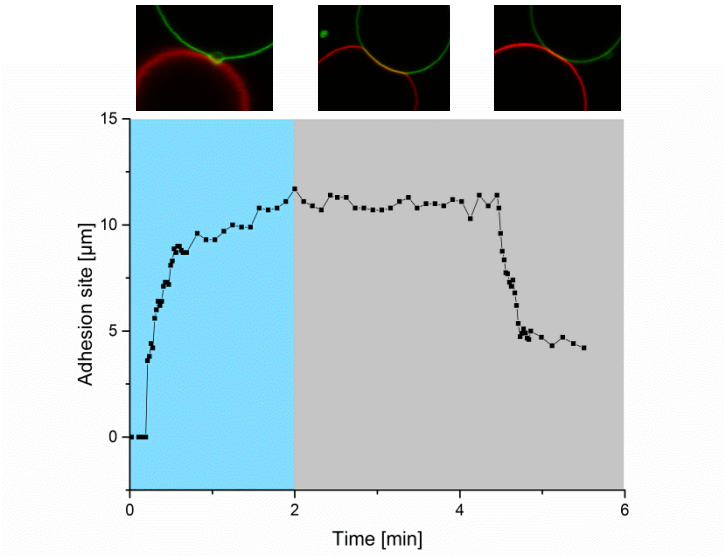

Figure 2.3.4 Adhesion site vs time over a sequential illumination and dark period. Two GUVs are in close proximity but not interacting, as shown in the first picture. During blue light illumination the GUVs interact, shown by deformation as seen in the second microscopy picture and a sharp increase in adhesion site. When the light is turned off the adhesion is reversed, seen by a sharp decline in adhesion site.

In general, we observe that the adhesion is determined by two vesicles of opposite type coming into proximity and not by the activation of the iLID protein with blue light, which happens within seconds of blue light illumination.[169]

The rational for this observation is that as long as the interaction partners iLID and Nano, which are immobilized on the GUVs, are not close enough to each other they cannot interact and hence there is no adhesion between the vesicles. However, as soon as the vesicles achieve their first contact the adhesion is very abrupt. Evidence for this was observed in our experiments (Figure 2.3.5): within a few seconds of first contact (marked by arrow at each curve in the respective colors) the adhesion site increases abruptly. In total the time between the initial contact and the formation of the stable adhesion is less than 1 min, during which there is a sharp increase in contact area between the GUVs. After this initial period, the area of the interaction site stabilizes. The final length of adhesion site dependents on the size of the two vesicles and the amount of excess membrane of the deflated vesicle

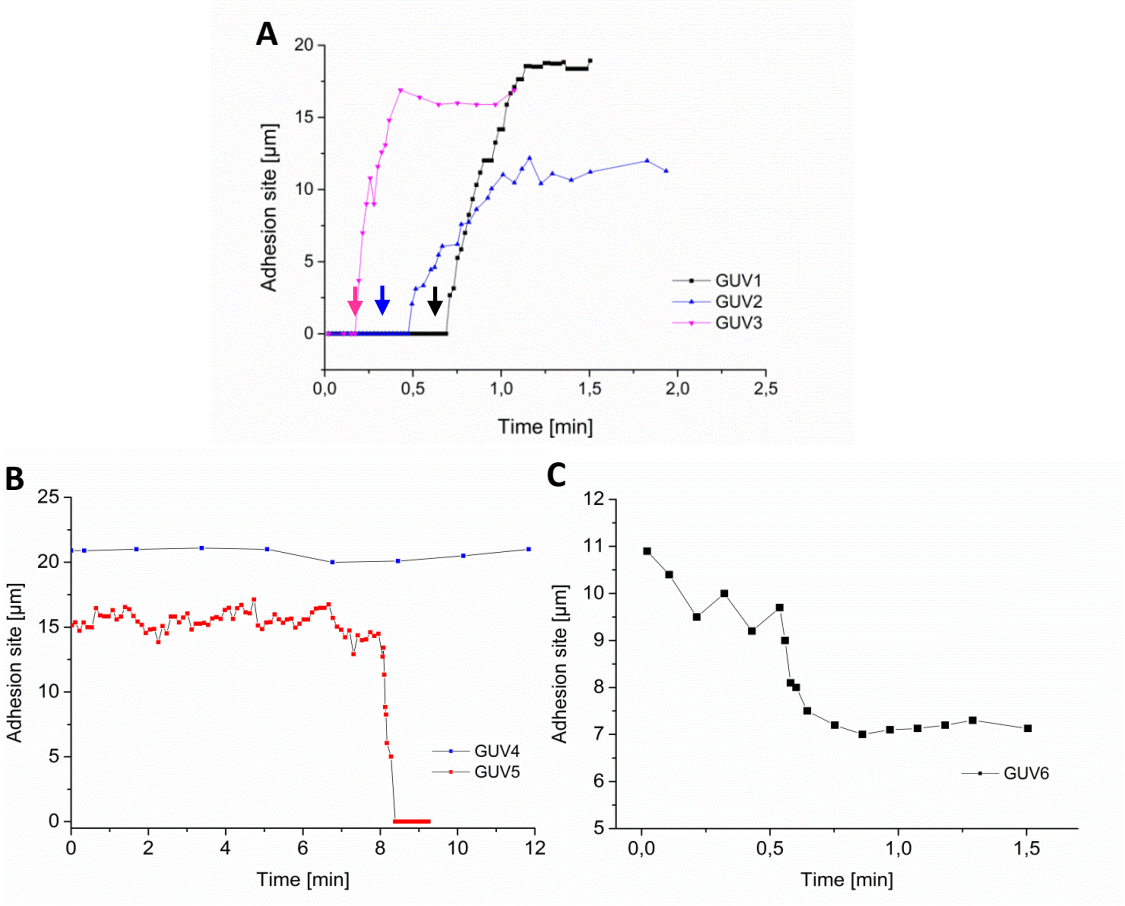

Figure 2.3.5 Adhesion site vs time. A) Examples of adhesion of three different GUVs under blue light illumination. After initial contact the adhesion is formed very fast marked by a steep increase in adhesion site. The process takes less than 30 s. The arrows mark time of first contact point, being close enough to form protein interactions. B) Examples of reversed adhesion in the dark. GUV4 shows the case of no reversion, when the GUVs stay attached. GUV5 shows the case of full reversion. The reversion occurs on a time scale of minutes. D) Example of partial reversion in the dark. The GUV shows a sharp decline of adhesion area, but an adhesion site of ca. 7 µm remains.

To analyze reversion the adhesion in the dark, the length of the adhesion site was measured from the time point of turning the blue light off. The reversion of adhesion takes place on a time scale of minutes (Figure 2.3.5 B/C). This is in correlation with the reversion kinetics of GUV-to-surface adhesion (see chapter 2.2). As might be expected, reversion occurs with an inverse growth of adhesion site interaction length in comparison to that seen during adhesion. There are three different modes discernable in reversion. As already mentioned, reversion is dependent on the deformation of the GUV, distinguishing between full reversion (Figure 2.3.5 B GUV 4), partial reversion (Figure 2.3.5 C, Figure 2.3.6) and no reversion (Figure 2.3.5 B GUV 5). In full reversion the two GUVs separate fully from each other. In partial reversion a contact site is

reduced but not eliminated, probably due to close proximity and a missing force to actually move the GUVs apart. While harshly deformed GUVs do not show any change in adhesion site, lacking the energy to change from bowl to spherical shape.

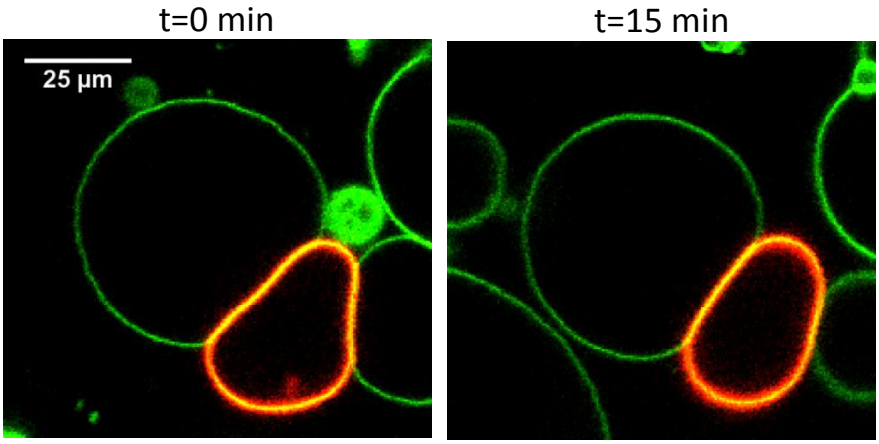

Figure 2.3.6 Example of reversion. The iLID functionalized vesicle (red) is trapped between multiple Nano-functionalized (green) vesicles and is deformed strongly. After 15 min in the dark the red GUV shows a distinct less deformed form, hinting reversion of strong adhesion.

To demonstrate that these photoswitchable GUV-GUV interactions can also be used to assemble proto tissues, these GUVs were assembled into larger assemblies using a microfluidic set up. Vesicles of both populations were captured in traps in a microfluidic chamber that can hold ca. 150 vesicles. The microfluidic chip has the benefit of confining 204 traps with 100 vesicles within a small area putting them into very close proximity (Figure 2.3.7). Following trapping, the interactions between the vesicles were then activated using visible blue light or were left non-adhering in the dark. Subsequently, the flow was reversed to remove the vesicles from the traps. While vesicles kept in the dark moved out of the traps as single GUVs, the vesicles under blue light illumination moved out in larger clusters.

Although we could observe this difference in vesicle clustering moving out of the microfluidic traps under both light and dark, the distinction between adhered and non-adhered vesicles was not as clear cut. This is presumable due to differences in forces caused by the internal flow within the chip. This is especially problematic under dark conditions where the gradual exit of single GUVs over time is not observed. Instead, many GUVs move out at once and single GUVs were observed once the GUVs left the trap. The results show that under dark conditions the GUVs remain unattached despite their close proximity, as observed by the presence of singular GUVs and small GUV

clusters of both species outside the traps following flow reversal (Figure 2.3.7A). In contrast, under light the GUVs form large aggregate structures that do not readily disassociate even under mechanical shear stresses (Figure 2.3.7B).

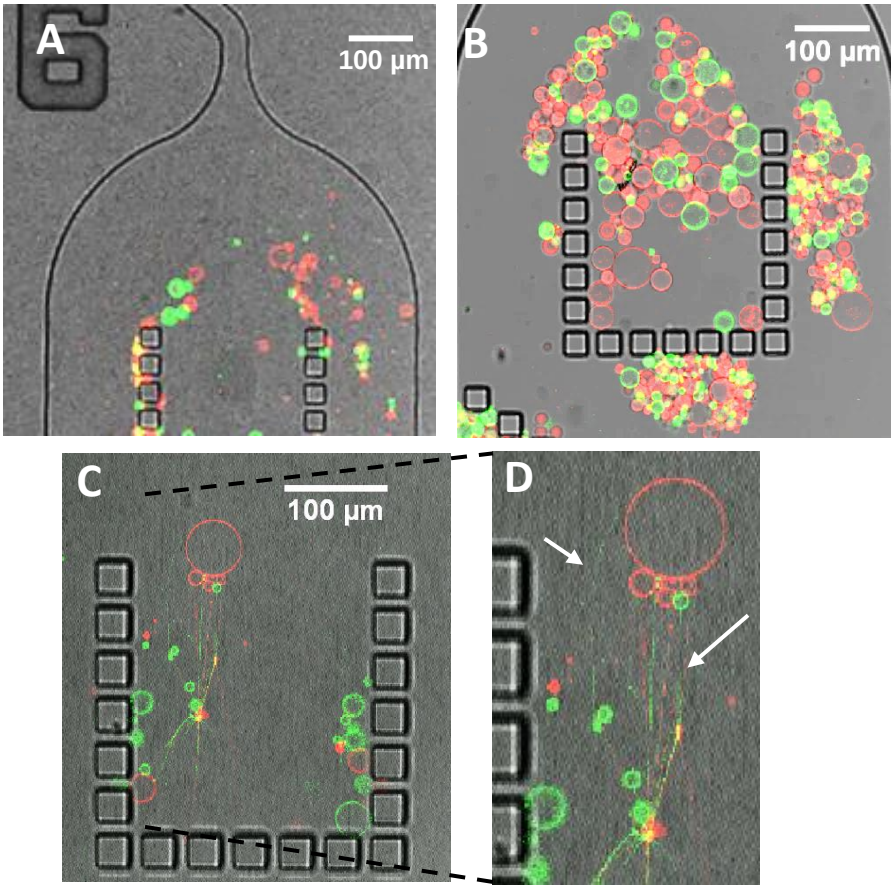

Figure 2.3.7 Microfluidic trapping. A) Reversion of the flow reveals the singular GUVs being extracted from the trap after leaving the sample 15 min in the dark. B) Cluster forming of vesicles after 15 min blue light illumination (488 nm) after reverse flow. C) Tubular forming at strongly adhered GUVs. D) Zoom of formed tubules. White arrows indicating the formed tubules.

Additionally, supporting our findings of light dependent adhesion is the formation of external lipid tubules between adhered vesicles under blue light upon separation by the reversed flow (Figure 2.3.7 C/D). This indicates strong adhesion between two vesicles, as it takes energy to extract the lipid molecules from the vesicle membranes to form the tubules while staying attached to the other vesicle.[213] This further supports the claim that the optogenetic proteins iLID-Nano are able to create strong adhesions between two different populations of vesicles.

Having established vesicle to vesicle adhesion, we were interested in whether cargo exchange is possible between the attached GUVs. The Nano-functionalized GUV population was loaded with mOrange, an orange fluorescent protein (Excitation: 548 nm, Emission 562 nm), while GUV population was not loaded with fluorescent proteins (Figure 2.3.8). When these two populations of GUVs were brought together and adhered under blue light, the fluorescent protein remains solely in its original Nano-functionalized GUV. There is no exchange of contents between the vesicles, confirming our expectation that the protein interaction only induces adhesion and not fusion of the vesicles.

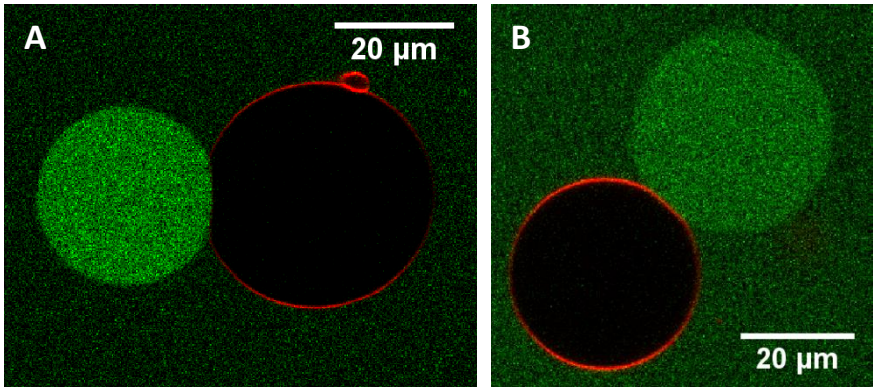

Figure 2.3.8 Light induced adhesion without cargo exchange. iLID functionalized GUV (red) interacts with Nano-functionalized, mOrange loaded (green) GUV after 15 min blue light illumination. There is no exchange of loading shown in the low intensity of green fluorescence in the iLID functionalized GUV even after 10 min of illumination.

Conclusion

We created a minimal system to mimic cell-cell adhesion with the optogenetic protein dimer iLID-Nano. The GUV-GUV adhesion was light-dependent and occurred reversibly within minutes between complementary vesicles. The use of visible light provides a biocompatible system for bringing two biomimetic compartments together and allows for the building up multi-vesicular assemblies, as shown in the bulk experiments. This is the first step towards a light-induced approach towards creating tissue like structures from minimal synthetic cells in a highly controlled way. In future, the light-controlled GUV-GUV interactions could be used to induce dynamic adhesion to achieve self-assembly of different synthetic cells and control the communication between them.

3 Summary and Outlook

Introducing cell functions into a minimal synthetic cell is a challenge that needs new tools, which can be precisely controlled in space and time. Optogenetic protein pairs like iLID-Micro/Nano offer such control and precision using visible blue light as a trigger. Additionally, this protein interaction is biocompatible, works under physiological conditions, and provides a reversible interaction with high spatial and temporal resolution. Combining such tools with minimal synthetic cells provides a platform to gain a deeper understanding of fundamental mechanisms in the modern cell and modulate synthetic cell behavior.

This thesis demonstrates the use of the iLID-Micro/Nano protein to mimic three fundamental processes where control is important: Protein patterning, cell motility, and cell to cell adhesion. Moreover, this light dependent protein interaction allowed one to trigger dynamic responses, which translated into equally dynamic and responsive behaviors in the minimal synthetic cells.

In the first part of the thesis, protein patterns were created on the surface of giant unilamellar vesicles (GUVs). Through blue light illumination a protein of interest (POI) fused to Nano could be recruited to iLID that was immobilized to a lipid surface. This process was reversible in the dark and could be repeated over multiple cycles. Additionally, the recruitment was dependent on the light intensity and highly specific to blue light (488 nm). Protein gradients were generated by the spatially controlled recruitment of proteins to one side of the GUV followed by the diffusion of this protein due to the fluidity of the lipid membrane. Moreover, proteins were patterned on a tissue-like assembly of GUVs. Illuminating different parts of the vesicle assembly allowed recruitment of the POI only to these specific regions. Due to the dynamic nature of this protein interaction, it was possible to create differently shaped patterns on the same surface at different time points. Thus, the iLID interaction with Nano was established as a platform to create protein patterns on different scales.

In the future, this platform could help to mimic and investigate natural protein clusters and patterns, as seen for example in cell migration, cell division and signaling, as the POI can be readily varied to correspond to the process under investigation. Furthermore, the complexity of this system could be further increased by combining the iLID-Nano interaction with other optogenetic dimers that respond to different wavelengths of light. Such a set-up would allow activating different proteins orthogonally, such that different proteins could be patterned simultaneously or sequentially. The protein patterning based on the iLID-Nano interaction is not limited to lipid membranes as it can be extended to

functionalized glass surfaces. In fact, this approach can be applied to any surface that is compatible with NTA functionalization, greatly expanding its scope. Lipid rafts, a phenomenon of cellular phospholipid-based membranes, and its influence on lipid cluster and pattern formation can be analyzed in detail as well physical properties of the membrane. GUVs provide the closest mimic to nature cells and therefore could be used in future to pattern desired proteins with high spatiotemporal.

The protein dimer iLID-Micro was used as mediator of reversible vesicle adhesion to a surface in the second part of the thesis. The iLID-Micro pair is especially suitable to mimic this adhesion as the thermodynamic and kinetic constants are very close to those of known cell adhesion proteins like integrin. Inducing adhesion of Micro functionalized GUVs to a surface functionalized with iLID with blue light in physiological conditions was possible with precise control and high spatial resolution. This was be quantified through the calculation of the adhesion energy in both the dark and light conditions, which showed significantly increased energies under blue light compared to the dark state. The high spatial resolution allowed for creating asymmetric adhesion, which is necessary to induce migration in a cell. By illuminating part of a GUV it was possible to create movement of the vesicle into the illuminated area. Repeating this over multiple cycles allowed the displacement of the GUV over a micrometer scale at a speed comparable to the movement of mammalian cells. This system provides the first evidence of light guided movement of a synthetic cell that mimics autonomous cell migration.

Achieving synthetic cell migration is a difficult and demanding task; nevertheless, we could demonstrate that optogenetic systems have the requisite properties to induce such a property in a synthetic cell. This approach can be expanded to optogenetic protein dimers activated by different wavelengths, allowing light guiding with different colors of light. Combining the different dimers would furthermore allow for a complex network of light guided vesicles. It would be possible to bring different families of vesicles together on a surface in a defined way as well as sort a mixture of vesicles into defined families, behavior that is known from embryonic development. This would a big step in synthetic biology mimic such complex and highly controlled processes. Even though we have shown that there is no need for the inner protein machinery to induce movement in a synthetic cell, to create a closer image to nature and gain greater insight into the natural workings of a cell, it would be interesting to connect this approach to an intracellular protein network. One interesting aspect would be implementing and connecting the contraction machinery of cells, as it occurs during cell motility, to the iLID dimer. Adhesion receptors are in nature closely connected to signaling pathway in the cell. To mimic motility in the full scope of nature and to investigate the influence of adhesion on

different signaling pathways, the iLID protein dimer could provide the adhesion receptor to connect to signaling pathways. To achieve that these internal pathways have to be developed though for a synthetic surrounding.

Further, the ability to adhere vesicles in a defined way could be used in the development of single vesicle experiments, as vesicles can be arranged in a defined way on a surface and adhered there. In single vesicle experiments today, the vesicles have to be either physically trapped or the through put is very low as every vesicle has to be considered separately. Adhering the vesicles in a spot by light makes it possible to trap multiple vesicles separately from each other and manipulate them at the same time without physical barriers.

The adhering and light guiding with the help the help of a light switchable dimer is a great first step towards synthetic motile cells, but the model can be expanded to achieve even more knowledge into the intricate workings of a cell.

The third part of the thesis explored the use of the iLID-Nano dimer to induce adhesion between vesicles. To mimic these two different GUV populations were functionalized with iLID and Nano. In close proximity and under blue light illumination they reversibly adhered to each other. They showed stable adhesion without fusion and the adhesion was able to withstand laminar flow. There was no evidence for loading exchange between the vesicles, confirming, that there was no fusion events induced by the light controlled adhesion. The interaction could also be scaled from single GUV-to-GUV adhesion to bulk experiments mimicking tissues.

To increase the complexity and applicability this approach to adhesion could be expanded: Through introducing channel proteins into the GUV[214] or the use of ionophores[215] the exchange of molecules between the vesicles could be induced. This would allow recreating information exchange between cells, as cells communicate inter alia by exchange of signaling molecules. The vesicles could be used as transporters of chemical cascades, only being triggered when the reactant filled vesicle is adhered and loading exchange initiated. Also, would allow to create synthetic cells with division of metabolism pathways. Only through adhesion and exchange of molecules between the cells the assembly would be able to reach its full potential, mimicking differentiated cells in higher organisms, each cell performing their specialized task.

With these proteins the vesicle-to-surface adhesion can clearly be distinguished from vesicle-to-vesicle adhesion, allowing mimicking these processes separate from each other. Combining vesicle-surface adhesion with vesicle-vesicle adhesion would give a great opportunity to investigate mechanisms of higher organisms, such as tissue build up

and tissue rearrangement. Different vesicle populations could be created and assembled in a desired architecture. It could be the mimic to investigate embryonic development on a completely synthetic platform. Also, the possibility of adding different optogenetic dimers to the system offers the possibility of creating adhesion systems that are kinetically and thermodynamically different but use the same trigger, provide the same chemistry and biocompatibility without influencing the already established system.

Here, it was demonstrated that light and optogenetic proteins, in this case the iLID-Nano/Micro dimers, deliver a useful tool in synthetic biology to induce contacts and to create protein patterns. As visible light is used biocompatible platforms that work under physiological conditions were created. This makes the precise spatial and temporal control and dynamics of the protein system available to synthetic biology to craft life-like functions into a synthetic system.

4 Materials and Methods

4.1 Materials

4.1.1 Laboratory Equipment

AccuBlock Digital Dry Bath Labnet	Labnet International Inc., Edison, USA
Analytical scale XS205 Dual range	Mettler-Toledo GmbH, Gießen Deutschland
Affinity column HisTrap™ HP (1 mL, 5 mL)	GE Healthcare Europe GmbH, Freiburg, Germany
Centrifuges:	
Avanti J-26S XP (rotors: JA-10 and JA-25.50)	Beckman Coulter Inc., Brea, USA
VWR Micro Star 17	VWR International GmbH, Darmstadt, Germany
Rotixa 50 RS	Andreas Hettich GmbH & Co.KG
Electroporator (MicroPulser™)	Bio-Rad Laboratories GmbH, Munich, Germany
Gel electrophoresis	Bio-Rad Laboratories GmbH, Munich, Germany
Hamilton glass syringe (1 mL, 25 µL)	Carl Roth GmbH + Co. KG, Karlsruhe, Germany
Ikatron thermometer	IKA®-Werke GmbH & Co. KG, Staufen Germany
Incubators:	
INCU-Line ® ILS6	VWR International GmbH, Darmstadt, Germany
Innova ® 44	New Brunswick Scientific Co., Inc., Enfield, USA
Ecotherm Incubator	Torrey Pines Scientific, Inc, Carlsbad, USA

Lamp Bulbs (blue, red, far-red), 15 Watts	Osram GmbH, Munich, Germany
Magnetic stirrer “color squid”	IKA®-Werke GmbH & Co. KG, Staufen Germany
Magnetic stirring hotplate Heidolph MR 3001 K	Sigma Aldrich, Munich, Germany
Membrane pump MZ2c	VACUUBRAND GMBH + CO KG, Wertheim, Germany
Microwave	C.Bomann GmbH, Kempen, Germany
Milli-Q® Synthesis water purification system	Merck KGaA, Darmstadt, Germany
with Q-Grad® 2 Purification Cartridge	
NanoDrop 8-sample Spectrophotometer ND-8000	Peqlab Biotechnologie GmbH, Erlangen, Germany
pH-meter Hanna HI 208	Sigma Aldrich, Munich, Germany
Pipetteboy accu-jet® pro	Brand GmbH + Co KG, Wertheim, Germany
Plasma system “Femto”	Diener electronic GmbH + Co. KG, Ebhausen, Germany
QCM-D (E1 and E4 system)	Q-Sense, Västra Frölunda, Sweden
QSense® flow module	Q-Sense, Västra Frölunda, Sweden
QSense® Window Module	Q-Sense, Västra Frölunda, Sweden
Scanner system ViewPix1100	EPSON Deutschland GmbH Meerbusch, Germany
Scales:	
Mettler PM460 DeltaRange	Mettler-Toledo GmbH, Gießen, Germany
Kern EMB 1000-2	KERN & SOHN GmbH, Balingen, Germany
Sonication bath	BANDELIN Electronic GmbH & Co. KG, Berlin, Germany

Teflon frame (ca. 40 mm x 24 mm)	Made by Feinmechanik MPIP
Ultrasonic homogenizer Omni Sonic Ruptor 400	Omni International Inc., Tulsa, USA
UV-VIS spectrometer	Lambda25, Perkin Elmer, Germany
Vacutherm vaccum oven VT6025	Fisher Scientific UK Ltd, Loughborough, United Kingdom
Vortex-Genie 1	Scientific Industries Inc., Bohemia, USA

4.1.2 Microscopes

Confocal microscope Leica SP5 63X water lens	Leica Microsystems GmbH, Wetzlar, Germany
Confocal microscope Leica SP8 63X water and oil lens	Leica Microsystems GmbH, Wetzlar, Germany

4.1.3 Software

ChemDraw Professional 17.0

Dfind β-Version

EndNote X8.2

Gimp 2.8.22

ImageJ 1.51g

Leica Application Suite X 3.0.1

MATLAB 2014a

Mestrenova 12.0

Microsoft office 2010 (Word, Excel, Power Point)

OriginPro 9.1

QSoft401 2.5

QTools 3.1

4.1.4 Chemicals

Acetic acid glacial	VWR International GmbH, Darmstadt, Germany
Acetone	VWR International GmbH, Darmstadt, Germany
40% Acrylamide/Bis Solution	Bio-Rad Laboratories GmbH, Munich, Germany
Agarose	Sigma Aldrich, Munich, Germany
Ammonium persulfate (APS)	Sigma Aldrich, Munich, Germany
Antibiotics:	
Ampicillin	Carl Roth GmbH + Co. KG, Karlsruhe, Germany
Kanamycin	Carl Roth GmbH + Co. KG, Karlsruhe, Germany
Chloramphenicol	Sigma Aldrich, Munich, Germany
Brilliant Blue R	Sigma Aldrich, Munich, Germany
Bromophenol Blue	Sigma Aldrich, Munich, Germany
Casein	Provided by Tom Robinson lab
Citric acid	Sigma Aldrich, Munich, Germany
Chloroform	Fisher Scientific UK Ltd, Loughborough, United Kingdom
Chloroform-d	Fisher Scientific UK Ltd, Loughborough, United Kingdom
Copper(II) sulfate pentahydrate ($CuSO_4x5H_2O$)	Sigma Aldrich, Munich, Germany
Diethyl ether	Sigma Aldrich, Munich, Germany
Dimethylformamid	
Dimethyl sulfoxide (DMSO)	Merck KGaA, Darmstadt, Germany
DL-Dithiothreitol (DTT)	Sigma Aldrich, Munich, Germany

1,1'-Dioctadecyl-3,3,3',3'-Tetramethylindodicarbocyanine (DiD)	Fisher Scientific UK Ltd, Loughborough, United Kingdom
1,1'-Dioctadecyl-3,3,3',3'-Tetramethylindocarbocyanine (DiI)	Fisher Scientific UK Ltd, Loughborough, United Kingdom
Ethylenediaminetetraacetic acid (EDTA)	Sigma Aldrich, Munich, Germany
Ethanol	VWR International GmbH, Darmstadt, Germany
Ethyl acetate	VWR International GmbH, Darmstadt, Germany
	Honeywell International Inc., New Jersey, United States
Glycerol	Sigma Aldrich, Munich, Germany
Glycine	Carl Roth GmbH + Co. KG, Karlsruhe, Germany
Hydrogen peroxide (35%) (H_2O_2)	Carl Roth GmbH + Co. KG, Karlsruhe, Germany
Hydrochloric acid (37%) (HCl)	VWR International GmbH, Darmstadt, Germany
Imidazole	Sigma Aldrich, Munich, Germany
Isopropyl-β-D-thiogalactopyranoside IPTG	Fisher Scientific GmbH, Schwerte,Germany
L-Ascorbic acid	Sigma Aldrich, Munich, Germany
β-Mercaptoethanol	Sigma Aldrich, Munich, Germany
Methanol	VWR International GmbH, Darmstadt, Germany
Nickel(II) chloride hexahydrate ($NiCl_2x6H_2O$)	Sigma Aldrich, Munich, Germany
NTA alkyne	Synthesized by Julia Ricken
H_3N-PEG_{3000}-N_3	Iris Biotech GmbH, Marktredwitz, Germany

Lipids:	
1,2-Dioleoyl-sn-glycero-3-phosphocholine (DOPC)	All from Avanti® Polar Lipids, Alabaster USA; Distributed by Sigma Aldrich, Munich, Germany
Palmitoyl-2-oleoylphosphatidylcholine (POPC)	
1-Palmitoyl-2-oleoyl-sn-glycero-3-phospho-(1'-rac-glycerol) (POPG)	
1,2-Dioleoyl-sn-glycero-3-[(N-(5-amino-1-carboxypentyl)iminodiacetic acid) succinyl] (DGS-NTA)	
N-succinyldioctadecylamine with three NTA groups (trisNTA-Suc-DODA)	Gift from Prof. R. Tampé Lab, Institute of Biochemistry, Goethe University Frankfurt, Germany
Phenylmethylsulfonylfluorid (PMSF)	Sigma Aldrich, Munich, Germany
Potassium Hydroxyde (KOH)	Carl Roth GmbH + Co. KG, Karlsruhe, Germany
Polydimethylsiloxane (PDMS)	Provided by Tom Robinson lab
Polyvinyl alcohol	VWR International GmbH, Darmstadt, Germany
2-Propanol	Biosolve BV, Valkenswaard, Netherlands
	Honeywell International Inc., New Jersey, United States
Phenylmethylsulfonyl fluoride (PMSF)	Sigma Aldrich, Munich, Germany
Sodium chloride (NaCl)	Sigma Aldrich, Munich, Germany
Sodium dodecyl sulfate (SDS)	Carl Roth GmbH + Co. KG, Karlsruhe, Germany
Sulfuric acid H_2SO_4 (95-97%)	Sigma Aldrich, Munich, Germany
Sucrose	Sigma Aldrich, Munich, Germany

N,N,N',N'-Tetranethyl-ethylenediamine (TEMED)	Sigma Aldrich, Munich, Germany
Toluene	Fisher Scientific GmbH, Schwerte,Germany
3-(Triethozysilyl)propyl isocyanate	Sigma Aldrich, Munich, Germany
Triethylamine	Sigma Aldrich, Munich, Germany
Trizma® base	Sigma Aldrich, Munich, Germany

4.1.5 Biochemicals

Bacterial medium:

Agar	Carl Roth GmbH + Co. KG, Karlsruhe, Germany
Luria-Bertani (LB)	Carl Roth GmbH + Co. KG, Karlsruhe, Germany
Bovine Serum Albumin (BSA)	Sigma Aldrich, Munich, Germany
Cholesterol	Sigma Aldrich, Munich, Germany
cOmplete Protease inhibitor cocktail tablets	Roche Diagnostics GmbH, Mannheim, Germany
QIAprep Spin Miniprep Kit	QIAGEN Inc., Hilden, Germany

Protein standards:

Color Protein Standard Broad Range	NEB GmbH, Frankfurt am Main, Germany
Unstained Protein Standard Broad Range (10 -200 kDa)	NEB GmbH, Frankfurt am Main, Germany

4.1.6 Disposables

Amicon centrifugal filter units, 15 mL (10 kDa, 100 kDa)	Merck KGaA, Darmstadt, Germany
Amicon centrifugal filter units, 50 mL (10 kDa, 100 kDa)	Merck KGaA, Darmstadt, Germany
Cellulose filters (0.22 µm and 0.45 µm)	Carl Roth GmbH + Co. KG, Karlsruhe, Germany
Cover slips (20 x 20 mm)	Carl Roth GmbH + Co. KG, Karlsruhe, Germany
Electroporation cuvettes (1 mm)	Bio-Rad Laboratories GmbH, Munich, Germany
Eppendorf® tubes (1.5 mL, 2 mL)	Eppendorf AG, Hamburg, Germany
Falcon® tubes (15 mL, 50 mL)	Greiner Bio-One, Frickenhausen, Germany
Microscope slides 24 x 60 mm (#1 and #1.5)	Carl Roth GmbH + Co. KG, Karlsruhe, Germany
Molecular sieves (3Å)	Carl Roth GmbH + Co. KG, Karlsruhe, Germany
Petri dishes (90 mm diameter, 14.2 mm height)	VWR International GmbH, Darmstadt, Germany
Plastic pipettes (5 mL, 10 mL)	Greiner CELLSTAR®, Sigma Aldrich, Munich, Germany
Pipette tips (10 µL, 100 µL, 1000 µL)	STARLAB GmbH, Hamburg, Germany
Silica oxid SiO_2 QCM-D sensors (QSX 303)	LOT-Quantum Design GmbH Darmstadt, Germany
UV-VIS semi-micro polystyrene cuvettes	Brand GmbH + Co KG, Wertheim, Germany
LoBind Eppendorf® tubes (1.5 mL)	Eppendorf AG, Hamburg, Germany

4.1.7 Buffers

Buffer A

50 mM TRIS pH 7.4

300 mM NaCl (add 1 mM DTT right before the purification)

Buffer A minimal

10 mM TRIS pH 7.4
100 mM NaCl

Buffer B

50 mM TRIS pH 7.4

300 mM NaCl

250 mM Imidazole (add 1 mM DTT right before the purification)

Buffer A minimal (experiments with GUVs)

10 mM TRIS pH 7.4

100 mM NaCl

Coomassie brilliant blue (1 L)

1 g brilliant blue

50% (v/v) Methanol

10% (v/v) Acetic Acid

40% MilliQ water

Destaining buffer

40% Methanol

10% Acetic acid

50% MilliQ water

10x SDS PAGE running buffer

250 mM TRIS

1,92 M glycine

1% SDS (w/v) in MilliQ water

TEV binding buffer

50 mM TRIS HCl pH 7.4

300 mM NaCl

30 mM imidazole

1 mM DTT

20x TEV reaction Buffer

1 M TRIS HCl pH 8.0

10 mM EDTA

(add 1 mM DTT right before the purification)

Protein loading dye

4xProtein loading dye (stored at -20 °C):

40% glycerol

240 mM TRIS pH 6.8

8% SDS

0.04% bromphenol blue

5% beta-mercaptoethanol

4.2 Methods

4.2.1 Protein expression and purification

pQE-80L iLID (C530M), pQE-80L MBP-SspB Nano and pQE-80L MBP-SspB R73Q Micro were gifts from Brian Kuhlman (Addgene plasmids # 60408, # 60409 and # 60410 respectively). pQE-80L iLID (C530M) expresses iLID with an N-terminal His6-tag, pQE-80L MBP-SspB Nano expresses Nano with N-terminal His6-MBP-TEV tag (His6-MBP-TEV-Nano, short Nano) and pQE-80L MBP-SspB R73Q Micro expresses Micro with an N-terminal His6-MBP-TEV tag (His6-MBP-TEV-Micro, short Micro). mOrange-GGS was a gift from Spatz Lab. The mOrange-GGS was inserted into the pQE-80L MBP-SspB Nano plasmid or pQE-80L MBP-SspB R73Q Micro after the BamH1 cutting site to yield His6-MBP-TEV-mOrange-Nano/Micro. The TEV cutting site was used to cleave the His6-tag after Ni^{2+}-NTA affinity purification to yield cutNano, cutMicro and cutmOrange-Nano, cutmOrange-Micro. His6-tagged TEV protease originated from the Wombacher Lab and was kindly provided as a glycerol stock of *E. coli* BL21 (DE3) co-transformed with pLysS (chloramphenicol) and pET N_TEV234 (kanamycin) plasmids.

All proteins were recombinantly expressed in *E. coli* following a standard protocol. In short, 10 mL overnight culture was inoculated into 1 L LB medium with the appropriate antibiotic and grown at 37 ^{o}C shaking at 200 rpm till the OD_{600} = 0.6-0.8. The protein expression was induced by addition of 500 µM IPTG (end concentration) and the cultures were grown overnight at 16 ^{o}C (with the exception of TEV protease, which was expressed at room temperature overnight). 1 L of harvested bacteria was resuspended in 20 mL of Buffer A (50 mM Tris, 300 mM NaCl, pH 7.4) with 100 mM PMSF (in methanol) and lysed by sonication. The lysate was separated by centrifugation and the proteins in the supernatant were purified using Ni^{2+}-NTA affinity columns with consequent gel filtration (HiLoad 16/600 Superdex 200 pg, GE Healthcare). For the purification of all proteins Buffer B was used as elution buffer for the Ni^{2+}-NTA affinity columns and all proteins were stored in Buffer A. Only for the His6-TEV protease a different storage buffer (50 mM Tris, 400 mM NaCl, 2 mM EDTA, pH 7.4) was used. The purity of proteins was checked on custom-made 12% SDS-PAGE gels (see Appendix). The protein concentration was determined by UV-Vis spectral analysis.

4.2.2 TEV cutting

To ensure that the protein recruitment due to the iLID-Nano binding and not because of the His6-tag-Ni^{2+}-NTA interaction[216], the His6-tag was cut off from His6-MBP-TEV-Nano and His6-MBP-TEV-mOrange-Nano using His6-TEV protease. The purified proteins were incubated with His6-TEV protease at 1:50 concentration ratio (protein : TEV protease) overnight at 4 ^{o}C (reaction buffer: 50 mM Tris, 0.5 mM EDTA, 1 mM DTT, pH 8.0). Then, the His6-TEV protease and the cut off fragment His6-MBP were removed by binding to a Ni^{2+}-NTA column, while the proteins without the His6-tag were collected in the flow through. The protein will from therfore be named with the prefix “cut”.

4.2.3 Electroporation

To 49.5 µL of electrocompetent DH5α *E. coli* 0.5 µL of the according plasmid DNA was added and mixed by pipetting. The mixture was transferred into a 0.1 cm Electroporation cuvette and a single electrical pulse was given (1.8 kV, according to the preprogrammed settings). Immediately after the pulse 450 µL LB medium were added to the bacteria and the suspension transferred into an Eppendorf tube. The bacteria were allowed to recover at 37 °C, 200 rpm for 1 h. The bacteria suspension was plated on a LB agar plate containing 50 µg/mL of appropriate antibiotic and incubated over night at 37 °C and colonies were picked, if necessary.

4.2.4 Chemical Transformation

To 48 µL of chemocompetent BL21 *E. coli* 2 µL of the according plasmid DNA were added and mixed gently in an Eppendorf tube. After 30 min incubation on ice the bacteria were heat shocked by putting the Eppendorf tube in a heating block at 42 °C for 45 s. The bacteria were transferred to ice immediately for another 2 min. Then 450 µL of LB media was added to the bacteria suspension and incubated at 37 °C for 1 h before plating the mixture on a LB agar plate with 50 µg/mL of appropriate antibiotic. The plate was incubated over night at 37 °C and colonies were picked if necessary.

4.2.5 Plasmid isolation with the QIAprep Spin Miniprep Kit (QIAGEN Inc., Hilden, Germany)

For the isolation of Plasmid DNA a colony was picked from a transformation and transferred to a starter culture (10 mL of LB media with appropriate antibiotic). After overnight incubation at 37 °C, 200 rpm the suspension was spun down (4000 rpm, 4 °C,

10 min) and the supernatant removed carefully without disturbing the pellet. The isolation was done according to the standard protocol. Namely the bacteria pellet was first resuspended in 250 µL Buffer P1, then 250 µL Buffer P 2 was added and the solution carefully inverted for six times. 350 µL Buffer N3 was added within a minute of inverting and again inverted six times. The resulting mixture was spun down (13000 rpm, RT, 10 min) to separate the cell debris from solution. The supernatant was added to a QIAprep 2.0 Spin column and through centrifugation (13000 rpm, RT, 10 min) the plasmid was bound to the column material. To clean the plasmid DNA 750 µL PE Buffer was added and sequential removed through centrifugation (13000 rpm, RT, 1 min). To elute the DNA 30 µL of water was added carefully to the surface of the column, allowed to stand for 1 min and eluted to a clean Eppendorf tube (13000 rpm, RT, 1 min). The concentration of the Plasmid was determined with UV-Vis Nanodrop analysis. The correct base order was determined by sequence analysis done by StarSEQ® GmbH, Mainz, Germany.

4.2.6 SDS-Gel

Table 4.2.1 Chemicals used for SDS-Gel preparation

Chemical/Solution	Stacking gel	Resolving gel (12%)
40% Acrylamid/Bisacrylamid	1.48 mL	7.5 mL
0.5 M Tris pH=6.8	3.78 mL	-
1,5 M Tris pH=8.8	-	6.25 mL
10% SDS	150 µL	250 µL
H2O	9.5 mL	10.9 mL
TEMED	15 µL	12.5 µL
10% APS	75 µL	125 µL
Total Volume	15 mL	25 mL

Four gels were cast at once. All components of the resolving gel were mixed, with APS and TEMED added at last and poured between two glas plates in a Biorad Mini-PROTEAN® Tetra Cell Casting Stand. The hight of gel was adjusted to fit the stacking

gel and overlayed with butanol to allow a straight surface. After the gel solified butanol was removed, APS and TEMED were added to the stacking gel and poured on top of the resolving gel. Immediately a comb was placed in the stacking gel. Excess of gel were removed carefully. After the stacking gel solidified the gels were either used immideiatly or stored in moist environment at 4 °C.

To run an SDS-PAGE 15 µL Protein were mixed with 5 µL protein loading dye and heated to 90 °C for 10 min to ensure full denaturation. 15 µL of this solution were loaded into the pockets of a SDS-gel with one pocket of 5 µL of protein ladder. The Gel was run at 120 mA und 200 V for 37 min. To stain the gel it was put in comassie blue staining solution and heated for 30 s in the microwave. After the gel remained a deep blue the comassie blue staining solution was removed, the gel rinsed with MilliQ and destaining solution was added. The gel was left in destaining solution under shaking for about 1.5 h until the gel showed the protein bands clearly. The gel was scanned for documentation.

4.2.7 SUV preparation

To prepare SUVs the following lipids were mixed in a glass flask: 10 mg/mL 1,2-Dioleoyl-sn-glycero-3-phosphocholine (DOPC) and 5 mol% 1,2-Dioleoyl-sn-glycero-3-[(N-(5-amino-1-carboxypentyl)iminodiacetic acid) succinyl] Ni^{2+} Salt (DGS-NTA-Ni^{2+}) diluted in chloroform. The lipids were carefully deposited as a thin layer to the flask walls by evaporating the chloroform in a nitrogen stream while simultaneously turning the flask.

The residing chloroform was removed by evaporation in vacuum for 1 h. 1 mL Buffer A minimal (10 mM TRIS, 100 mM NaCl, pH 7.4) in 3 mL MilliQ was added to hydrate the lipids, vortexed to ensure that the lipids are fully dissolved and transferred into an Eppendorf tube. The lipids were sonicated for about 1 min till the opaque solution turned clear right before use. Lipid solutions that where not used immediately were stored at -20 °C. Repeated DLS measurements (done by Polymeranalytics, MPIP, Mainz) revealed a constant hydration radius of around 130 nm.

4.2.8 QCM-D

All experiments were performed on a Qsense Analyzer with flow modules for dark measurements and window modules for blue light experiments. Blue light was shone through the window module with a standard 15 W blue light LED lamp. The flow rate was kept at 250 µL/min throughout the experiments.

The following components in Buffer A minimal (10 mM TRIS, 100 mM NaCl, pH 7.4) were washed over a SiO_2 QCM-D crystal at the respective time points and excess proteins or chemicals was washed away with Buffer A minimal after every step: 1) 10 mg/mL DOPC + 5 mol% DGS-NTA with 5 mM $CaCl_2$ to from a supported lipid bilayer, 2) 10 mM $NiCl_2$ for 5 min to load the NTA-groups with Ni^{2+}, 3) 1 mL of 1 µM iLID was flown over the sensor and the pump was stopped until the frequency stabilized. 1 mL of Nano or Micro (4) 250 nM, 5) 500 nM, 6) 1 µM and 7) 2 µM) was washed onto the sensor at increasing concentrations in a stepwise manner, where the pump was stopped and the next concentration was only added after the frequency was stable. Nano or Micro were washed away by flushing an excess of Buffer A minimal. 8) 250 mM imidazole for 3 min to confirm that iLID specifically binds to the lipid bilayer through the His-tag-Ni^{2+}-NTA interaction.

To calculate thermodynamic and kinetic constants the thickness of each layer was calculated using changes in frequency and dissipation in QTools (Bioline Scientific Inc.) according to the standard modelling protocol. The K_d was obtained by fitting the layer thickness at the respective Nano or Micro concentrations to a Hill-fit with one binding site. The k_{off} was computed from the wash off behaviour of Nano or Micro in QTools. The k_{on} was calculated from the relationship of K_d to k_{off}. The mean values were calculated from three technical and biological replicates and the errors are given as the standard deviation.

4.2.9 GUV formation and functionalization

GUVs were prepared using the assisted gel formation method.[63]

First 50 µL of polyvinyl alcohol solution (PVA, 145000 g/mol, 5% w/w in MilliQ, 100 mM sucrose) were dried in a thin layer on top of a 60 x 24 mm glass slide at 50 ^{o}C for 30 min. Then, 5 µL of a lipid solution were dried on the PVA layer at 30 ^{o}C or under vacuum for 1 h. Then a chamber was built on the glass slide with the help of a Teflon frame (ca. 40 mm x 24 mm) and a second glass slide. The lipids were hydrated using ca. 1 mL of Bufer A minimal for 1 h at room temperature allowing GUV formation. The chamber was then inverted and GUVs were harvested. Proteins were immobilized on the GUVs through the His-tag-Ni^{2+}-NTA interaction by adding proteins to a final concentration of 10 nM (if not stated differently) to 100 µL harvested GUVs in suspension and incubating for 30 min in the dark.

Lipid solutions used:

10 mg/mL 1-Palmitoyl-2-oleoylphosphatidylcholine (POPC) + 10 mol% 1-palmitoyl-2-oleoyl-sn-glycero-3-phospho-(1'-rac-glycerol) (POPG) + 0.1 mol% 1,2-dioleoyl-sn-glycero-3-[(N-(5-amino-1-carboxypentyl)iminodiacetic acid) succinyl] Ni^{2+} Salt (DGS-NTA-Ni^{2+}) + 1 mol% 1,1'-Dioctadecyl-3,3,3',3'-Tetramethylindodicarbo-cyanine (DiD) or 1 mol% 1,1'-dioctadecyl-3,3,3',3'-tetramethylindocarbocyanine (DiI) dye in chloroform

10 mg/mL POPC, 10 mol% POPG, 0.5 mol% DGS-NTA-Ni^{2+} and 1 mol% DiD dye in chloroform

10 mg/mL POPC, 10 mol% POPG, 1 mol% DGS-NTA-Ni^{2+} and 1 mol% DiD dye in chloroform

10 mg/mL POPC, 10 mol% POPG, 0.1 mol% DGS-NTA-Ni^{2+}, 20 mol% cholesterol and 1 mol% DiD dye in chloroform

10 mg/mL POPC, 10 mol% POPG, 0.1 mol% DGS-NTA-Ni^{2+}, 40 mol% cholesterol and 1 mol% DiD dye in chloroform

10 mg/mL DOPC + 10 mol% POPG + 0.1 mol% DGS-NTA-Ni^{2+} + 1 mol% DiD in chloroform

If not stated otherwise, all lipids were purchased from Avanti Polar Lipids.

4.2.10 Microscopy light soureces

The light power was measured using a LabMax-TOP meter with an OP-2 VIS power sensor (Coherent Inc.). The sensor was positioned over the microscope objective and the laser power (Argon laser, 488 nm) was measured for different power percentages (1%, 2%, 5%, 10% and 20%) through the 63x water objective (Table 4.2.2).

Table 4.2.2 Light power at different laser power percentage.

Laser power percentage	**Mean power ± Standard deviation [nW]**
1%	70.8 ± 2.7
2%	151.3 ± 5.6
5%	575.5 ± 21
10%	1790 ± 71
20%	6330 ± 238

4.2.11 Protein recruitment to GUVs

For imaging a chamber was build from a cut of Eppendorf tube glued to a clean glass slide (24 x 60 mm) with silica grease. The chamber was incubated with 3% bovine serum albumin (BSA w/v in water) for 20 min prior to the experiment to prevent protein adsorption and the bursting of the GUVs. The chamber was washed 3 times with Buffer A. Afterwards, a solution of iLID functionalized GUVs with DID dye mixed in a 1:1 ratio with a solution of 50 nM Nano-mOrange was transferred into the chamber.

The imaging was performed either on a Leica SP5 laser scanning confocal microscope (for all the experiments except for the patterning) or a Leica SP8 laser scanning confocal microscope with a FRAP (Fluorescence Recovery after Photobleaching) module (for the patterning experiments). An argon laser (488nm) was used to illuminate the samples with the blue light continuously in given intesities and the TRITC channel was used to detect mOrange (excitation max: 557 nm; emission max: 576 nm). A HeNe laser was used to excite the DiD dye (excitation max: 644 nm; emission max: 665 nm) in the GUVs. There is DiD bleed through to the TRITC channel, however despite the bleaching of the DiD dye over time, the intensity of the GUV fluorescence increased under blue light illumination. Illumination with far-red light was done with a standard far-red LED lamp, 15 W, 700-800 nm.

For the quantification of the protein recruitment to GUVs the mean fluorescence intensity of a whole GUV was analysed. The fluorescence intensity of the data point $t = 0$ was subtracted from all other data points. All the data was then normalized by setting the maximum value to 100 and calculating the percentage of intensity change. The experiments were repeated multiple times, minimum 3 GUVs analysed in each case.

4.2.12 Effect of lipid fluidity on protein recruitment and adhesion

GUVs with a different fluidity were prepared to compare the dependence of protein recruitment on the lipid membrane fluidity. To modulate the fluidity we added 20 mol% or 40 mol% choleserol to the used lipid preparation (10 mg/mL POPC + 10 mol% POPG + 0.1 mol% DGS-NTA-Ni^{2+} + 1 mol% DiD). Additionally, a 1,2-dioleoyl-*sn*-glycero-3-phosphocholine (DOPC) (10 mg/mL DOPC + 10 mol% POPG + 0.1 mol% DGS-NTA-Ni^{2+} + 1 mol% DiD) lipid preparation was used for the comparison.

The GUVs were prepared, hydrated with Buffer A minimal, harvested and functionalized with iLID protein (10 nM) as described above. After 30 min incubation in the dark 25 nM final concentration of mOrange-Nano was added to the chamber. The GUVs were illuminated with a 488 nm laser (Argon laser, 5%) through 63x water objective for

15 min, while continuously acquiring fluorescent images for Nano-mOrange in TRITC channel (excitation max: 557 nm; emission max: 576 nm) and DID in Cy5 channel (excitation max: 644 nm; emission max: 665 nm) .

4.2.13 Protein recruitment to ROI

The protein recruitment to a region of interest (ROI) was performed following the same protocol as in the protein recruitment to the whole GUV. In this case only a small ROI on the side of a GUV was constantly illuminated with blue light (488 nm, 5% power), while acquiring images at 1 image/s in the TRITC channel (excitation max: 557 nm; emission max: 576 nm) for up to 30 min.

4.2.14 Protein recruitment to a single GUV

For the protein recruitment to a single GUV experiments the GUVs (10 mg/mL 1-Palmitoyl-2-oleoylphosphatidylcholine (POPC) + 10 mol% 1-palmitoyl-2-oleoyl-sn-glycero-3-phospho-(1'-rac-glycerol) (POPG) + 0.1 mol% 1,2-dioleoyl-sn-glycero-3-[(N-(5-amino-1-carboxypentyl)iminodiacetic acid) succinyl] (DGS-NTA) Ni^{2+} Salt + 1 mol% 1,1'-Dioctadecyl-3,3,3',3'-Tetramethylindodicarbo-cyanine (DiD) dye in chloroform, from Avanti Polar Lipids) were prepared, hydrated with Buffer A minimum and harvested as described above. The GUVs were then incubated with 10 nM iLID for 30 min in the dark and afterwards 25 nM final concentration of mOrange-Nano was added to the chamber. The GUVs were allowed to settle and a region with several GUVs close but not touching each other was chosen. One of the GUVs in the field of view was illuminated with a 488 nm laser (Argon laser, 5%) through 63x water objective for 15 min, while the other GUVs were not illuminated. Fluorescent images for mOrange-Nano in TRITC channel (excitation max: 557 nm; emission max: 576 nm) and DID in Cy5 channel (excitation max: 644 nm; emission max: 665 nm) were acquired simultaneously for the whole field of view.

4.2.15 Patterning on GUV carpet

For the patterning experiments a layer of GUVs (4 mM total lipid concentration, POPC + 10% POGP + 1 % N-succinyldioctadecylamine with three NTA groups (trisNTA-Suc-DODA)[217] was prepared as described above, leaving out the harvesting step and working directly with the hydrated layer of GUVs in the hydration chamber. For the hydration step a modified buffer with lower salt concentrations was used to prevent the

GUVs from bursting (10 mM Tris, 150 mM NaCl, pH 7.4). The GUVs were then incubated with 10 nM iLID for 30 min in the dark and afterwards 50 nM mOrange-Nano was flushed into the chamber. To create a pattern the FRAP-Module of the Leica SP8 laser scanning confocal microscope was used to define the ROI. The regions of interest were illuminated with a 496 nm laser for up to 1 min, and fluorescent images for mOrange-Nano were acquired simultaneously.

4.2.16 Surface functionalization and passivation

Standard microscopy slides (60 mm x 24 mm, # 1.5) were functionalized with PEG-NTA as previously described with either 100% or 10%PEG-NTA.[202] The NTA-groups were the loaded with Ni^{2+} by incubating the surfaces in 100 mM $NiCl_2$ solution for 15 min, RT. The surfaces were thoroughly washed by placing them in two consequential Buffer A minimal baths. Then the surfaces were incubated with 1 µM iLID or Micro solution for 30 min at room temperature and again thoroughly washed with buffer immediately before use. The sample was always handled in the dark or under red light by a standard red 15 W LED lamp.

To passivate microscopy slides to prevent GUV bursting or absorption of protein, the slides were incubated with 3 wt% BSA solution in MilliQ for 15 min, RT. The excess was washed off with MiliQ and dried in a nitrogen stream before immediate use.

4.2.17 Protein recruitment to functionalized glass surfaces

The 20x20 mm glass surfaces were functionalized with Ni^{2+}-NTA terminated PEG as previously described.[202]

Subsequently, each surface was incubated with 100 µL of 10 µM iLID, which can bind to the surface through His-tag-Ni^{2+}-NTA interaction, and briefly washed with Buffer A. The surfaces were incubated either in the dark or under blue light (488 nm, light intensity of 0.63 mW/m^2) for 30 min with 1 µM Nano-mOrange solution, briefly washed with excess of Buffer A, and mounted on glass slides with 50 µL Mowiol 4-88. Fluorescence images were acquired in TRITC channel using an inverted fluorescence microscope (DMi8, Leica) through the 40x air objective. The mean fluorescence of each surface was then quantified with ImageJ and the results were statistically analysed for significance with the Mann-Whitney test.

4.2.18 Synthesis of $(CH_3CH_2O)_3Si$-PEG_{3000}-azid

The synthesis was performed as previously described.[202] Namely, 1 equiv. of H_3N-PEG_{3000}-N_3 (Iris Biotech GmbH, Marktredwitz, Germany) was dissolved in ca. 10 mL dry DMF under argon atmosphere. 1.1 equiv. of 3-(Triethoxysilyl)-propylisocyanate was added and the reaction mixture was stirred at RT for 24 h. Next the solution was cooled to 0 °C and an excess of diethyl ether added till a white precipitation was detected. The precipitate was collected through centrifugation (4000 rpm, 4 °C, 5 min), filtered off, washed with chilled diethyl ether and dried under vacuum. ^{1}H NMR [300 MHz, CDCl3] δ 4.45 (m, 2H, N_3-CH_2), 3.83−3.48 (m, 1165H; O−CH2), 3.41 (m, 4H, CH_2-C=O, N-CH_2), 2.92 (br s, 2H, Si−CH2−CH2−C*H*2), 1.77 (br s, 2H, Si−CH2−C*H*2), 1.22 (m, 9H, CH3), 0.65 (br s, 2H, Si−C*H*2) (for NMR see Appendix).

4.2.19 Deflated GUV preparation

To deflate GUV´s the functionalized GUV preparation was left standing open to air for ca. 1 h at RT to increase the salt concentration of the Buffer and thus diffusion of water out of the GUV.

4.2.20 Imaging of GUV adhesion to surface

Press-to-Seal™ silicon isolators were used to create a chamber between a functionalized and a passivated microscopy slide to prevent evaporation of the imaging sample. Into this chamber a drop of 10 µL of functionalized GUV solution with 10 µL buffer was introduced. For imaging, a Leica SP5 laser scanning confocal microscope with a FRAP (Fluorescence Recovery after Photobleaching) module with a 63x water objective was used. The 633 nm laser was used to image the lipid dye DiD and thus the membrane (indicated in red in microscopy pictures). In the case of membrane staining with DiI the 561 nm laser was used for imaging. The surface was detected by the transmission light channel and imaged in reflection with the 561 nm laser (indicated in green in microscopy pictures). For imaging the adhesion of GUVs, (x,z) cross-section (relative to the substrate in the (x,y) plane) confocal scans were obtained at varying sample heights. If not indicated otherwise, the sample was observed in the (x,z) plane and illuminated continuously with blue light (488 nm Laser) and 1 scan per ca. 2 s was acquired using 633 nm excitation light. Following illumination protocol was used: about 30 s of dark, then ca. 10 min of blue light exposure with the 488 nm laser at 10% laser intensity (1790 ± 71 nW), followed by another ca. 10 min observation without 488 nm in the dark to show reversibility. The observation was stopped when no further reversion was visible.

The GUVs were always imaged at the position of maximum diameter between adhering GUV segment and the substrate. The shown pictures were scaled compared to the spherical GUVs in solution to avoid distortion of the image. To image multiple adhesions of the same GUV the same protocol was used as described above but the illumination time with the 488 nm laser and the reversion time in the dark were reduced to 5 min each. The dark/light cycle was repeated up to 4 times.

4.2.21 Analysis of Micro distribution over the GUV

The experiment was performed the same way as described above (imaging of GUV adhesion) with following changes. Instead of functionalizing the GUVs with Micro, His-tagged Micro-mOrange was used, making it possible to observe the Micro-mOrange distribution over the GUV in the TRITC channel on a confocal microscope. The GUVs were observed in the x,z plane at 1 scan ca. every 2 s. The GUVs were initially imaged in the dark for about 30 s and then exposed to blue light for ca. 15 min with the 488 nm laser at 10% laser intensity. The mOrange fluorescence was analysed with ImageJ software, measuring the mean intensity of fluorescence before and after adhesion at the adhesion site and the top of the GUV and subtracting the contribution of the surface reflection at the adhesion site.

4.2.22 Quantification of adhesion energy

Adhesion energies were estimated from the global shape of the GUV as described in detail elsewhere[120]. Images were obtained by confocal microscopy and were corrected for optical aberrations and other distortions by calibration to spherical GUV in solution. Adhering GUV area, volume and substrate-membrane contact area were extracted from (x,z) cross-section scans by image analysis (Image J 1.52b). Using the obtained geometry parameters, adhesion energies were estimated from analytical approximations of shape equations describing adhering vesicles (method termed „First method of image analysis" in Ref.[120]). The method relies on the measurements of adhesion area and GUV area and volume. Area and volume were extracted from three dimensional reconstructions obtained by confocal microscopy (vertical cross sections). The analysis assumed axisymmetric GUV shapes and area and volume were found by integration of the vesicle contour. Because shape fluctuations lead to distortions during this analysis, up two four measurements were obtained per GUV and the median value for area and volume was used. The relation between adhesion energy W rescaled by the membrane bending rigidity κ can be expressed to a leading order in $R - R_0$ as [209]:

$$(1)\ W/\kappa \approx \frac{2}{(R-R_0)^2}\left(\frac{\cos\left(\frac{\theta_0}{2}\right)}{1+\sin\left(\frac{\theta_0}{2}\right)}\right)^2$$

where the angle θ_0 and radius R_0 only depend on the area and volume of the GUV.[209] The change in GUV adhesion energies between dark and light activated state was found by measurement of adhesion area radius R for a given set of θ_0, R_0 values measured on an individual GUV.

4.2.23 Quantification of adhesion kinetics

The GUV adhesion and unbinding kinetics were quantified by the change of GUV-substrate contact area during light activation or incubation in the dark. Time-series from confocal (x,z) scans were obtained and quantification was performed by automated image analysis. Micrographs of GUV membrane signal and water-substrate interfaces were binarized individually (ImageJ 1.52b). The overlap (*co-localisation)* between the two channels was estimated by multiplication of the two binary images. Further image processing (Gaussian filtering and subsequent edge detection) was used to find an estimate of the adhesion area of the GUV at each time-point (MATLAB 2014a). The adhesion area is a measure of the change of adhesion energy as long the GUV area and volume stay approximately constant which is usually the case during the experiments, see eq. (1).

4.2.24 Light guiding

To observe the GUVs the same settings imaging settings were used as described above with the following changes: The GUVs were observed in x,y-direction in the immediate vicinity of the glass substrate (z=0 position), where the adhesion area of the GUV with the glass substrate could be observed. A region of interest (ROI) was chosen such that it included ca. half of the GUV adhesion area and a vesicle-free region of similar surface area. The ROI was illuminated continuously with blue light (488 nm Laser) at 10% laser intensity (1790 ± 71 nW) and the GUV's movement was monitored by acquiring 1 scan every 2 s using 633 nm laser light excitation till the GUV stopped movement into the illuminated area. Then the ROI was adjusted such that again half of the GUV was within the ROI and the new ROI was illuminated using the same settings. Depending on the size of ROI every ROI was illuminated for ca. 1-2 min.

To analyse the speed of GUV movement, the GUV images were binarized with ImageJ1.8 and holes were filled by using the ImageJ. Subsequently, the centre of mass

of the GUV was determined for each time point using the analyse particle tool in ImageJ1.8. From the coordinates of the centre of mass the displacement was calculated for each time interval and the speed was calculated for 8 different GUVs.

4.2.25 Protein loading of GUVs

The GUVs were prepared as described before (4.2.9 GUV formation and functionalization). In case of loading of GUVs with a fluorescent protein (mOrange without His-tag, cutmOrange) 1 µM (end concentration) of protein was added to the hydration buffer. The GUVs were left standing at RT for 1 h for the GUVs to form, before harvesting them. They were diluted with Buffer A minimal at least 1:1 till the flourescence showed a clear difference of outside buffer and GUV loading. They were functionalied with iLID as before.

4.2.26 GUV-GUV-interaction and reversion

All glas surfaces were passivated before the experiments with BSA. A chamber was built with two passivated glass slides and a Press-to-Seal^{TM} insolator. The iLID functionalized DiD GUVs were mixed 1:1 with Buffer in the chamber and according to the experiment the appropiate DiI GUV preparation (deflated, functionalized with nano, and/or loaded) was added. The sample was allowed to settle for ca. 15 to 30 min before microscopy started. Two GUVs in relative vicinity were chosen and illuminated with a 488 nm laser (Argon laser, 10%) through 63x water objective for 15 min. DiI was imaged in the TRITC channel (excitation max: 557 nm; emission max: 576 nm) and DID in Cy5 channel (excitation max: 644 nm; emission max: 665 nm) was acquired simultaneously for the whole field of view.

To determine the light dependence of the interaction the observed GUVs were kept in dark for at least 1 min before illumination with blue light. For reversion experiments, two GUVs in vicinity or with already showing adhesion where illuminated at least 10 min with blue light before the 488 nm laser was stopped while continously imaging.

4.2.27 Kinetic analysis of GUV-GUV interaction and reversion

To analyse the kinetic behavior of the GUV-GUV interaction 4 examples of adhesion and 4 examples of reversion were analysed by measuring the interaction area between the vesicles over time. The time lines of adhesion where analyzed with the ImageJ1.8 line tool by measuring the length of the site of green and red fluorescence overlay every 2 to

5 pictures (ca. every 5 s), in times of fast change every picture was analysed (every ca. 1 s). The length change was depicted against the time with OriginPro9.1.

4.2.28 Microfluidic bulk experiment

GUVs were prepared as described before (4.2.9 GUV formation and functionalization). They were then injected into a casein passivated polydimethylsiloxane (PDMS) microfluidic chamber with 204 of traps (provided by Tom Robinsion lab). The GUVs functionalized with iLID (DiD) and Nano (DiD) were captured in the traps in a random order. One trap was chosen that showed the best ratio (ideally 1:1) between iLID and Nano functionalized GUVs as well as the GUVs with the least imperfections. The chamber was then either illuminated with 488 nm Laser light at 10% or kept in the dark for at least 15 min. After that the GUVs were pushed out of the chamber by applying a reverse flow in steps from 0.1 µL/min to 0.8 µL/min while continuously imaging the chamber.

5 Bibliography

1. Xu, C., S. Hu, and X. Chen, *Artificial cells: from basic science to applications.* Mater Today (Kidlington), 2016. **19**, 516-532.

2. Blain, J.C. and J.W. Szostak, *Progress toward synthetic cells.* Annu Rev Biochem, 2014. **83**, 615-40.

3. Gopfrich, K., I. Platzman, and J.P. Spatz, *Mastering Complexity: Towards Bottom-up Construction of Multifunctional Eukaryotic Synthetic Cells.* Trends Biotechnol, 2018. **36**, 938-951.

4. Schwille, P., *Bottom-Up Synthetic Biology: Engineering in a Tinkerer's World.* Science, 2011. **333**, 1252-1254.

5. Auslander, S., D. Auslander, and M. Fussenegger, *Synthetic Biology-The Synthesis of Biology.* Angew Chem, 2017. **56**, 6396-6419.

6. Dzieciol, A.J. and S. Mann, *Designs for life: protocell models in the laboratory.* Chem Soc Rev, 2012. **41**, 79-85.

7. Roberts, M.A., et al., *Synthetic biology: biology by design.* Microbiology, 2013. **159**, 1219-20.

8. Glass, J.I., et al., *Essential genes of a minimal bacterium.* Proc Natl Acad Sci USA, 2006. **103**, 425-30.

9. Luisi, P.L., P. Walde, and T. Oberholzer, *Lipid vesicles as possible intermediates in the origin of life.* Curr Opin Colloid Interface Sci, 1999. **4**, 33-39.

10. Clomburg, J.M. and R. Gonzalez, *Biofuel production in Escherichia coli: the role of metabolic engineering and synthetic biology.* Appl Microbiol Biotechnol, 2010. **86**, 419-34.

11. Madhavan, A., et al., *Synthetic Biology and Metabolic Engineering Approaches and Its Impact on Non-Conventional Yeast and Biofuel Production.* Front Energy Res, 2017. **5**.

12. Oldham, P., S. Hall, and G. Burton, *Synthetic biology: mapping the scientific landscape.* PLoS One, 2012. **7**, e34368.

13. Luisi, P.L., F. Ferri, and P. Stano, *Approaches to semi-synthetic minimal cells: a review.* Naturwissenschaften, 2006. **93**, 1-13.

14. Salehi-Reyhani, A., O. Ces, and Y. Elani, *Artificial cell mimics as simplified models for the study of cell biology.* Exp Biol Med (Maywood), 2017. **242**, 1309-1317.

15. Matosevic, S., *Synthesizing artificial cells from giant unilamellar vesicles: state-of-the art in the development of microfluidic technology.* Bioessays, 2012. **34**, 992-1001.

16. Schmidt, D. and Y.K. Cho, *Natural photoreceptors and their application to synthetic biology.* Trends Biotechnol, 2015. **33**, 80-91.

17. Schwille, P., et al., *MaxSynBio: Avenues Towards Creating Cells from the Bottom Up.* Angew Chem, 2018. **57**, 13382-13392.

18. Choi, H.J. and C.D. Montemagno, *Artificial organelle: ATP synthesis from cellular mimetic polymersomes.* Nano Lett, 2005. **5**, 2538-42.

19. Oesterhelt, D. and W. Stoeckenius, *Rhodopsin-Like Protein from Purple Membrane of Halobacterium-Halobium.* Nature-New Biology, 1971. **233**,149.

20. Otrin, L., et al., *Toward Artificial Mitochondrion: Mimicking Oxidative Phosphorylation in Polymer and Hybrid Membranes.* Nano Lett, 2017. **17**, 6816-6821.

21. Weiss, M., et al., *Sequential bottom-up assembly of mechanically stabilized synthetic cells by microfluidics.* Nat Mater, 2018. **17**, 89-96.

22. Erb, T.J., P.R. Jones, and A. Bar-Even, *Synthetic metabolism: metabolic engineering meets enzyme design.* Curr Opin Chem Biol, 2017. **37**, 56-62.

23. Schwander, T., et al., *A synthetic pathway for the fixation of carbon dioxide in vitro.* Science, 2016. **354**, 900-904.

24. Ostwald, W., *On the assumed isomerism of red and yellow mercury oxide and the surface-tension of solid bodies.* Zeitschrift Fur Physikalische Chemie--Stochiometrie Und Verwandtschaftslehre, 1900. **34**, 495-503.

25. Haluska, C.K., et al., *Time scales of membrane fusion revealed by direct imaging of vesicle fusion with high temporal resolution.* Proc Natl Acad Sci USA, 2006. **103**, 15841-15846.

26. Kurihara, K., et al., *Self-reproduction of supramolecular giant vesicles combined with the amplification of encapsulated DNA.* Nat Chem, 2011. **3**, 775-81.

27. Georgiev, V.N., et al., *Area Increase and Budding in Giant Vesicles Triggered by Light: Behind the Scene.* Adv Sci, 2018. **5**, 1800432

28. Osawa, M. and H.P. Erickson, *Liposome division by a simple bacterial division machinery.* Proc Natl Acad Sci USA, 2013. **110**, 11000-4.

29. Pierschbacher, M.D. and E. Ruoslahti, *Cell attachment activity of fibronectin can be duplicated by small synthetic fragments of the molecule.* Nature, 1984. **309**, 30-3.

30. Schrum, J.P., T.F. Zhu, and J.W. Szostak, *The origins of cellular life.* Cold Spring Harb Perspect Biol, 2010. **2**, a002212.

31. Huang, X., et al., *Interfacial assembly of protein-polymer nano-conjugates into stimulus-responsive biomimetic protocells.* Nat Commun, 2013. **4**, 2239.

32. Gebicki, J.M. and M. Hicks, *Ufasomes Are Stable Particles Surrounded by Unsaturated Fatty-Acid Membranes.* Nature, 1973. **243**, 232-234.

33. Chen, I.A. and J.W. Szostak, *A kinetic study of the growth of fatty acid vesicles.* Biophys J, 2004. **87**, 988-98.

34. Mansy, S.S., *Membrane transport in primitive cells.* Cold Spring Harb Perspect Biol, 2010. **2**, a002188.

35. Shum, H.C., et al., *Double emulsion templated monodisperse phospholipid vesicles.* Langmuir, 2008. **24**, 7651-3.

36. Ugrinic, M., et al., *Microfluidic formation of proteinosomes.* Chem Commun, 2018. **54**, 287-290.

37. Liu, X., et al., *Hierarchical Proteinosomes for Programmed Release of Multiple Components.* Angew Chem, 2016. **55**, 7095-100.

38. Li, M., X. Huang, and S. Mann, *Spontaneous growth and division in self-reproducing inorganic colloidosomes.* Small, 2014. **10**, 3291-8.

39. Huang, X., et al., *Design and construction of higher-order structure and function in proteinosome-based protocells.* J Am Chem Soc, 2014. **136**, 9225-34.

40. Chang, T.M.S., *Semipermeable Microcapsules.* Science, 1964. **146**, 524.

41. Discher, D.E. and A. Eisenberg, *Polymer vesicles.* Science, 2002. **297**, 967-73.

42. Kamat, N.P., J.S. Katz, and D.A. Hammer, *Engineering Polymersome Protocells.* J Phys Chem Lett, 2011. **2**, 1612-1623.

43. Li, M., et al., *Synthetic cellularity based on non-lipid micro-compartments and protocell models.* Curr Opin Chem Biol, 2014. **22**, 1-11.

44. Petit, J., et al., *A modular approach for multifunctional polymersomes with controlled adhesive properties.* Soft Matter, 2018. **14**, 894-900.

45. Petit, J., et al., *Vesicles-on-a-chip: A universal microfluidic platform for the assembly of liposomes and polymersomes.* Eur Phys J E Soft Matter, 2016. **39**, 59.

46. Chu, L.Y., et al., *Controllable monodisperse multiple emulsions.* Angew Chem, 2007. **46**, 8970-4.

47. Wilson, D.A., R.J. Nolte, and J.C. van Hest, *Autonomous movement of platinum-loaded stomatocytes.* Nat Chem, 2012. **4**, 268-74.

48. Discher, B., et al., *Tough polysomes: soft giant vesicles made from large-molecular-weight diblock copolymer.* Biophys J, 1999. **76**, A435-A435.

49. Kumar, M., et al., *Highly permeable polymeric membranes based on the incorporation of the functional water channel protein Aquaporin Z.* Proc Natl Acad Sci USA, 2007. **104**, 20719-20724.

50. Kim, K.T., et al., *A Polymersome Nanoreactor with Controllable Permeability Induced by Stimuli-Responsive Block Copolymers.* Adv Mater, 2009. **21**, 2787.

51. Cheng, Z.L. and A. Tsourkas, *Paramagnetic porous polymersomes.* Langmuir, 2008. **24**, 8169-8173.

52. Pickering, S.U., *Emulsions.* J Chem Soc, 1907. **91**, 2001-2021.

53. Dinsmore, A.D., et al., *Colloidosomes: Selectively permeable capsules composed of colloidal particles.* Science, 2002. **298**, 1006-1009.

54. Li, M., et al., *In vitro gene expression and enzyme catalysis in bio-inorganic protocells.* Chem Sci, 2011. **2,** 1739.

55. Li, M., et al., *Electrostatically gated membrane permeability in inorganic protocells.* Nat Chem, 2013. **5**, 529-36.

56. Hsu, M.F., et al., *Self-assembled shells composed of colloidal particles: Fabrication and characterization.* Langmuir, 2005. **21**, 2963-2970.

57. Thompson, K.L. and S.P. Armes, *From well-defined macromonomers to sterically-stabilised latexes to covalently cross-linkable colloidosomes: exerting control over multiple length scales.* Chem Commun, 2010. **46**, 5274-6.

58. Fenz, S.F. and K. Sengupta, *Giant vesicles as cell models.* Integr Biol, 2012. **4**, 982-95.

59. Fenz, S.F., R. Merkel, and K. Sengupta, *Diffusion and intermembrane distance: case study of avidin and E-cadherin mediated adhesion.* Langmuir, 2009. **25**, 1074-85.

60. Menger, F.M. and M.I. Angelova, *Giant vesicles: Imitating the cytological processes of cell membranes.* Acc Chem Res, 1998. **31**, 789-797.

61. Bangham, A.D., M.M. Standish, and J.C. Watkins, *Diffusion of univalent ions across the lamellae of swollen phospholipids.* J Mol Biol, 1965. **13**, 238-52.

62. Reeves, J.P. and R.M. Dowben, *Formation and Properties of Thin-Walled Phospholipid Vesicles.* J Cell Physiol, 1969. **73**, 49.

63. Weinberger, A., et al., *Gel-assisted formation of giant unilamellar vesicles.* Biophys J, 2013. **105**, 154-64.

64. Angelova, M.I. and D.S. Dimitrov, *Liposome Electroformation.* Faraday Discuss, 1986. **81**, 303.

65. Deshpande, S., et al., *Octanol-assisted liposome assembly on chip.* Nat Commun, 2016. **7**, 10447.

66. Kahya, N., *Protein-protein and protein-lipid interactions in domain-assembly: lessons from giant unilamellar vesicles.* Biochim Biophys Acta, 2010. **1798**, 1392-8.

67. Singer, S.J. and G.L. Nicolson, *The Fluid Mosaic Model of the Structure of Cell Membranes.* Science, 1972. **175**, 720.

68. Veatch, S.L. and S.L. Keller, *Separation of liquid phases in giant vesicles of ternary mixtures of phospholipids and cholesterol.* Biophys J, 2003. **85**, 3074-3083.

69. Lingwood, D. and K. Simons, *Lipid rafts as a membrane-organizing principle.* Science, 2010. **327**, 46-50.

70. Dezi, M., et al., *Detergent-mediated incorporation of transmembrane proteins in giant unilamellar vesicles with controlled physiological contents.* Proc Natl Acad Sci USA, 2013. **110**, 7276-81.

71. Kuruma, Y., et al., *A synthetic biology approach to the construction of membrane proteins in semi-synthetic minimal cells.* Biochim Biophys Acta, 2009. **1788**, 567-74.

72. Gaul, V., et al., *The lateral diffusion and fibrinogen induced clustering of platelet integrin alphaIIbbeta3 reconstituted into physiologically mimetic GUVs.* Integr Biol, 2015. **7**, 402-11.

73. Streicher, P., et al., *Integrin reconstituted in GUVs: a biomimetic system to study initial steps of cell spreading.* Biochim Biophys Acta, 2009. **1788**, 2291-300.

74. Nii, T. and F. Ishii, *Encapsulation efficiency of water-soluble and insoluble drugs in liposomes prepared by the microencapsulation vesicle method.* Int J Pharm, 2005. **298**, 198-205.

75. Fischer, A., A. Franco, and T. Oberholzer, *Giant vesicles as microreactors for enzymatic mRNA synthesis.* ChemBioChem, 2002. **3**, 409-17.

76. Shohda, K.-i. and T. Sugawara, *DNA polymerization on the inner surface of a giant liposome for synthesizing an artificial cell model.* Soft Matter, 2006. **2**, 402–408.

77. Tsumoto, K., et al., *Giant liposome as a biochemical reactor: Transcription of DNA and transportation by laser tweezers.* Langmuir, 2001. **17**, 7225-7228.

78. Walde, P. and S. Ichikawa, *Enzymes inside lipid vesicles: Preparation, reactivity and applications.* Biomol Eng, 2001. **18**, 143-177.

79. Kretschmer, S. and P. Schwille, *Toward Spatially Regulated Division of Protocells: Insights into the E. coli Min System from in Vitro Studies.* Life, 2014. **4**, 915-28.

80. Kretschmer, S. and P. Schwille, *Pattern formation on membranes and its role in bacterial cell division.* Curr Opin Cell Biol, 2016. **38**, 52-9.

81. Banerjee, R., *Liposomes: applications in medicine.* J Biomater Appl, 2001. **16**, 3-21.

82. Hartman, N.C. and J.T. Groves, *Signaling clusters in the cell membrane.* Curr Opin Cell Biol, 2011. **23**, 370-6.

83. Dillard, P., et al., *Nano-clustering of ligands on surrogate antigen presenting cells modulates T cell membrane adhesion and organization.* Integr Biol, 2016. **8**, 287-301.

84. Schweizer, J., et al., *Geometry sensing by self-organized protein patterns.* Proc Natl Acad Sci USA, 2012. **109**, 15283-8.

85. Zieske, K., G. Chwastek, and P. Schwille, *Protein Patterns and Oscillations on Lipid Monolayers and in Microdroplets.* Angew Chem, 2016. **55**, 13455-13459.

86. Golestaneh, A.F. and B. Nadler, *Modeling of cell adhesion and deformation mediated by receptor-ligand interactions.* Biomech Model Mechanobiol, 2016. **15**, 371-87.

87. Wehrle-Haller, B., *Assembly and disassembly of cell matrix adhesions.* Curr Opin Cell Biol, 2012. **24**, 569-81.

88. Maheshwari, G., et al., *Cell adhesion and motility depend on nanoscale RGD clustering.* J Cell Sci, 2000. **113**, 1677-1686.

89. Pearson, D. and A.D. Abell, *Structural optimization of photoswitch ligands for surface attachment of alpha-chymotrypsin and regulation of its surface binding.* Chemistry, 2010. **16**, 6983-92.

90. Rudd, A.K., J.M. Valls Cuevas, and N.K. Devaraj, *SNAP-Tag-Reactive Lipid Anchors Enable Targeted and Spatiotemporally Controlled Localization of Proteins to Phospholipid Membranes.* J Am Chem Soc, 2015. **137**, 4884-7.

91. Zhang, J., et al., *Photoswitched protein adsorption on electrostatically self-assembled azobenzene films.* ChemPhysChem, 2012. **13**, 2671-5.

92. Bhagawati, M., et al., *Native Laser Lithography of His-Tagged Proteins by Uncaging of Multivalent Chelators.* J Am Chem Soc, 2010. **132**, 5932.

93. Gatterdam, V., et al., *Three-dimensional protein networks assembled by two-photon activation.* Angew Chem, 2014. **53**, 5680-4.

94. Hengsakul, M. and A.E.G. Cass, *Protein patterning with a photoactivatable derivative of biotin.* Bioconjugate Chem, 1996. **7**, 249-254.

95. Reuther, C., et al., *Programmable patterning of protein bioactivity by visible light.* Nano Lett, 2014. **14**, 4050-7.

96. Chen, Z., et al., *Photon upconversion lithography: patterning of biomaterials using near-infrared light.* Adv Mater, 2015. **27**, 2203-6.

97. Weis, P. and S. Wu, *Light-Switchable Azobenzene-Containing Macromolecules: From UV to Near Infrared.* Macromol Rapid Commun, 2018. **39**, 1700220.

98. Terai, T., et al., *Rational development of caged-biotin protein-labeling agents and some applications in live cells.* Chem Biol, 2011. **18**, 1261-72.

99. Green, N.M., *Avidin .1. Use of [14c]Biotin for Kinetic Studies and for Assay.* Biochem J, 1963. **89**, 585.

100. Laboria, N., R. Wieneke, and R. Tampe, *Control of nanomolar interaction and in situ assembly of proteins in four dimensions by light.* Angew Chem, 2013. **52**, 848-53.

101. Doh, J. and D.J. Irvine, *Photogenerated polyelectrolyte bilayers from an aqueous-processible photoresist for multicomponent protein patterning.* J Am Chem Soc, 2004. **126**, 9170-1.

102. Wegner, S.V., O.I. Senturk, and J.P. Spatz, *Photocleavable linker for the patterning of bioactive molecules.* Sci Rep, 2015. **5**, 18309.

103. DeForest, C.A. and D.A. Tirrell, *A photoreversible protein-patterning approach for guiding stem cell fate in three-dimensional gels.* Nat Mater, 2015. **14**, 523-31.

104. Chen, X., et al., *"Molecular Activity Painting": Switch-like, Light-Controlled Perturbations inside Living Cells.* Angew Chem, 2017. **56**, 5916-5920.

105. You, C., et al., *Affinity capturing for targeting proteins into micro and nanostructures.* Anal Bioanal Chem, 2009. **393**, 1563-70.

106. McMillen, P. and S.A. Holley, *Integration of cell-cell and cell-ECM adhesion in vertebrate morphogenesis.* Curr Opin Cell Biol, 2015. **36**, 48-53.

107. Anderson, L.R., T.W. Owens, and M.J. Naylor, *Integrins in development and cancer.* Biophys Rev, 2014. **6**, 191-202.

108. Ni, H. and J. Freedman, *Platelets in hemostasis and thrombosis: role of integrins and their ligands.* Transfusion and Apheresis Science, 2003. **28**, 257-264.

109. Hynes, R.O., *Integrins: bidirectional, allosteric signaling machines.* Cell, 2002. **110**, 673-87.

110. Mui, K.L., C.S. Chen, and R.K. Assoian, *The mechanical regulation of integrin-cadherin crosstalk organizes cells, signaling and forces.* J Cell Sci, 2016. **129**, 1093-100.

111. Weber, G.F., M.A. Bjerke, and D.W. DeSimone, *Integrins and cadherins join forces to form adhesive networks.* J Cell Sci, 2011. **124**, 1183-93.

112. Gumbiner, B.M., *Regulation of cadherin-mediated adhesion in morphogenesis.* Nat Rev Mol Cell Biol, 2005. **6**, 622-34.

113. Fuchs, E. and S. Raghavan, *Getting under the skin of epidermal morphogenesis.* Nat Rev Genet, 2002. **3**, 199-209.

114. Gahmberg, C.G., et al., *Regulation of integrin activity and signalling.* Biochim Biophys Acta, 2009. **1790**, 431-44.

115. Takagi, J., et al., *Global conformational rearrangements in integrin extracellular domains in outside-in and inside-out signaling.* Cell, 2002. **110**, 599-611.

116. Klezovitch, O. and V. Vasioukhin, *Cadherin signaling: keeping cells in touch.* F1000Res, 2015. **4**, 550.

117. Yap, A.S., C.M. Niessen, and B.M. Gumbiner, *The juxtamembrane region of the cadherin cytoplasmic tail supports lateral clustering, adhesive strengthening, and interaction with p120ctn.* J Cell Biol, 1998. **141**, 779-89.

118. Burute, M. and M. Thery, *Spatial segregation between cell-cell and cell-matrix adhesions.* Curr Opin Cell Biol, 2012. **24**, 628-36.

119. Tsai, J. and L. Kam, *Rigidity-dependent cross talk between integrin and cadherin signaling.* Biophys J, 2009. **96**, L39-41.

120. Steinkuhler, J., et al., *Modulating Vesicle Adhesion by Electric Fields.* Biophys J, 2016. **111**, 1454-1464.

121. Bolognesi, G., et al., *Sculpting and fusing biomimetic vesicle networks using optical tweezers.* Nat Commun, 2018. **9**, 1882.

122. Richard, A., et al., *Fusogenic supramolecular vesicle systems induced by metal ion binding to amphiphilic ligands.* Proc Natl Acad Sci USA, 2004. **101**, 15279-15284.

123. Sommerdijk, N.A.J.M., et al., *Stereodependent fusion and fission of vesicles: Calcium binding of synthetic gemini phospholipids containing two phosphate groups.* J Am Chem Soc, 1997. **119**, 4338-4344.

124. Frohnmayer, J.P., et al., *Minimal synthetic cells to study integrin-mediated adhesion.* Angew Chem, 2015. **54**, 12472-8.

125. Pontani, L.L., I. Jorjadze, and J. Brujic, *Cis and Trans Cooperativity of E-Cadherin Mediates Adhesion in Biomimetic Lipid Droplets.* Biophys J, 2016. **110**, 391-399.

126. Chiruvolu, S., et al., *Higher-Order Self-Assembly of Vesicles by Site-Specific Binding.* Science, 1994. **264**, 1753-1756.

127. Villringer, S., et al., *Lectin-mediated protocell crosslinking to mimic cell-cell junctions and adhesion.* Sci Rep, 2018. **8**, 1932.

128. NopplSimson, D.A. and D. Needham, *Avidin-biotin interactions at vesicle surfaces: Adsorption and binding, cross-bridge formation, and lateral interactions.* Biophys J, 1996. **70**, 1391-1401.

129. Parolini, L., et al., *Controlling Self-Assembly Kinetics of DNA-Functionalized Liposomes Using Toehold Exchange Mechanism.* ACS Nano, 2016. **10**, 2392-8.

130. Stengel, G., R. Zahn, and F. Hook, *DNA-induced programmable fusion of phospholipid vesicles.* J Am Chem Soc, 2007. **129**, 9584.

131. Robert, E., et al., *Mimicking and Understanding the Agglutination Effect of the Antimicrobial Peptide Thanatin Using Model Phospholipid Vesicles.* Biochemistry, 2015. **54**, 3932-41.

132. Warner, J.M., E. Karatekin, and B. O'Shaughnessy, *Model of SNARE-mediated membrane adhesion kinetics.* PLoS One, 2009. **4**, e6375.

133. Kong, L., et al., *Temporal Control of Membrane Fusion through Photolabile PEGylation of Liposome Membranes.* Angew Chem, 2016. **55**, 1396-400.

133. Kong, L., et al., *Temporal Control of Membrane Fusion through Photolabile PEGylation of Liposome Membranes.* Angew Chem, 2016. **55**, 1396-400.

134. Siton-Mendelson, O. and A. Bernheim-Groswasser, *Toward the reconstitution of synthetic cell motility.* Cell Adh Migr, 2016. **10**, 461-474.

135. Joseph, A., et al., *Chemotactic synthetic vesicles: Design and applications in blood-brain barrier crossing.* Sci Adv, 2017. **3**, e1700362.

136. Bente, K., et al., *Biohybrid and Bioinspired Magnetic Microswimmers.* Small, 2018, e1704374.

137. Brochard-Wyart, F., et al., *Hydrodynamic narrowing of tubes extruded from cells.* Proc Natl Acad Sci USA, 2006. **103**, 7660-7663.

138. Koster, G., et al., *Force barriers for membrane tube formation.* Phys Rev Lett, 2005. **94**, 068101.

139. Heuvingh, J., et al., *ARF1-mediated actin polymerization produces movement of artificial vesicles.* Proc Natl Acad Sci USA, 2007. **104**, 16928-33.

140. Upadhyaya, A., et al., *Probing polymerization forces by using actin-propelled lipid vesicles.* Proc Natl Acad Sci USA, 2003. **100**, 4521-6.

141. Fygenson, D.K., J.F. Marko, and A. Libchaber, *Mechanics of microtubule-based membrane extension.* Phys Rev Lett, 1997. **79**, 4497-4500.

142. Carvalho, K., et al., *Cell-sized liposomes reveal how actomyosin cortical tension drives shape change (vol 110, pg 16456, 2013).* Proc Natl Acad Sci USA, 2013. **110**, 19969-19969.

143. Loiseau, E., et al., *Shape remodeling and blebbing of active cytoskeletal vesicles.* Science Advances, 2016. **2**, e150046.

144. Bruggemann, D., J.P. Frohnmayer, and J.P. Spatz, *Model systems for studying cell adhesion and biomimetic actin networks.* Beilstein J Nanotechnol, 2014. **5**, 1193-202.

145. Maiuri, P., et al., *Actin flows mediate a universal coupling between cell speed and cell persistence.* Cell, 2015. **161**, 374-86.

146. Cortese, J.D., et al., *Actin polymerization induces a shape change in actin-containing vesicles.* Proc Natl Acad Sci USA, 1989. **86**, 5773-7.

147. Keber, F.C., et al., *Topology and dynamics of active nematic vesicles.* Science, 2014. **345**, 1135-9.

148. Tsai, F.C., B. Stuhrmann, and G.H. Koenderink, *Encapsulation of active cytoskeletal protein networks in cell-sized liposomes.* Langmuir, 2011. **27**, 10061-71.

149. Takiguchi, K., et al., *Transformation of actoHMM assembly confined in cell-sized liposome.* Langmuir, 2011. **27**, 11528-35.

150. Asahi, R., et al., *Visible-light photocatalysis in nitrogen-doped titanium oxides.* Science, 2001. **293**, 269-71.

151. Guglielmi, G., H.J. Falk, and S. De Renzis, *Optogenetic Control of Protein Function: From Intracellular Processes to Tissue Morphogenesis.* Trends Cell Biol, 2016. **26**, 864-874.

152. Pathak, G.P., et al., *Benchmarking of optical dimerizer systems.* ACS Synth Biol, 2014. **3**, 832-8.

153. Johnson, H.E., et al., *The Spatiotemporal Limits of Developmental Erk Signaling.* Dev Cell, 2017. **40**, 185-192.

154. Harper, S.M., L.C. Neil, and K.H. Gardner, *Structural basis of a phototropin light switch.* Science, 2003. **301**, 1541-4.

155. Karunarathne, W.K.A., P.R. O'Neill, and N. Gautam, *Subcellular optogenetics - controlling signaling and single-cell behavior.* J Cell Sci, 2015. **128**, 15-25.

156. Chen, F. and S.V. Wegner, *Blue Light Switchable Bacterial Adhesion as a Key Step toward the Design of Biofilms.* ACS Synth Biol, 2017. **6**, 2170-2174.

157. Shi, F., et al., *Optogenetic Control of Endoplasmic Reticulum-Mitochondria Tethering.* ACS Synth Biol, 2018. **7**, 2-9.

158. Nguyen, T., C.S. Yang, and C.B. Pickett, *The pathways and molecular mechanisms regulating Nrf2 activation in response to chemical stress.* Free Radic Biol Med, 2004. **37**, 433-41.

159. Moan, J. and M.J. Peak, *Effects of UV radiation of cells.* J Photochem Photobiol B, 1989. **4**, 21-34.

160. Chervyachkova, E. and S.V. Wegner, *Reversible Social Self-Sorting of Colloidal Cell-Mimics with Blue Light Switchable Proteins.* ACS Synth Biol, 2018. **7**, 1817-1824.

161. Kawano, F., F. Shi, and M. Yazawa, *Optogenetics: Switching with red and blue.* Nat Chem Biol, 2017. **13**, 573-574.

162. Ash, C., et al., *Effect of wavelength and beam width on penetration in light-tissue interaction using computational methods.* Lasers Med Sci, 2017. **32**, 1909-1918.

163. Kaberniuk, A.A., A.A. Shemetov, and V.V. Verkhusha, *A bacterial phytochrome-based optogenetic system controllable with near-infrared light.* Nat Methods, 2016. **13**, 591-7.

164. Proft, J. and N. Weiss, *From opto- to radio-genetics: A switch in the wavelength.* Commun Integr Biol, 2012. **5**, 227-9.

165. Redchuk, T.A., et al., *Near-infrared optogenetic pair for protein regulation and spectral multiplexing.* Nat Chem Biol, 2017. **13**, 633-639.

166. Deisseroth, K., *Optogenetics.* Nat Methods, 2011. **8**, 26-9.

167. Liu, Q. and C.L. Tucker, *Engineering genetically-encoded tools for optogenetic control of protein activity.* Curr Opin Chem Biol, 2017. **40**, 17-23.

168. Muller, K. and W. Weber, *Optogenetic tools for mammalian systems.* Mol Biosyst, 2013. **9**, 596-608.

169. Guntas, G., et al., *Engineering an improved light-induced dimer (iLID) for controlling the localization and activity of signaling proteins.* Proc Natl Acad Sci USA, 2015. **112**, 112-7.

170. Konold, P.E., et al., *Unfolding of the C-Terminal Jalpha Helix in the LOV2 Photoreceptor Domain Observed by Time-Resolved Vibrational Spectroscopy.* J Phys Chem Lett, 2016. **7**, 3472-6.

171. Shimizu-Sato, S., et al., *A light-switchable gene promoter system.* Nat Biotechnol, 2002. **20**, 1041-4.

172. Levskaya, A., et al., *Synthetic biology: engineering Escherichia coli to see light.* Nature, 2005. **438**, 441-2.

173. Wang, X., X. Chen, and Y. Yang, *Spatiotemporal control of gene expression by a light-switchable transgene system.* Nat Methods, 2012. **9**, 266-9.

174. Taslimi, A., et al., *An optimized optogenetic clustering tool for probing protein interaction and function.* Nat Commun, 2014. **5**, 4925.

175. Kawano, F., et al., *Engineered pairs of distinct photoswitches for optogenetic control of cellular proteins.* Nat Commun, 2015. **6**, 6256.

176. Kennedy, M.J., et al., *Rapid blue-light-mediated induction of protein interactions in living cells.* Nat Methods, 2010. **7**, 973-5.

177. Lungu, O.I., et al., *Designing photoswitchable peptides using the AsLOV2 domain.* Chem Biol, 2012. **19**, 507-17.

178. Zimmerman, S.P., et al., *Tuning the Binding Affinities and Reversion Kinetics of a Light Inducible Dimer Allows Control of Transmembrane Protein Localization.* Biochemistry, 2016. **55**, 5264-71.

179. Zhu, J., et al., *Photoadduct Formation from the FMN Singlet Excited State in the LOV2 Domain of Chlamydomonas reinhardtii Phototropin.* J Phys Chem Lett, 2016. **7**, 4380-4384.

180. Benedetti, L., et al., *Light-activated protein interaction with high spatial subcellular confinement.* Proc Natl Acad Sci USA, 2018. **115**, E2238-E2245.

181. O'Neill, P.R., et al., *Membrane Flow Drives an Adhesion-Independent Amoeboid Cell Migration Mode.* Dev Cell, 2018. **46**, 9-22 e4.

182. Zimmerman, S.P., et al., *Cells lay their own tracks - optogenetic Cdc42 activation stimulates fibronectin deposition supporting directed migration.* J Cell Sci, 2017. **130**, 2971-2983.

183. O'Neill, P.R., V. Kalyanaraman, and N. Gautam, *Subcellular optogenetic activation of Cdc42 controls local and distal signaling to drive immune cell migration.* Mol Biol Cell, 2016. **27**, 1442-50.

184. Wu, Y.I., et al., *A genetically encoded photoactivatable Rac controls the motility of living cells.* Nature, 2009. **461**, 104-8.

185. Ji, C., F. Fan, and X. Lou, *Vesicle Docking Is a Key Target of Local PI(4,5)P2 Metabolism in the Secretory Pathway of INS-1 Cells.* Cell Rep, 2017. **20**,1 409-1421.

186. Yu, Q., et al., *Photocontrolled reversible self-assembly of dodecamer nitrilase.* Bioresour Bioprocess, 2017. **4**, 36.

187. Filipponi, L., et al., *Protein patterning by microcontact printing using pyramidal PDMS stamps.* Biomed Microdevices, 2016. **18**, 9.

188. Setlow, R.B., *The wavelengths in sunlight effective in producing skin cancer: a theoretical analysis.* Proc Natl Acad Sci USA, 1974. **71**, 3363-6.

189. Muller, K., et al., *A red/far-red light-responsive bi-stable toggle switch to control gene expression in mammalian cells.* Nucleic Acids Res, 2013. **41**, e77.

190. Saka, S.K., et al., *Multi-protein assemblies underlie the mesoscale organization of the plasma membrane.* Nat Commun, 2014. **5**, 4509.

191. Wu, F., et al., *Multistability and dynamic transitions of intracellular Min protein patterns.* Mol Syst Biol, 2016. **12**, 873.

192. Hao, J., et al., *Differential expression patterns of the dentin matrix proteins during mineralized tissue formation.* Bone, 2004. **34**, 921-32.

193. Lata, S., et al., *High-affinity adaptors for switchable recognition of histidine-tagged proteins.* J Am Chem Soc, 2005. **127**, 10205-15.

194. Smith, A.S. and U. Seifert, *Vesicles as a model for controlled (de-) adhesion of cells: a thermodynamic approach.* Soft Matter, 2007. **3**, 275-289.

195. Hoesli, C.A., et al., *A fluorophore-tagged RGD peptide to control endothelial cell adhesion to micropatterned surfaces.* Biomaterials, 2014. **35**, 879-90.

196. Marchi-Artzner, V., et al., *Adhesion of Arg-Gly-Asp (RGD) peptide vesicles onto an integrin surface: Visualization of the segregation of RGD ligands into the adhesion plaques by fluorescence.* Langmuir, 2003. **19**, 835-841.

197. Anamelechi, C.C., et al., *Streptavidin binding and endothelial cell adhesion to biotinylated fibronectin.* Langmuir, 2007. **23**, 12583-8.

198. Cardoso Dos Santos, M., C. Vezy, and R. Jaffiol, *Nanoscale characterization of vesicle adhesion by normalized total internal reflection fluorescence microscopy.* Biochim Biophys Acta, 2016. **1858**, 1244-53.

199. Maiuri, P., et al., *The first World Cell Race.* Curr Biol, 2012. **22**, R673-5.

200. Bartelt, S.M., et al., *Dynamic blue light-switchable protein patterns on giant unilamellar vesicles.* Chem Commun, 2018. **54**, 948-951.

201. Yüz, S.G., J. Ricken, and S.V. Wegner, *Independent Control over Multiple Cell Types in Space and Time Using Orthogonal Blue and Red Light Switchable Cell Interactions.* Advanced Science, 2018. **5**, 1800446.

202. Schenk, F.C., et al., *Dual-functionalized nanostructured biointerfaces by click chemistry.* Langmuir, 2014. **30**, 6897-905.

203. Seifert, U. and R. Lipowsky, *Adhesion of vesicles.* Phys Rev A, 1990. **42**, 4768-4771.

204. Dimova, R., *Recent developments in the field of bending rigidity measurements on membranes.* Adv Colloid Interface Sci, 2014. **208**,225-34.

205. Hudson, S.V., et al., *Modeling the Kinetics of Integrin Receptor Binding to Hepatic Extracellular Matrix Proteins.* Scientific Reports, 2017. **7**, 12444.

206. Litvinov, R.I., et al., *Resolving two-dimensional kinetics of the integrin alphaIIbbeta3-fibrinogen interactions using binding-unbinding correlation spectroscopy.* J Biol Chem, 2012. **287**, 35275-85.

207. Germer, M., et al., *Kinetic analysis of integrin-dependent cell adhesion on vitronectin--the inhibitory potential of plasminogen activator inhibitor-1 and RGD peptides.* Eur J Biochem, 1998. **253**, 669-74.

208. Kim, J.K., et al., *A novel binding site in collagen type III for integrins alpha1beta1 and alpha2beta1.* J Biol Chem, 2005. **280**, 32512-20.

209. Tordeux, C., J.B. Fournier, and P. Galatola, *Analytical characterization of adhering vesicles.* Phys Rev E Stat Nonlin Soft Matter Phys, 2002. **65**, 041912.

210. Steinkuhler, J., et al., *Membrane fluctuations and acidosis regulate cooperative binding of "marker of self" CD47 with macrophage checkpoint receptor SIRPalpha.* J Cell Sci, 2018. *132*, jcs216770.

211. Weikl, T.R., et al., *Adhesion of membranes via receptor–ligand complexes: Domain formation, binding cooperativity, and active processes.* Soft Matter, 2009. **5**, 3213–3224.

212. Suzuki, Y., et al., *Photoinduced Fusion of Lipid Bilayer Membranes.* Langmuir, 2017. **33**, 2671-2676.

213. Lipowsky, R., *Spontaneous tubulation of membranes and vesicles reveals membrane tension generated by spontaneous curvature.* Faraday Discuss., 2013. **161**, 305-331.

214. Garten, M., et al., *Reconstitution of a transmembrane protein, the voltage-gated ion channel, KvAP, into giant unilamellar vesicles for microscopy and patch clamp studies.* J Vis Exp, 2015, 52281.

215. Pressman, B.C., *Biological Applications of Ionophores.* Annu Rev Biochem, 1976. **45**, 501-530.

216. Beers, E.P. and J. Callis, *Utility of Polyhistidine-Tagged Ubiquitin in the Purification of Ubiquitin-Protein Conjugates and as an Affinity Ligand for the Purification of Ubiquitin-Specific Hydrolases.* J Biol Chem, 1993. **268**, 21645-21649.

217. Grunwald, C., et al., *In situ assembly of macromolecular complexes triggered by light.* Proc Natl Acad Sci USA, 2010. **107**, 6146-51.

Appendix

5.1 Nucleotide and amino acid sequences of optogenetic proteins

5.1.1 iLID

Nucleotide sequence

ATGAGAGGATCGCATCACCATCACCATCACGGATCCGGGGAGTTTCTGGCAACCACACTGGAAC
GGATCGAGAAAAATTTCGTGATTACTGATCCGAGACTGCCTGACAACCCAATCATTTTTGCGAG
CGATTCCTTCCTGCAGCTGACAGAATATTCTCGGGAAGAGATCCTGGGGCGCAATTGCCGTTTT
CTGCAGGGACCCGAGACAGACCGTGCCACTGTTCGGAAAATCAGAGATGCTATTGACAACCAGA
CTGAAGTGACCGTTCAGCTGATCAATTATACCAAGAGCGGCAAGAAGTTCTGGAACGTGTTCCA
CCTGCAGCCGATGCGCGATTATAAGGGCGACGTCCAGTACTTCATTGGCGTGCAGCTGGATGGC
ACCGAACGTCTTCATGGCGCCGCTGAGCGTGAGGCGGTCATGCTGATCAAAAAGACAGCCTTTC
AGATTGCTGAGGCAGCGAACGACGAAAATTACTTTTAA

Amino acid sequence

MRGSHHHHHHGSGEFLATTLERIEKNFVITDPRLPDNPIIFASDSFLQLTEYSREEILGRNCRF
LQGPETDRATVRKIRDAIDNQTEVTVQLINYTKSGKKFWNVFHLQPMRDYKGDVQYFIGVQLDG
TERLHGAAEREAVMLIKKTAFQIAEAANDENYF-

5.1.2 MBP-SspB-Nano

Nucleotide sequence

ATGAGAGGATCGCATCACCATCACCATCACGGATCTAAAATCGAAGAAGGTAAACTGGTAATCT
GGATTAACGGCGATAAAGGCTATAACGGTCTCGCTGAAGTCGGTAAGAAATTCGAGAAAGATAC
CGGAATTAAAGTCACCGTTGAGCATCCGGATAAACTGGAAGAGAAATTCCCACAGGTTGCGGCA
ACTGGCGATGGCCCTGACATTATCTTCTGGGCACACGACCGCTTTGGTGGCTACGCTCAATCTG
GCCTGTTGGCTGAAATCACCCCGGACAAAGCGTTCCAGGACAAGCTGTATCCGTTTACCTGGGA
TGCCGTACGTTACAACGGCAAGCTGATTGCTTACCCGATCGCTGTTGAAGCGTTATCGCTGATT
TATAACAAAGACCTGCTGCCGAACCCGCCAAAAACCTGGGAAGAGATCCCGGCGCTGGATAAAG
AACTGAAAGCGAAAGGTAAGAGCGCGCTGATGTTCAACCTGCAAGAACCGTACTTCACCTGGCC
GCTGATTGCTGCTGACGGGGGTTATGCGTTCAAGTATGAAAACGGCAAGTACGACATTAAAGAC
GTGGGCGTGGATAACGCTGGCGCGAAAGCGGGTCTGACCTTCCTGGTTGACCTGATTAAAAACA
AACACATGAATGCAGACACCGATTACTCCATCGCAGAAGCTGCCTTTAATAAAGGCGAAACAGC
GATGACCATCAACGGCCCGTGGGCATGGTCCAACATCGACACCAGCAAAGTGAATTATGGTGTA
ACGGTACTGCCGACCTTCAAGGGTCAACCATCCAAACCGTTCGTTGGCGTGCTGAGCGCAGGTA
TTAACGCCGCCAGTCCGAACAAAGAGCTGGCAAAAGAGTTCCTCGAAAACTATCTGCTGACTGA

TGAAGGTCTGGAAGCGGTTAATAAAGACAAACCGCTGGGTGCCGTAGCGCTGAAGTCTTACGAG
GAAGAGTTGGCGAAAGATCCACGTATTGCCGCCACTATGGAAAACGCCCAGAAAGGTGAAATCA
TGCCGAACATCCCGCAGATGTCCGCTTTCTGGTATGCCGTGCGTACTGCGGTGATCAACGCCGC
CAGCGGTCGTCAGACTGTCGATGAAGCCCTGAAAGACGCGCAGACTAATTCGAGCTCGAACAAC
AACAACAATAACAATAACAACAACCTCGGGATCGAGGGAACGACCGAAAACCTGTATTTTCAGG
GATCCAGCTCCCCGAAACGCCCTAAGCTGCTGCGTGAATATTACGATTGGCTGGTTGATAACAG
CTTTACCCCATATCTGGTGGTGGATGCCACATACCTGGGCGTGAACGTGCCCGTGGAGTATGTG
AAAGACGGTCAGATCGTGCTGAATCTGTCTGCAAGTGCGACCGGCAACCTGCAACTGACAAATG
ATTTTATCCAGTTCAACGCCCGCTTTAAGGGCGTGTCTCGTGAACTGTATATCCCGATGGGTGC
CGCTCTGGCCATTTACGCTCGCGAGAACGGCGATGGTGTGATGTTCGAACCAGAAGAAATCTAT
GACGAGCTGAATATTGGTTAA

Amino acid sequence

MRGSHHHHHHGSKIEEGKLVIWINGDKGYNGLAEVGKKFEKDTGIKVTVEHPDKLEEKFPQVAA
TGDGPDIIFWAHDRFGGYAQSGLLAEITPDKAFQDKLYPFTWDAVRYNGKLIAYPIAVEALSLI
YNKDLLPNPPKTWEEIPALDKELKAKGKSALMFNLQEPYFTWPLIAADGGYAFKYENGKYDIKD
VGVDNAGAKAGLTFLVDLIKNKHMNADTDYSIAEAAFNKGETAMTINGPWAWSNIDTSKVNYGV
TVLPTFKGQPSKPFVGVLSAGINAASPNKELAKEFLENYLLTDEGLEAVNKDKPLGAVALKSYE
EELAKDPRIAATMENAQKGEIMPNIPQMSAFWYAVRTAVINAASGRQTVDEALKDAQTNSSSNN
NNNNNNNNLGIEGTTENLYFQGSSSPKRPKLREYYDWLVDNSFTPYLVVDATYLGVNVPVEYVK
DGQIVLNLSASATGNLQLTNDFIQFNARFKGVSRELYIPMGAALAIYARENGDGVMFEPEEIYD
ELNIG-

5.1.3 MBP-SspB-Micro

Nucleotide sequence

ATGAGAGGATCGCATCACCATCACCATCACGGATCTAAAATCGAAGAAGGTAAACTGGTAATCT
GGATTAACGGCGATAAAGGCTATAACGGTCTCGCTGAAGTCGGTAAGAAATTCGAGAAAGATAC
CGGAATTAAAGTCACCGTTGAGCATCCGGATAAACTGGAAGAGAAATTCCCACAGGTTGCGGCA
ACTGGCGATGGCCCTGACATTATCTTCTGGGCACACGACCGCTTTGGTGGCTACGCTCAATCTG
GCCTGTTGGCTGAAATCACCCCGGACAAAGCGTTCCAGGACAAGCTGTATCCGTTTACCTGGGA
TGCCGTACGTTACAACGGCAAGCTGATTGCTTACCCGATCGCTGTTGAAGCGTTATCGCTGATT
TATAACAAAGACCTGCTGCCGAACCCGCCAAAAACCTGGGAAGAGATCCCGGCGCTGGATAAAG
AACTGAAAGCGAAAGGTAAGAGCGCGCTGATGTTCAACCTGCAAGAACCGTACTTCACCTGGCC
GCTGATTGCTGCTGACGGGGGTTATGCGTTCAAGTATGAAAACGGCAAGTACGACATTAAAGAC
GTGGGCGTGGATAACGCTGGCGCGAAAGCGGGTCTGACCTTCCTGGTTGACCTGATTAAAAACA

AACACATGAATGCAGACACCGATTACTCCATCGCAGAAGCTGCCTTTAATAAAGGCGAAACAGC
GATGACCATCAACGGCCCGTGGGCATGGTCCAACATCGACACCAGCAAAGTGAATTATGGTGTA
ACGGTACTGCCGACCTTCAAGGGTCAACCATCCAAACCGTTCGTTGGCGTGCTGAGCGCAGGTA
TTAACGCCGCCAGTCCGAACAAAGAGCTGGCAAAAGAGTTCCTCGAAAACTATCTGCTGACTGA
TGAAGGTCTGGAAGCGGTTAATAAAGACAAACCGCTGGGTGCCGTAGCGCTGAAGTCTTACGAG
GAAGAGTTGGCGAAAGATCCACGTATTGCCGCCACTATGGAAAACGCCCAGAAAGGTGAAATCA
TGCCGAACATCCCGCAGATGTCCGCTTTCTGGTATGCCGTGCGTACTGCGGTGATCAACGCCGC
CAGCGGTCGTCAGACTGTCGATGAAGCCCTGAAAGACGCGCAGACTAATTCGAGCTCGAACAAC
AACAACAATAACAATAACAACAACCTCGGGATCGAGGGAACGACCGAAAACCTGTATTTTCAGG
GATCCAGCTCCCCGAAACGCCCTAAGCTGCTGCGTGAATATTACGATTGGCTGGTTGATAACAG
CTTTACCCCATATCTGGTGGTGGATGCCACATACCTGGGCGTGAACGTGCCCGTGGAGTATGTG
AAAGACGGTCAGATCGTGCTGAATCTGTCTGCAAGTGCGACCGGCAACCTGCAACTGACAAATG
ATTTTATCCAGTTCAACGCCCAGTTTAAGGGCGTGTCTCGTGAACTGTATATCCCGATGGGTGC
CGCTCTGGCCATTTACGCTCGCGAGAACGGCGATGGTGTGATGTTCGAACCAGAAGAAATCTAT
GACGAGCTGAATATTGGTTAA

Amino acid sequence

MRGSHHHHHHGSKIEEGKLVIWINGDKGYNGLAEVGKKFEKDTGIKVTVEHPDKLEEKFPQVAA
TGDGPDIIFWAHDRFGGYAQSGLLAEITPDKAFQDKLYPFTWDAVRYNGKLIAYPIAVEALSLI
YNKDLLPNPPKTWEEIPALDKELKAKGKSALMFNLQEPYFTWPLIAADGGYAFKYENGKYDIKD
VGVDNAGAKAGLTFLVDLIKNKHMNADTDYSIAEAAFNKGETAMTINGPWAWSNIDTSKVNYGV
TVLPTFKGQPSKPFVGVLSAGINAASPNKELAKEFLENYLLTDEGLEAVNKDKPLGAVALKSYE
EELAKDPRIAATMENAQKGEIMPNIPQMSAFWYAVRTAVINAASGRQTVDEALKDAQTNSSSNN
NNNNNNNNLGIEGTTENLYFQGSSSPKRPKLLREYYDWLVDNSFTPYLVVDATYLGVNVPVEYV
KDGQIVLNLSASATGNLQLTNDFIQFNAQFKGVSRELYIPMGAALAIYARENGDGVMFEPEEIY
DELNIG-

5.1.4 Nano-mOrange

Nucleotide sequence

ATGAGAGGATCGCATCACCATCACCATCACGGATCTAAAATCGAAGAAGGTAAACTGGTAATCT
GGATTAACGGCGATAAAGGCTATAACGGTCTCGCTGAAGTCGGTAAGAAATTCGAGAAAGATAC
CGGAATTAAAGTCACCGTTGAGCATCCGGATAAACTGGAAGAGAAATTCCCACAGGTTGCGGCA
ACTGGCGATGGCCCTGACATTATCTTCTGGGCACACGACCGCTTTGGTGGCTACGCTCAATCTG
GCCTGTTGGCTGAAATCACCCCGGACAAAGCGTTCCAGGACAAGCTGTATCCGTTTACCTGGGA
TGCCGTACGTTACAACGGCAAGCTGATTGCTTACCCGATCGCTGTTGAAGCGTTATCGCTGATT

TATAACAAAGACCTGCTGCCGAACCCGCCAAAAACCTGGGAAGAGATCCCGGCGCTGGATAAAG
AACTGAAAGCGAAAGGTAAGAGCGCGCTGATGTTCAACCTGCAAGAACCGTACTTCACCTGGCC
GCTGATTGCTGCTGACGGGGGTTATGCGTTCAAGTATGAAAACGGCAAGTACGACATTAAAGAC
GTGGGCGTGGATAACGCTGGCGCGAAAGCGGGTCTGACCTTCCTGGTTGACCTGATTAAAAACA
AACACATGAATGCAGACACCGATTACTCCATCGCAGAAGCTGCCTTTAATAAAGGCGAAACAGC
GATGACCATCAACGGCCCGTGGGCATGGTCCAACATCGACACCAGCAAAGTGAATTATGGTGTA
ACGGTACTGCCGACCTTCAAGGGTCAACCATCCAAACCGTTCGTTGGCGTGCTGAGCGCAGGTA
TTAACGCCGCCAGTCCGAACAAAGAGCTGGCAAAAGAGTTCCTCGAAAACTATCTGCTGACTGA
TGAAGGTCTGGAAGCGGTTAATAAAGACAAACCGCTGGGTGCCGTAGCGCTGAAGTCTTACGAG
GAAGAGTTGGCGAAAGATCCACGTATTGCCGCCACTATGGAAAACGCCCAGAAAGGTGAAATCA
TGCCGAACATCCCGCAGATGTCCGCTTTCTGGTATGCCGTGCGTACTGCGGTGATCAACGCCGC
CAGCGGTCGTCAGACTGTCGATGAAGCCCTGAAAGACGCGCAGACTAATTCGAGCTCGAACAAC
AACAACAATAACAATAACAACAACCTCGGGATCGAGGGAACGACCGAAAACCTGTATTTTCAGG
GATCCGTGAGCAAGGGCGAGGAGAATAACATGGCCATCATCAAGGAGTTCATGCGCTTCAAGGT
GCGCATGGAGGGCTCCGTGAACGGCCACGAGTTCGAGATCGAGGGCGAGGGCGAGGGCCGCCCC
TACGAGGGCTTTCAGACCGCTAAGCTGAAGGTGACCAAGGGTGGCCCCCTGCCCTTCGCCTGGG
ACATCCTGTCCCCTCAGTTCACCTACGGCTCCAAGGCCTACGTGAAGCACCCCGCCGACATCCC
CGACTACTTCAAGCTGTCCTTCCCCGAGGGCTTCAAGTGGGAGCGCGTGATGAACTTCGAGGAC
GGCGGCGTGGTGACCGTGACCCAGGACTCCTCCCTCCAGGACGGCGAGTTCATCTACAAGGTGA
AGCTGCGCGGCACCAACTTCCCCTCCGACGGCCCCGTAATGCAGAAGAAGACCATGGGCTGGGA
GGCCTCCTCCGAGCGGATGTACCCCGAGGACGGCGCCCTGAAGGGCGAGATCAAGATGAGGCTG
AAGCTGAAGGACGGCGGCCACTACACCTCCGAGGTCAAGACCACCTACAAGGCCAAGAAGCCCG
TGCAGCTGCCCGGCGCCTACATCGTCGGCATCAAGTTGGACATCACCTCCCACAACGAGGACTA
CACCATCGTGGAACAGTACGAACGCGCCGAGGGCCGCCACTCCACCGGCGGCATGGACGAGCTG
TACAAGGGAGGAAGTGGTACCAGCTCCCCGAAACGCCCTAAGCTGCTGCGTGAATATTACGATT
GGCTGGTTGATAACAGCTTTACCCCATATCTGGTGGTGGATGCCACATACCTGGGCGTGAACGT
GCCCGTGGAGTATGTGAAAGACGGTCAGATCGTGCTGAATCTGTCTGCAAGTGCGACCGGCAAC
CTGCAACTGACAAATGATTTTATCCAGTTCAACGCCCGCTTTAAGGGCGTGTCTCGTGAACTGT
ATATCCCGATGGGTGCCGCTCTGGCCATTTACGCTCGCGAGAACGGCGATGGTGTGATGTTCGA
ACCAGAAGAAATCTATGACGAGCTGAATATTGGTTAA

Amino acid sequence

MRGSHHHHHHGSKIEEGKLVIWINGDKGYNGLAEVGKKFEKDTGIKVTVEHPDKLEEKFPQVAA
TGDGPDIIFWAHDRFGGYAQSGLLAEITPDKAFQDKLYPFTWDAVRYNGKLIAYPIAVEALSLI
YNKDLLPNPPKTWEEIPALDKELKAKGKSALMFNLQEPYFTWPLIAADGGYAFKYENGKYDIKD

VGVDNAGAKAGLTFLVDLIKNKHMNADTDYSIAEAAFNKGETAMTINGPWAWSNIDTSKVNYGV
TVLPTFKGQPSKPFVGVLSAGINAASPNKELAKEFLENYLLTDEGLEAVNKDKPLGAVALKSYE
EELAKDPRIAATMENAQKGEIMPNIPQMSAFWYAVRTAVINAASGRQTVDEALKDAQTNSSSNN
NNNNNNNNLGIEGTTENLYFQGSVSKGEENNMAIIKEFMRFKVRMEGSVNGHEFEIEGEGEGRP
YEGFQTAKLKVTKGGPLPFAWDILSPQFTYGSKAYVKHPADIPDYFKLSFPEGFKWERVMNFED
GGVVTVTQDSSLQDGEFIYKVKLRGTNFPSDGPVMQKKTMGWEASSERMYPEDGALKGEIKMRL
KLKDGGHYTSEVKTTYKAKKPVQLPGAYIVGIKLDITSHNEDYTIVEQYERAEGRHSTGGMDEL
YKGGSGTSSPKRPKLLREYYDWLVDNSFTPYLVVDATYLGVNVPVEYVKDGQIVLNLSASATGN
LQLTNDFIQFNARFKGVSRELYIPMGAALAIYARENGDGVMFEPEEIYDELNIG-

5.1.5 Micro-mOrange

Nucleotide sequence

ATGAGAGGATCGCATCACCATCACCATCACGGATCTAAAATCGAAGAAGGTAAACTGGTAATCT
GGATTAACGGCGATAAAGGCTATAACGGTCTCGCTGAAGTCGGTAAGAAATTCGAGAAAGATAC
CGGAATTAAAGTCACCGTTGAGCATCCGGATAAACTGGAAGAGAAATTCCCACAGGTTGCGGCA
ACTGGCGATGGCCCTGACATTATCTTCTGGGCACACGACCGCTTTGGTGGCTACGCTCAATCTG
GCCTGTTGGCTGAAATCACCCCGGACAAAGCGTTCCAGGACAAGCTGTATCCGTTTACCTGGGA
TGCCGTACGTTACAACGGCAAGCTGATTGCTTACCCGATCGCTGTTGAAGCGTTATCGCTGATT
TATAACAAAGACCTGCTGCCGAACCCGCCAAAAACCTGGGAAGAGATCCCGGCGCTGGATAAAG
AACTGAAAGCGAAAGGTAAGAGCGCGCTGATGTTCAACCTGCAAGAACCGTACTTCACCTGGCC
GCTGATTGCTGCTGACGGGGGTTATGCGTTCAAGTATGAAAACGGCAAGTACGACATTAAAGAC
GTGGGCGTGGATAACGCTGGCGCGAAAGCGGGTCTGACCTTCCTGGTTGACCTGATTAAAAACA
AACACATGAATGCAGACACCGATTACTCCATCGCAGAAGCTGCCTTTAATAAAGGCGAAACAGC
GATGACCATCAACGGCCCGTGGGCATGGTCCAACATCGACACCAGCAAAGTGAATTATGGTGTA
ACGGTACTGCCGACCTTCAAGGGTCAACCATCCAAACCGTTCGTTGGCGTGCTGAGCGCAGGTA
TTAACGCCGCCAGTCCGAACAAAGAGCTGGCAAAAGAGTTCCTCGAAAACTATCTGCTGACTGA
TGAAGGTCTGGAAGCGGTTAATAAAGACAAACCGCTGGGTGCCGTAGCGCTGAAGTCTTACGAG
GAAGAGTTGGCGAAAGATCCACGTATTGCCGCCACTATGGAAAACGCCCAGAAAGGTGAAATCA
TGCCGAACATCCCGCAGATGTCCGCTTTCTGGTATGCCGTGCGTACTGCGGTGATCAACGCCGC
CAGCGGTCGTCAGACTGTCGATGAAGCCCTGAAAGACGCGCAGACTAATTCGAGCTCGAACAAC
AACAACAATAACAATAACAACAACCTCGGGATCGAGGGAACGACCGAAAACCTGTATTTTCAGG
GATCCGTGAGCAAGGGCGAGGAGAATAACATGGCCATCATCAAGGAGTTCATGCGCTTCAAGGT
GCGCATGGAGGGCTCCGTGAACGGCCACGAGTTCGAGATCGAGGGCGAGGGCGAGGGCCGCCCC
TACGAGGGCTTTCAGACCGCTAAGCTGAAGGTGACCAAGGGTGGCCCCCTGCCCTTCGCCTGGG
ACATCCTGTCCCCTCAGTTCACCTACGGCTCCAAGGCCTACGTGAAGCACCCCGCCGACATCCC

CGACTACTTCAAGCTGTCCTTCCCCGAGGGCTTCAAGTGGGAGCGCGTGATGAACTTCGAGGAC
GGCGGCGTGGTGACCGTGACCCAGGACTCCTCCCTCCAGGACGGCGAGTTCATCTACAAGGTGA
AGCTGCGCGGCACCAACTTCCCCTCCGACGGCCCCGTAATGCAGAAGAAGACCATGGGCTGGGA
GGCCTCCTCCGAGCGGATGTACCCCGAGGACGGCGCCCTGAAGGGCGAGATCAAGATGAGGCTG
AAGCTGAAGGACGGCGGCCACTACACCTCCGAGGTCAAGACCACCTACAAGGCCAAGAAGCCCG
TGCAGCTGCCCGGCGCCTACATCGTCGGCATCAAGTTGGACATCACCTCCCACAACGAGGACTA
CACCATCGTGGAACAGTACGAACGCGCCGAGGGCCGCCACTCCACCGGCGGCATGGACGAGCTG
TACAAGGGAGGAAGTGGTACCAGCTCCCCGAAACGCCCTAAGCTGCTGCGTGAATATTACGATT
GGCTGGTTGATAACAGCTTTACCCCATATCTGGTGGTGGATGCCACATACCTGGGCGTGAACGT
GCCCGTGGAGTATGTGAAAGACGGTCAGATCGTGCTGAATCTGTCTGCAAGTGCGACCGGCAAC
CTGCAACTGACAAATGATTTTATCCAGTTCAACGCCCAGTTTAAGGGCGTGTCTCGTGAACTGT
ATATCCCGATGGGTGCCGCTCTGGCCATTTACGCTCGCGAGAACGGCGATGGTGTGATGTTCGA
ACCAGAAGAAATCTATGACGAGCTGAATATTGGTTAA

Amino acid sequence

MRGSHHHHHHGSKIEEGKLVIWINGDKGYNGLAEVGKKFEKDTGIKVTVEHPDKLEEKFPQVAA
TGDGPDIIFWAHDRFGGYAQSGLLAEITPDKAFQDKLYPFTWDAVRYNGKLIAYPIAVEALSLI
YNKDLLPNPPKTWEEIPALDKELKAKGKSALMFNLQEPYFTWPLIAADGGYAFKYENGKYDIKD
VGVDNAGAKAGLTFLVDLIKNKHMNADTDYSIAEAAFNKGETAMTINGPWAWSNIDTSKVNYGV
TVLPTFKGQPSKPFVGVLSAGINAASPNKELAKEFLENYLLTDEGLEAVNKDKPLGAVALKSYE
EELAKDPRIAATMENAQKGEIMPNIPQMSAFWYAVRTAVINAASGRQTVDEALKDAQTNSSSNN
NNNNNNNNLGIEGTTENLYFQGSVSKGEENNMAIIKEFMRFKVRMEGSVNGHEFEIEGEGEGRP
YEGFQTAKLKVTKGGPLPFAWDILSPQFTYGSKAYVKHPADIPDYFKLSFPEGFKWERVMNFED
GGVVTVTQDSSLQDGEFIYKVKLRGTNFPSDGPVMQKKTMGWEASSERMYPEDGALKGEIKMRL
KLKDGGHYTSEVKTTYKAKKPVQLPGAYIVGIKLDITSHNEDYTIVEQYERAEGRHSTGGMDEL
YKGGSGTSSPKRPKLLREYYDWLVDNSFTPYLVVDATYLGVNVPVEYVKDGQIVLNLSASATGN
LQLTNDFIQFNAQFKGVSRELYIPMGAALAIYARENGDGVMFEPEEIYDELNIG-

5.1.6 mOrange

Nucleotide sequence

GTGAGCAAGGGCGAGGAGAATAACATGGCCATCATCAAGGAGTTCATGCGCTTCAAGGTGCGCA
TGGAGGGCTCCGTGAACGGCCACGAGTTCGAGATCGAGGGCGAGGGCGAGGGCCGCCCCTACGA
GGGCTTTCAGACCGCTAAGCTGAAGGTGACCAAGGGTGGCCCCCTGCCCTTCGCCTGGGACATC
CTGTCCCCTCAGTTCACCTACGGCTCCAAGGCCTACGTGAAGCACCCCGCCGACATCCCCGACT

ACTTCAAGCTGTCCTTCCCCGAGGGCTTCAAGTGGGAGCGCGTGATGAACTTCGAGGACGGCGG
CGTGGTGACCGTGACCCAGGACTCCTCCCTCCAGGACGGCGAGTTCATCTACAAGGTGAAGCTG
CGCGGCACCAACTTCCCCTCCGACGGCCCCGTAATGCAGAAGAAGACCATGGGCTGGGAGGCCT
CCTCCGAGCGGATGTACCCCGAGGACGGCGCCCTGAAGGGCGAGATCAAGATGAGGCTGAAGCT
GAAGGACGGCGGCCACTACACCTCCGAGGTCAAGACCACCTACAAGGCCAAGAAGCCCGTGCAG
CTGCCCGGCGCCTACATCGTCGGCATCAAGTTGGACATCACCTCCCACAACGAGGACTACACCA
TCGTGGAACAGTACGAACGCGCCGAGGGCCGCCACTCCACCGGCGGCATGGACGAGCTGTACAA
GGGAGGAAGTGGTACCAGCTCCCCGAAACGCCCTAAGCTGCTGCGTGAATATTACGATTGGCTG
GTTGATAACAGCTTTACCCCATATCTGGTGGTGGATGCCACATACCTGGGCGTGAACGTGCCCG
TGGAGTATGTGAAAGACGGTCAGATCGTGCTGAATCTGTCTGCAAGTGCGACCGGCAACCTGCA
ACTGACAAATGATTTTATCCAGTTCAACGCCCGCTTTAAGGGCGTGTCTCGTGAACTGTATATC
CCGATGGGTGCCGCTCTGGCCATTTACGCTCGCGAGAACGGCGATGGTGTGATGTTCGAACCAG
AAGAAATCTATGACGAGCTGAATATTGGTTAA

Amino acid sequence

MAIIKEFMRFKVRMEGSVNGHEFEIEGEGEGRPYEGFQTAKLKVTKGGPLPFAWDILSPQFTYG
SKAYVKHPADIPDYFKLSFPEGFKWERVMNFEDGGVVTVTQDSSLQDGEFIYKVKLRGTNFPSD
GPVMQKKTMGWEASSERMYPEDGALKGEIKMRLKLKDGGHYTSEVKTTYKAKKPVQLPGAYIVG
IKLDITSHNEDYTIVEQYERAEGRHSTGGMDELYKGGSGTSSPKRPKLLREYYDWLVDNSFTPY
LVVDATYLGVNVPVEYVKDGQIVLNLSASATGNLQLTNDFIQFNARFKGVSRELYIPMGAALAI
YARENGDGVMFEPEEIYDELNIG-

5.2 12% SDS-Gel of used proteins

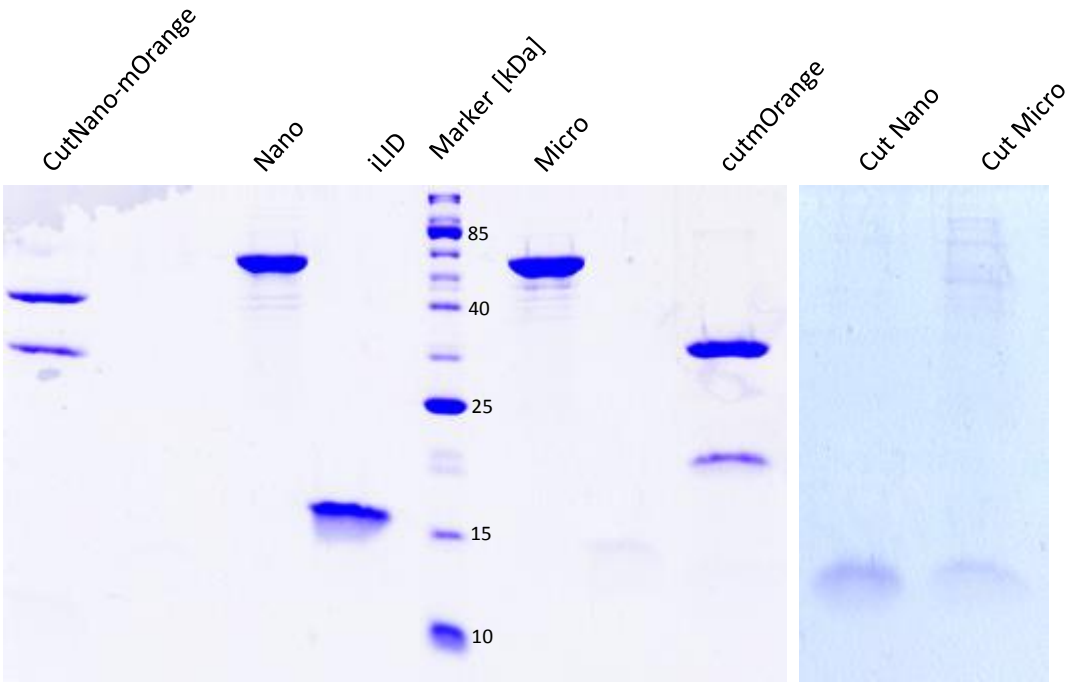

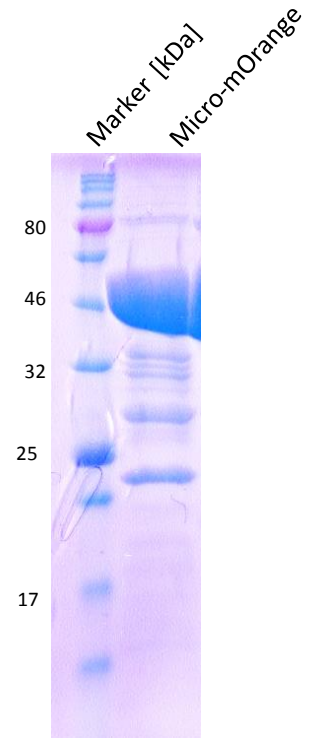

5.3 Reaction scheme of glass surface passivation and click reaction

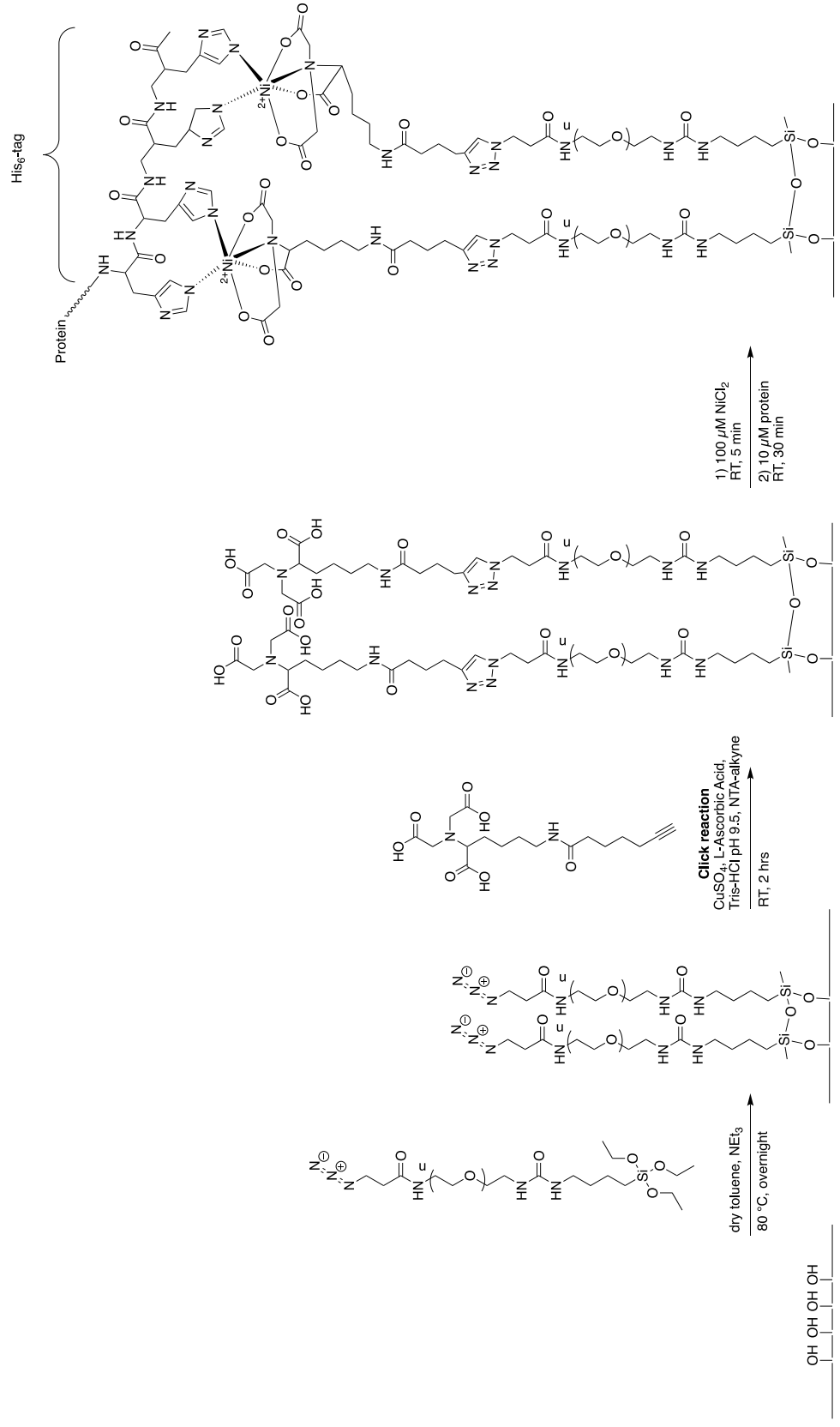

5.4 DLS Measurements to determine hydration radius for SUVs

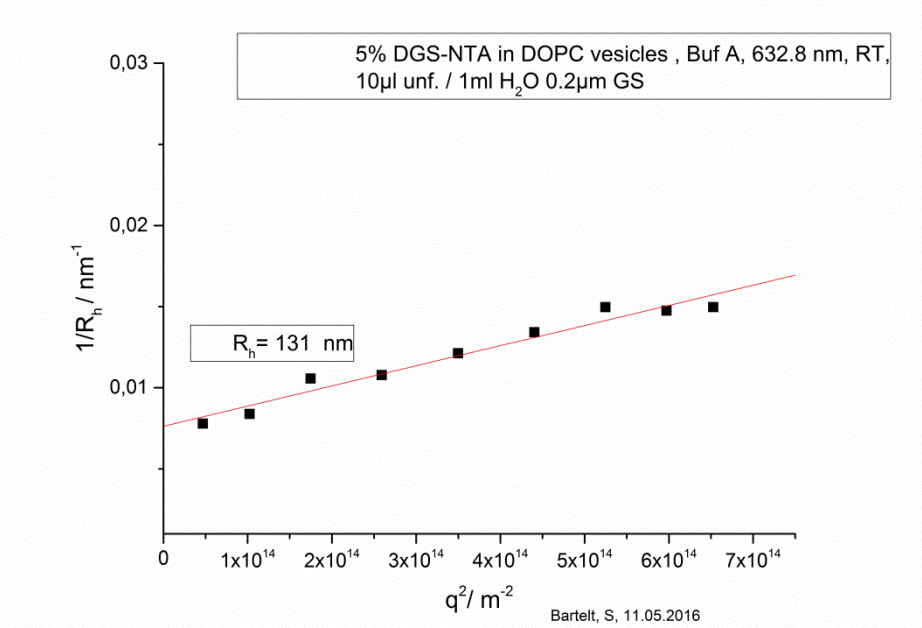

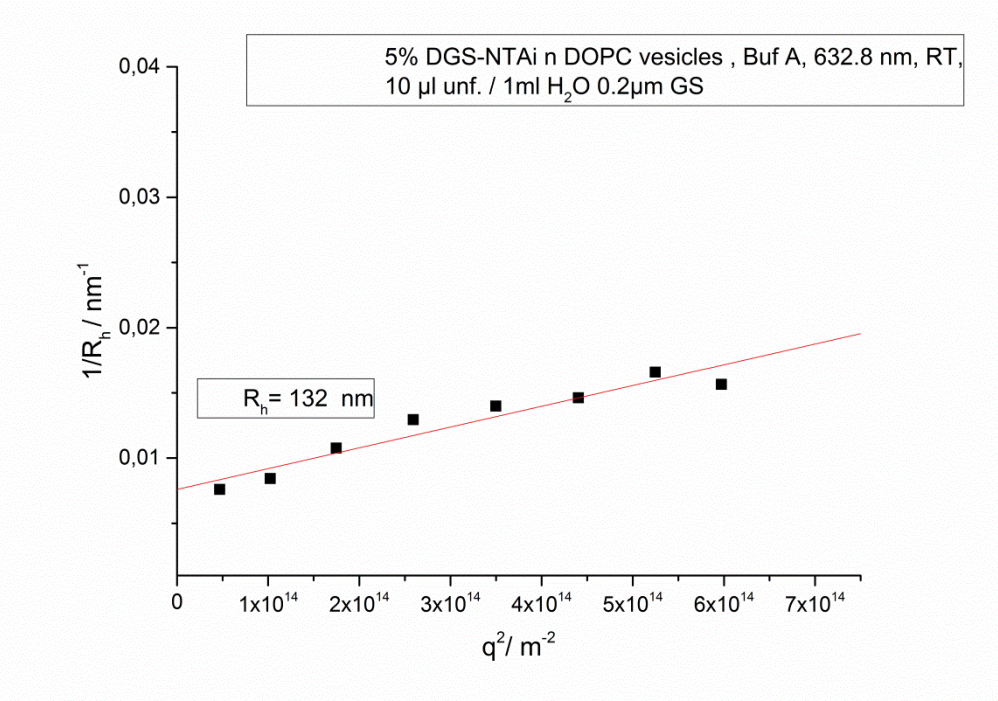

5.5 ^{1}H-NMR of $(CH_3CH_2O)_3Si$-PEG_{3000}-azid

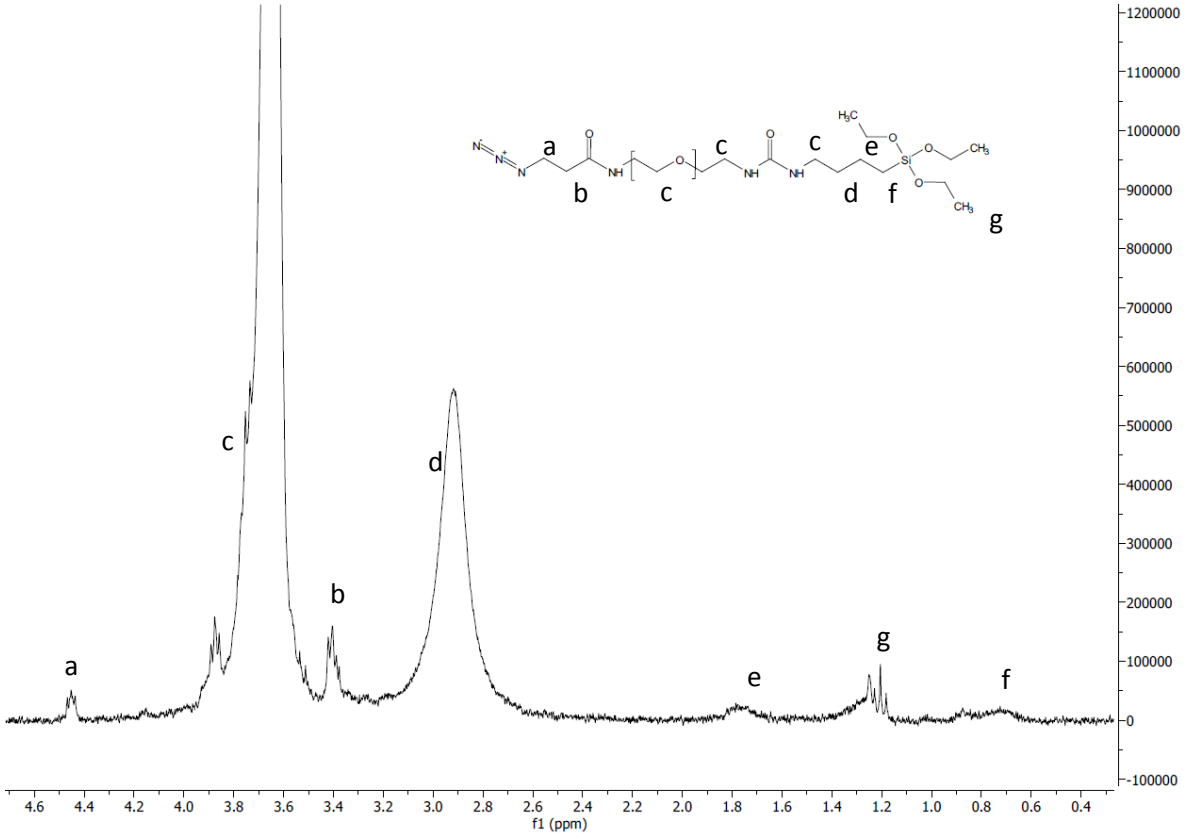

5.6 List of Publications

S. M. Bartelt*, E. Chervyachkova*,J. Steinkühler, J. Ricken, R. Wieneke, R. Tampé, R. Dimova and S. V. Wegner: Dynamic blue light-switchable protein patterns on giant unilamellar vesicles, **Chem. Comm.**, 2018,**54**, 948-95

S. M. Bartelt*, J. Steinkühler*, R. Dimova and S. V. Wegner: Light-guided motility of a minimal synthetic cell. **Nano Lett.,** 2018, **18**, 7268-7274. doi:10.1021/acs.nanolett.8b03469.

D. Xu, S.M. Bartelt, S. Rasoulinejad, F. Chen, S. V. Wegner: Green Light Lithography: A general strategy to create active protein and cell micropatterns. (sumitted)